ON THE MODELING AND SCREENOUT DETECTION BASED ON A SIMPLIFIED MODEL OF HYDRAULIC FRACTURING

By

JORGE CHIRIBOGA

Bachelor of Science

Pontificia Universidad Catolica del Peru

Lima, Peru

1990

Subbmitted to the Faculty of the
Graduate College of the
Oklahoma State University
in partial fulfillment of
the requirements for
the Degree of
MASTER OF SCIENCE
December, 1994

ON THE MODELING AND SCREENOUT DETECTION

BASED ON A SIMPLIFIED MODEL OF

HYDRAULIC FRACTURING

Thesis Approved:

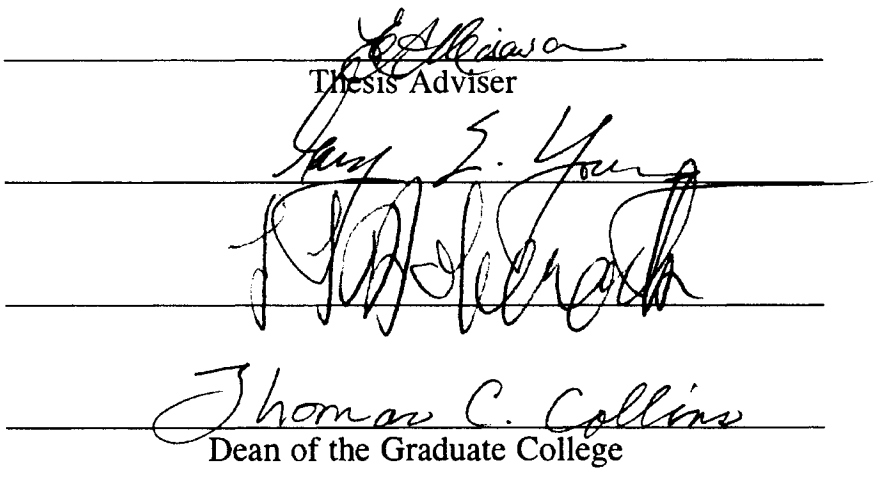

Thesis Adviser

Dean of the Graduate College

ACKNOWLEDGMENTS

I wish to express my sincere appreciation and thanks to my thesis adviser, Dr. Eduardo Misawa, for his guidance, and support throughout this graduate project. Many thanks to Dr. Gary Young, who began as my project advisor, and gave me valuable support whenever I needed. Many thanks to Dr. Larry Hoberock for serving on my committee.

Sincere thanks to my unforgettable friends May-Win, John Newton, Michael Moan, and Mike Arrington who made my staying at this School pleasurable. All of you made me feel at home.

I would like to express my deepest gratitude and admiration to my parents, Vicky and Carlos, for being my total support through every step of my education, and for being by my side whenever I needed them. Your teachings will never be forgotten.

I also want to thank the financial support provided by the Commission for Educational Exchange between United States and Peru (Fulbright Program), and the Pontificia Universidad Catolica del Peru that gave me this unique opportunity to come to USA.

Finally I want to thank the financial support given to this project from Halliburton Services and the Oklahoma Center for the Advancement of Science and Technology (OCAST).

TABLE OF CONTENTS

LIST OF TABLES

LIST OF FIGURES

NOMENCLATURE

σ_x	stress in the horizontal plane
σ_y	stress in the horizontal plane
τ_{xy}	shear stress in the horizontal plane
u_x	displacement vector
u_y	displacement vector
$w(x,t)$	maximum width of the fracture at x, at instant t
p	pressure
h	height of the fracture
υ	Poisson's ratio of rock formation
G	shear rate
q	flow rate per unit time
q_l	volume rate of fluid loss to the formation per unit length of the fracture
$A(x, t)$	cross-sectional area of the fracture
t	instant of time
$\tau(x)$	time at which the filtration starts
q_0	constant flow rate at fracture entrance
μ	Newtonian fracturing-fluid viscosity
K_l	overall fluid-loss coeficcient

$L(t)$	fracture length
p	uniformly distributed pressure applied to the fracture wall
L_0	wetted fracture lenght
K_c	critical-stress intensity factor
f_L	fraction of fracture length
Δp	net pressure
$V(t)$	volume of the fracture at instant t
V_{sp}	spurt loss
t_p	time at which pumping stops
r	radial coordinate
p_w	fluid pressure at wellbore
w	wellbore
R	fracture radius
K'	power-law consistency index
n	power-law flow behavior index
q_i	generalized coordinates
$\dot{q}_i$	time derivative of q_i
α	lumped parameter
β	lumped parameter
γ	lumped parameter
Δp_w	net pressure at the wellbore
Q	dimensionless flow rate

W	dimensionless width of the fracture
f_{LO}	dimensionless wetted fracture length
$I(f_{LO})$	dimensionless parameter
C_1	constant
$\dot{p}$	time derivativative of the pressure
C_2	constant
$\hat{P}(k)$	estimation of pressure at step k
$P(k)$	measured value of pressure at step k
$\hat{P}_N$	estimated normalized pressure
P_N	normalized pressure
q_N	normalized flow rate
t_N	normalized time
P_{max}	maximum pressure
q_{max}	maximum flow rate
t_{max}	maximum time
α_N	normalized parameter α
β_N	normalized parameter β
Δt_k	sample period
$S_{\alpha_N}^{\hat{P}_N}$	sensitivity of $\hat{P}_N$ with respect to α_N
$S_{\beta_N}^{\hat{P}_N}$	sensitivity of $\hat{P}_N$ with respect to β_N

J	cost function
$w(k)$	weighting factor
$e(k)$	error
∇J	cost function gradient
φ	regressor vector
θ	parameter vector
λ	forgetting factor

CHAPTER 1

INTRODUCTION

Generalities

The hydraulic fracturing process has been in practice since 1947, and there has been a lot of research, and success in many areas related to it. One of the most complex areas of research has always been the modeling of the fracture propagation itself. Among these models we can find the classical two-dimensional models, the three-dimensional models, and the pseudo-three dimensional models. But, in spite of all the technology available today that has made possible the development of more and more complex models, there is still uncertainty about how the fracture actually propagates.

One of the drawbacks of the current models is that they do not control the development of the fracture propagation itself as well as detecting, and correcting some related problems while the process is being performed. Most of the fracturing processes are carried out by following a given job schedule that gives the operators a short margin of freedom. All the deviations with respect to the expected propagation of the fracture are diagnosed by experts who base their decisions on what they have learned by years of practice in the field.

A basic requirement to develop a system, that takes into account all of the above, is the availability to a dynamic model that provides the time histories of both the fracture geometry and the net fracturing pressure.

Among all of the currently available models, the pseudo-3D ones are the only ones that provide these kinds of profiles but their accessibility, for public research, is restricted due to proprietary rights. This thesis shall try to make a contribution to this problem.

Scope and Contribution of this Thesis

According to what has been stated in the previous Section, we shall focus this work on the development of a dynamic model. We shall constrain this model to grow only in two-dimensions by assuming that we have a fixed height along the fracture. We shall also make use of the same premises in which the classical 2-D models such as the PKN, GdK and Radial models are based. Even though we shall use the same approach as they did, regarding the use of the fracture mechanics and fluid mechanics equations, we shall solve them under other criteria such that, at the end of this analysis, we shall have available a dynamic model.

This model shall have as a unique input the slurry rate pumped into the formation; and the predicted net Bottom Hole Pressure (BHP) as its output. It will assume a non-Newtonian fluid, and account for in-situ parameters such as the shear stress, Poisson's ratio, and fluid-loss coefficient.

We chose this pressure as the main output because it can be directly measured in the field, and, as such, provide an estimation of the accuracy of the model

The main contribution of this thesis is precisely related to this dynamic model. By working with the classical 2-D models, we developed a dynamic model that helped

to provide a fault detection scheme to detect screenout in the hydraulic fracturing process.

Overview

In this section we will show how this thesis is organized, and give a brief summary of what each chapter is about.

Chapter 2 states the problem by first defining what a hydraulic fracturing process is as well as explaining some details about the so-called screenout phenomenon. It also gives additional background to the problems that motivated this work.

Chapter 3 outlines the main characteristics of the classical 2-D models (PKN, GdK and Radial models) by giving the premises upon which they are based as well as the fundamental equations from which they were developed. We shall take some of those equations as starting points in order to develop our own models but solving them with a different approach such that we get a dynamic model. Some of the relevant features of each model are also outlined. In addition to these 2-D models, we also review some relevant characteristics of the pseudo 3-D dynamic models.

Chapter 4 shows the development of the 2-D dynamic models. It shows the fundamental equations on which they are based, and shows with some detail the steps that led to the final equations. Intensive algebra was involved in the development of these equations but we show here the intermediate steps that we consider could be useful if the reader wants to go through them as an exercise. It also states the main assumptions we took in order to develop them.

Chapter 5 shows some linear system identification techniques that we used in order to validate the proposed PKN model. We generated a pressure profile, by using the proposed PKN dynamic equation, as a test profile, and used it as a means to verify the accuracy of the estimation algorithm. Once the accuracy of the estimator was considered reasonably adequate, we applied it to field data, and modified the parameters such that we were able to distinguish the screenout fault.

Chapter 6 analyzes the results that we obtained at each step on this work as well as a perspective view of the results of this research.

Chapter 7 and 8 summarize the conclusions, and suggestions for future research.

CHAPTER 2

PROBLEM STATEMENT

According to [1]," The hydraulic fracturing process consists of blending special chemicals to make the appropriate fracturing fluid and then pumping the blended fluid into the pay zone at high enough rates and pressures to wedge and extend a fracture hydraulically. First, a neat fluid, called pad, is pumped to initiate the fracture and to establish propagation. This is followed by a slurry of fluid mixed with a propping agent (often called proppant). This slurry continues to extend the fracture and concurrently carries the proppant deeply into the fracture. After the materials are pumped, the chemical breaks back to a lower viscosity and flows back out of the well, leaving a highly conductive propped fracture for oil and/or gas to flow easily from the extremities of the formation into the well". The process is depicted in Fig. 2.1.

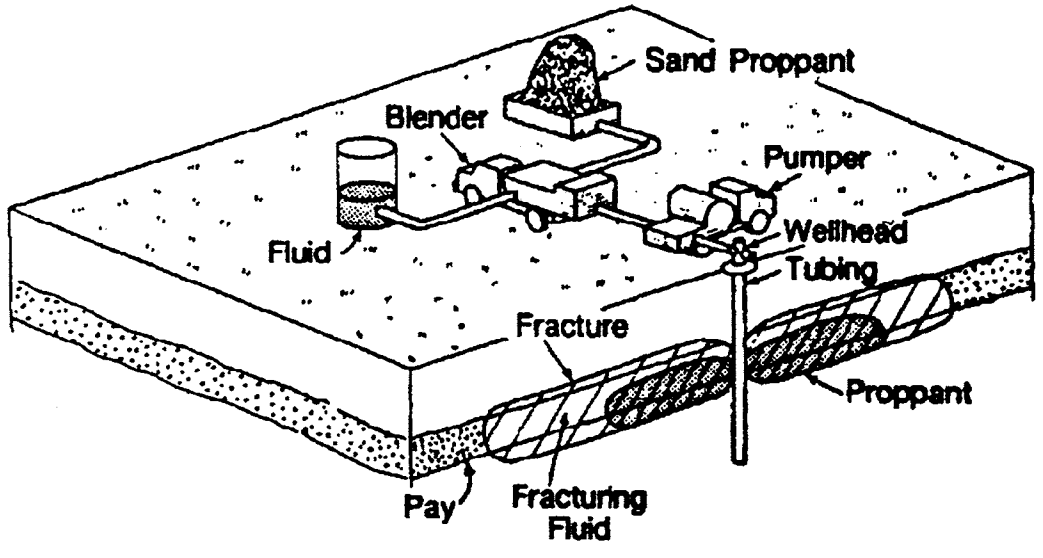

Fig. 2.1- The Fracturing Process. [1]

Even though the fracturing process was introduced in 1947, and has now become a standard procedure, there are still some uncertainties to be solved in spite of the high rate of success observed. One major problem encountered in this process is the so called screenout phenomenon.

In the course of fracturing treatment, sometimes, the pressure needed to keep pumping the fluid into the fracture exceeds the limitations of the injection well conduit, wellhead equipment, or pumping units. This condition is referred to as screenout [2]. When this condition is reached, the process has to be stopped. Screenouts usually occur because of some restrictions of the fluid flow that increase the frictional-pressure drop. Fig. 2.2. gives a graphic representation of the problem.

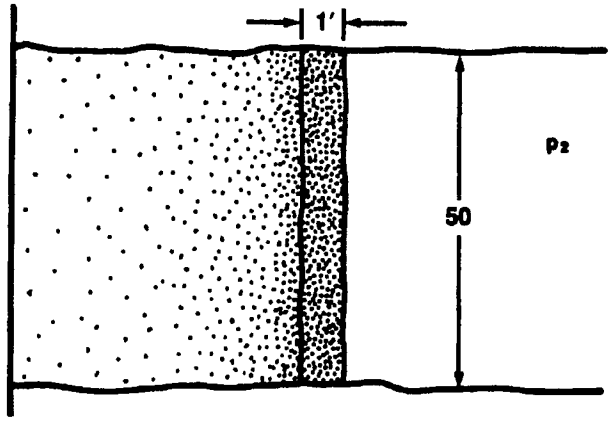

Fig. 2.2. Schematic of proppant blockage inside a hydraulic fracture. [2]

Rock mechanics and fracture mechanics play an important role in the study of this complex process. Among some of the factors that have been identified for the theoretical analysis, we have the variations of in-situ stresses existing in different layers of the rock, variations in mechanical rock properties (elastic modulus, Poisson's ratio),

fracturing fluid's viscosity, fluid loss parameters, fluid pressure gradients, geometry of the fracture, etc. Some of these in-situ variables, such as the geometry and the permeability of the fracture, are not possible to measure directly in the field at the current state of the technology. Many attempts have been made to overcome this problem by making different assumptions that have led to different models. The models have evolved from the very primitive Carter-type models (that completely ignored the rock mechanics), going through the ones with known heights (PKN, GdK, and Radial models) [3], also known as the 2-D models, until the most recent ones that take advantage of more computer power such as the 3-D models [16] [17]. However, experience leads us to believe that there is still a difference between the predicted geometries and the actual ones in the field. Fig. 2.3 depicts this situation.

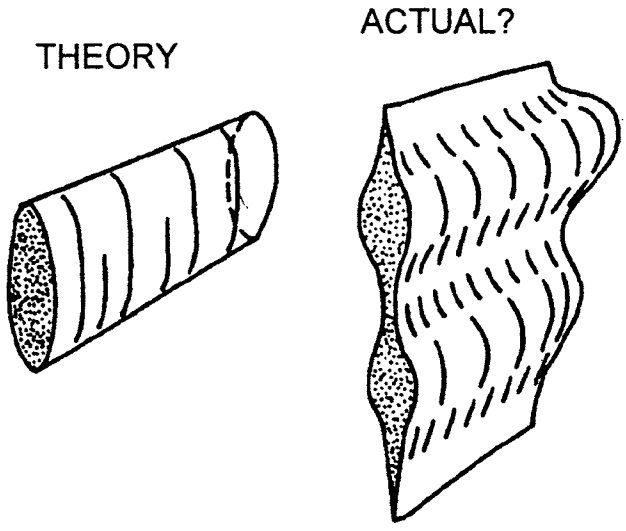

Fig. 1.3. Theoretical fracture-propagation models vs. possible actual in-situ behavior. [1]

The aim of any model is to predict the geometry of the fracture (length, width, and height). The early models assumed some geometry (by assuming the shape and the height for example). The latest ones, such as the 3-D, do not make any geometrical assumption, and solve the problem by using the finite elements technique.

Even though the aim of any model is to predict the geometry of the fracture, it would also be useful if the model could give some insights about the process itself such as the ability to predict screenout on-the-fly.

Taking all these factors into account, the aim of this work is the developing of a fault detection algorithm that will allow to detect screenout. But, in order to do so, we need to rely on a physically based model that could provide some insight about the process itself, and that will be the first problem to be solved in this work, followed by the fault detection itself.

CHAPTER 3

TWO-DIMENSIONAL FRACTURE PROPAGATION MODELS

Overview

In order to estimate the resultant geometry of a hydraulic process two different disciplines must be combined: fluid mechanics, and fracture mechanics. The role of fluid mechanics is to establish the pressure distribution inside the fracture, and the role of fracture mechanics is to establish the resultant shape of the fracture. However, in the case of the 2-D models, the fracture boundary in the plane of propagation is specified in advance. All these models are based on the assumption that the fracture deforms in a linear elastic manner.

In addition to that we have the compatibility condition that states that the fracture geometry and the pressure distribution creating it must be such that each one of them will produce the other one. However this condition is extremely hard to verify, and one must usually assume a pressure distribution, calculate the fracture opening resulting from it, and assume that the compatibility condition is met [4].

In this chapter we shall show the corresponding relations of the width, the length or radius of the pre-defined fracture geometries for the 2-D models such as the PKN, GdK, and Radial models. For details, consult the original papers [5], [6], and [7].

We shall assume a Newtonian fluid for the three cases for the sake of clearness. Similar results can be obtained for non-Newtonian fluids by incorporating the so-called power-law into the same analysis.

The PKN Model

This model (Fig. 3.1) was developed based on the premises published by Sneddon [8] which later Nordgren [7] used to compute the fracture length and width, at any value of time during the process, by solving a numerical differential equation. The assumptions under which this model is valid are [2]

- The fracture has a constant height, h, independent of fracture length.
- The fracturing fluid pressure, p, is constant in vertical cross sections perpendicular to the direction of the propagation, and it equals the rock stress perpendicular to the fracture plane, σ_H, at the tip of the fracture.
- Each vertical cross section deforms individually and is not affected by its neighbors.
- The injection rate into the fracture, q_0, is constant.

In [8] Sneddon considered the distribution of stress in the interior of an infinite two-dimensional elastic medium when a very thin internal crack $-h \le y \le h$, $x=0$ (Fig. 3.1) is opened under the action of a pressure which was considered to vary in magnitude along the length of the crack. He considered the stress in that medium described by three components of stress σ_x, σ_y and τ_{xy}. The corresponding components of the displacement vector were denoted by u_x and u_y. Under these conditions, the differential equations determining the stress components are

$$\frac{\partial \sigma_x}{\partial x} + \frac{\partial \tau_{xy}}{\partial y} = 0 \qquad (3.1)$$

$$\frac{\partial \tau_{xy}}{\partial x} + \frac{\partial \sigma_y}{\partial y} = 0 \qquad (3.2)$$

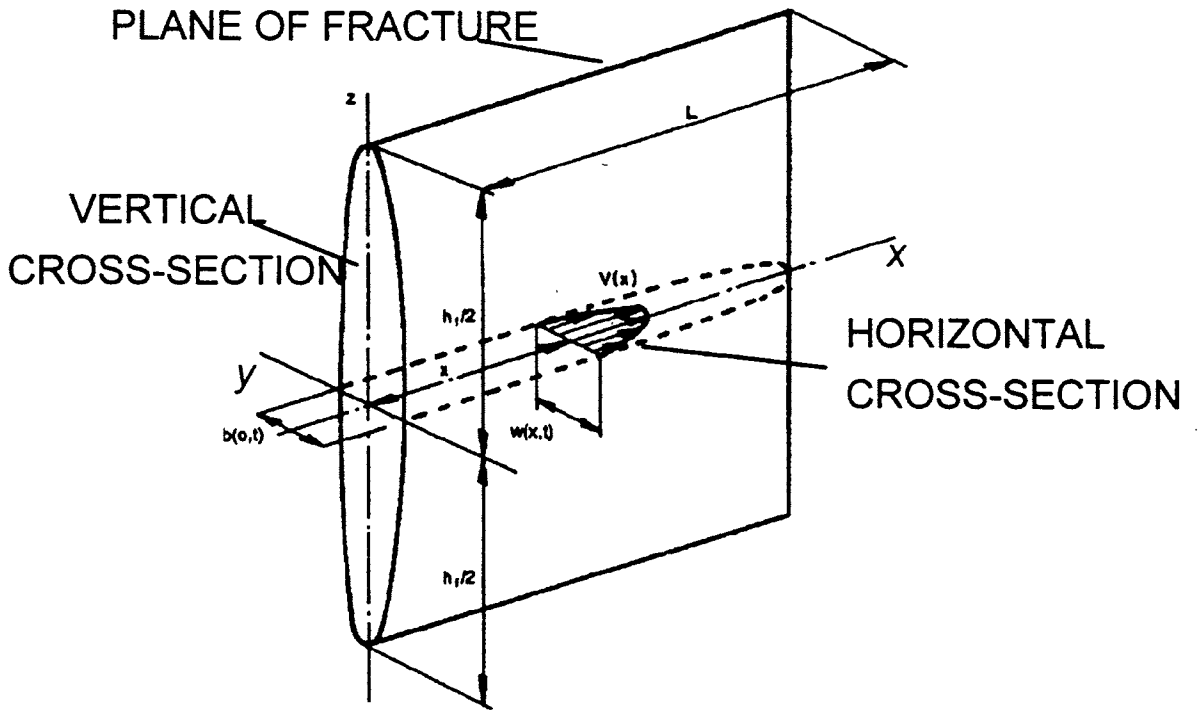

Fig. 3.1 Schematic representation of the PKN model. [2]

The boundary conditions to be satisfied are that all the components of stress and of the displacement vector must tend to zero as x^2+y^2 tends to infinity, and that

(i) $\tau_{xy}= 0$, for all values of y,

(ii) $\sigma_x= - p(y)$, $|y| \leq h$,

$u_x= 0$, $|y| \leq h$

For the case of a uniform pressure, p, along the vertical section of the fracture, Sneddon solves this partial differential equations and finds,

$$w(x,t) = \frac{(1- \upsilon)(p(x,t)-\sigma_H)}{G} \sqrt{h^2 - y^2} \qquad (3.3)$$

where $w(x,t)$ is the maximum width of the fracture at the distance x from the wellbore at instant t; υ is the Poisson's ratio; σ_H is the in-situ minimum stress, and G is the shear rate.

The Eq. 3.3 represents the fracture mechanics of the process, and must be solved simultaneously with fluid mechanics. In order to do that Daneshy [2] uses it in combination with the local-continuity equation

$$\frac{\partial q(x,t)}{\partial x} + q_l(x,t) + \frac{\partial A(x,t)}{\partial t} = 0 \tag{3.4}$$

where $q(x,t)$ represents the flow rate (volume per unit time) through a cross section; $q_l(x,t)$ is the volume rate of fluid loss to the formation per unit length of fracture, and $A(x,t)$ is the vertical cross-sectional area of the fracture (elliptical). They are given by

$$A(x,t) = \frac{\pi h}{4} w(x,t) \tag{3.5}$$

$$q_l(x,t) = \frac{2hK_l}{\sqrt{t-\tau(x)}} \tag{3.6}$$

where K_l represents the overall fluid-loss coefficient as measured in laboratory tests and $\tau(x)$ represents the time at which the filtration starts.

The Eq. 3.6 represents the fluid-loss into the formation as proposed by Carter [2]. In his theory, he assumes that the fluid is flowing in a rectangular slit of constant height and width as well as a constant flow rate. Only the fracture length, $L(t)$, is assumed to be variable. Even though Carter's assumptions differ from those assumed for this and other models, it has been found to give a good approximation for the fluid-loss into the formation.

These equations are combined with the fluid pressure gradient in the propagating or x direction, determined by the flow resistance in a narrow, elliptical flow channel. For Newtonian flow behavior we have,

$$\frac{\partial p(x,t)}{\partial x} = -\frac{64}{\pi}\frac{q_0\mu}{w^3(x,t)h} \tag{3.7}$$

Combining the above equations we get the partial differential equation $w(x,t)$,

$$\frac{G}{64(1-\upsilon)h\mu}\frac{\partial^2 w^4}{\partial x^2} - \frac{\partial w}{\partial t} - \frac{8K_I}{\pi\sqrt{t-\tau(x)}} = 0 \tag{3.8}$$

where $\tau[L(t')]= t'$, for $0<t'<t$, and subject to initial conditions

$$w(x,0)=0$$

and boundary conditions

$$w(x,t)=0,\ x>L$$

and

$$-\frac{\partial w^4(0,t)}{\partial x} = \frac{256\mu(1-\upsilon)q_0}{\pi G}$$

for a one sided fracture. A numerical solution for this set of equations was proposed by Nordgren [7].

The major characteristic of this model is that it predicts an increase in fracture length with an increase in the treatment pressure. This model has been found to give good results for long duration treatments when long fractures are obtained but gives narrower fractures than the ones observed in the field [2].

The GdK Model

This model (Fig. 3.2) was developed based on the premises published by Khristianovic and Zheltov [9], and the so-called equilibrium condition proposed by

Barenblatt [10]. Geertsma and de Klerk combined them later in [6]. The assumptions under which this model is valid are [2]

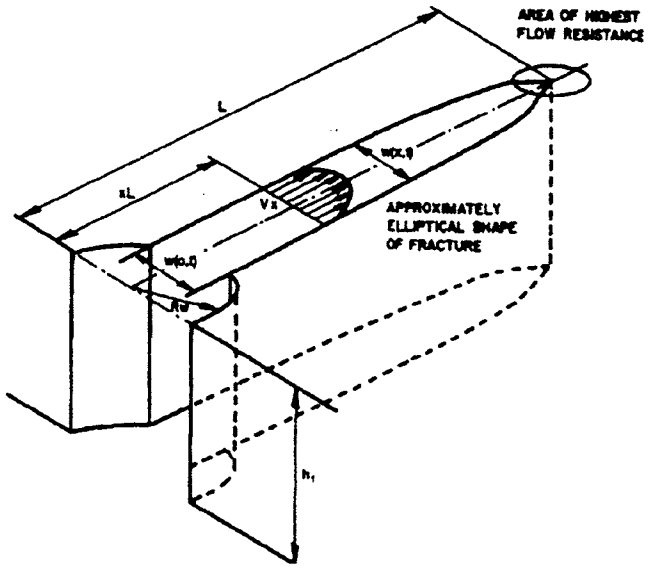

Fig. 3.2 Schematic representation of the GdK model. [2]

- The height of the fracture, h, is fixed.
- The width of the fracture, $w(x,t)$, is constant in the vertical direction.
- The injection rate into the fracture, q_0, is constant.
- The fluid pressure gradient in the propagating direction is calculated by [3],

$$p(0,t) - p(x,t) = \frac{12\mu q_0}{h} \int_0^x \frac{du}{w^3(u,t)} \tag{3.9}$$

The main difference of this model with respect to the PKN model is that it assumes an approximately constant distribution of pressure applied to most of the fracture wall. The main pressure-fall along the fracture occurs in a comparatively narrow zone near the tip of the fracture [9]. This is the condition established by the fracture mechanics. Therefore the pressure distribution in the fracture can be taken as follows,

$$p(f_L,t) = \overline{p(t)} \text{ for } 0 \le f_L \le f_{L_0} \tag{3.10}$$

$$p(f_L,t) = 0 \text{ for } f_{L_0} < f_L \le 1$$

where L_0 is the length of the wetted fracture with $f_{L0} = L_0/L$ close to unity. With this pressure distribution, the Barenblatt's condition establishes that,

$$f_{L_0} = \frac{L_0}{L} = \sin\left(\frac{\pi}{2}\,\frac{\sigma_H}{p} + \frac{K_c}{p\sqrt{L}}\right) \tag{3.11}$$

where K_c is the critical stress-intensity factor.

With the exception of the tip of the fracture, where Barenblatt's condition has to be verified, the shape of the fracture in the horizontal plane is elliptical, and it reaches its maximum value at the wellbore. Geertsma [2] showed a general expression for the width of the fracture,

$$w(x,t) = \frac{4(1-\upsilon)}{\pi G} L(t) \int_{\frac{x}{L}}^{1} \frac{f_{L2}\,df_{L2}}{\sqrt{f_{L2}^{\,2} - L(t)^2}} \int_0^{f_{L2}} \frac{\Delta p(f_{L1})\,df_{L1}}{\sqrt{u^2 - f_{L1}^{\,2}}} \tag{3.12}$$

where f_{L1}, and f_{L2} are all fractions of fracture length, and

$$\Delta p(f_{L1}) = p(f_{L1}) - \sigma_H(f_{L1}) \tag{3.13}$$

Now, by taking the pressure distribution established by Eq. 3.10, we get an expression for the fracture width [2] at any position x and instant t

$$w(x,t) = \frac{2(1-\upsilon)}{G} L(t)(\overline{p(t)} - \sigma_H)\sqrt{1 - \left(\frac{x}{L(t)}\right)^2} \tag{3.14}$$

The Eq. 3.14, that represents the fracture mechanics for the GdK model, is now solved simultaneously with the mass balance equation,

$$\frac{dV(t)}{dt} = q_0 - q_l(t) - 2V_{sp}h\frac{dL}{dt} \tag{3.15}$$

where $V(t)$ is the total volume of the fracture, q_l is the total fluid-loss into the formation, and V_{sp} is the spurt loss.

The total volume of the fracture, V, is evaluated taking into account the elliptical shape of the fracture in the horizontal cross sections,

$$V(t) = \frac{\pi}{4} hw(0,t)L(t) \tag{3.16}$$

The total fluid-loss is then evaluated according to,

$$q_l(t) = 2K_l h\int_0^t \frac{dL}{dt}\frac{d\tau}{\sqrt{t-\tau}} \tag{3.17}$$

This set of equations is solved [2] for the length, L, and the maximum width, w, of the fracture at the end of the process when the pumps are shut down,

$$L = \frac{q_0}{16\pi hK_l^2}[\pi w(0,t_p) + 8V_{sp}](\frac{2\alpha_L}{\sqrt{\pi}} - 1 + e^{\alpha_L^2}\text{erfc}\,\alpha_L) \tag{3.18}$$

$$w(0,t_p) = 2.27[\frac{(1-\upsilon)\mu q_0 L^2}{Gh}]^{\frac{1}{4}} \tag{3.19}$$

with

$$\alpha_L = \frac{8K_l\sqrt{\pi t}}{\pi w(0,t_p) + 8V_{sp}} \tag{3.20}$$

and t_p represents the time when the pumps stop.

The outstanding characteristic of this model is that it predicts an increase in fracture length with a decrease in the treatment pressure. On the other hand, this model

predicts relatively larger fracture widths than the ones predicted by the PKN model that seem to be closer to reality in many field cases [2].

The Radial Model

As it is the case of linear propagation for the GdK model, the situation near the tip of the fracture is essentially the same for the radial case, depicted in Fig. 3.3. We have an approximately constant distribution of pressure along the fracture, with a smooth closing region of low pressure near the tip of the fracture. The considerations here are:

- The height of the fracture, h, is fixed.
- The width of the fracture, $w(r,t)$, is constant in the vertical direction.
- The injection rate into the fracture, q_0, is constant.
- The fluid pressure gradient in the propagating direction is calculated by [3],

$$p(r,t) = p_w(t) - \frac{6\mu q_0}{\pi \bar{w}^3(r,t)} \ln \frac{r}{R_w} \tag{3.21}$$

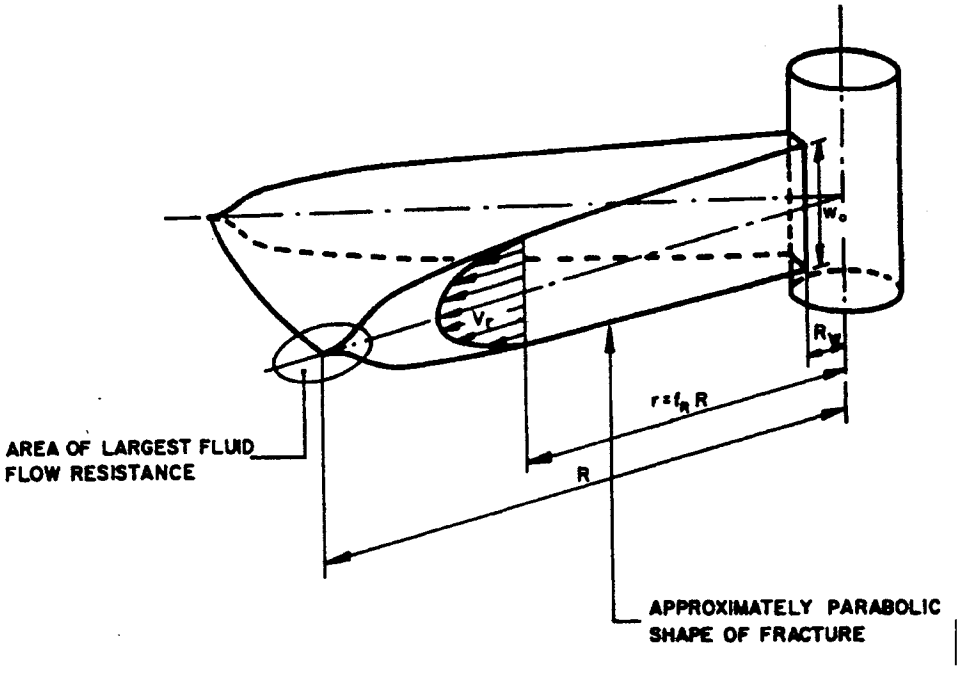

Fig. 3.3 Schematic representation of the Radial model. [2]

where $\bar{w}$ represents the average width of the propagating fracture, R_w the wellbore radius, and p_w the wellbore net pressure.

The Barenblatt's equilibrium condition is expressed in this case as

$$\int_{R_w}^{1} \frac{\rho p(\rho) d\rho}{\sqrt{(1-\rho^2)}} = \sigma_H \tag{3.22}$$

where $\rho = r/R$.

Applying the mass balance equation to this model (Eq. 3.15), the Carter's equation for fluid-loss (Eq. 3.17), and the total volume of the fracture as,

$$V(t) = \frac{8\pi}{15} w_w(t) R^2(t) \tag{3.23}$$

provided that $R_W/R << 1$, the solution of this set of equations is [9]

$$w(0) \sim 2.15[\frac{\mu q_0 R(1-\upsilon)}{G}]^{\frac{1}{4}} \tag{3.24}$$

$$\alpha_r = \frac{15K_I\sqrt{\pi t}}{4w(0,t_p)+15V_{sp}} \tag{3.25}$$

$$R^2 = \frac{q_0}{30\pi^2 K_I^2}[4w(0,t_p)+15V_{sp}](\frac{2\alpha_r}{\sqrt{\pi}} - 1 + e^{\alpha_r^2}\text{erfc}\,\alpha_r) \tag{3.26}$$

where Eq. 3.24 is taken as an approximation for $w(0, t_p)$.

This model seems most applicable only for the early stages of fracture growth, *i.e*, for small values of t, and, as in the case of the GdK model, it predicts wider fractures than the PKN model [2].

Effect of non-Newtonian Fluids

Throughout these models, the authors have assumed Newtonian fluids in the fracturing process, and this is one of the main drawbacks of these models. We have to take into account that most of the fracturing fluids used today exhibit a non-Newtonian behavior, and, as such, we need to develop models that take this factor into account in order to have a more accurate representation of this process.

These non-Newtonian fluids can be characterized by different models [11]. The most popular among them is the so-called power-law that replaces the Newton's one-parameter (viscosity) fluid law with a two-parameter relation, *i.e.*, the power-law consistency index and the power-law behavior index, that still allows adequate manipulation of the equations. Depending on the assumed geometry in which the fluid flows, we have a different equation that relates the fluid pressure gradient with the fluid flow rate [12]. The equation for the power-law fluid is given by

$$\tau = K' \dot{\gamma}^{n} \tag{3.27}$$

where τ is the shear stress (lbf/ft^2), K' is the power-law consistency index ($lbf\text{-}sec^n/ft^2$), n is the power-law index and $\dot{\gamma}$ is the shear rate (sec^{-1}).

The Pseudo 3-D Models

These models were developed from the PKN and GdK models by removing the restriction of constant fracture height. They calculate fracture width as a function of position and pressure, and apply a fracture propagation criterion to length and height.

These models can be classified in two categories: [16] (1) models that divide the fracture along its length into "cells" and use local cell geometry to relate fracture opening with fluid pressure and (2) models that use a parametric representation of the total fracture geometry. The following is a brief description [16] of the currently available pseudo 3-D dynamic models.

RES (FRACPRO). [16] It uses measured values of flow rate, proppant concentration, and fluid rheology parameters to calculate the time history of the pressure drop down at a wellbore of variable deviation and diameter. The time history of the fracture growth is also calculated.

Chevron 2D Fracturing Simulator. [16] This model can predict the propagation of constant-height, hydraulically induced, vertical fractures for a power-law fluid. It calculates mass flux, fracture width, pressure, and length as functions of time. It is based on the PKN and the GdK models.

MFRAC-II. [16] This model calculates fracture length, upper and lower heights, width, net pressure, fluid efficiency, and geometry parameters as functions of time. It also includes options for the GdK and PKN models.

Summary

In this chapter we have briefly outlined the different relations of the 2-D models. They have given us an idea of the different assumptions in which they are based upon as well as the different approaches taken in order to solve the corresponding fracture and rock mechanics relations.

In the case of the PKN model, Eq. 3.8 provides a solution for the width of the fracture at any given position and instant of time. For the GdK model, Eq. 3.18 provides an estimate of the fracture length by the time the pumps are shut down as well as an estimation for the width of the fracture. Also, in the case of the Radial model, Eq. 3.26 provides an estimate for the radius of the fracture after the pumps are shut down but it must make use of an approximation (Eq. 3.24).

Note here that the authors made different assumptions in order to solve the complex relations existing in this process, and some of them looked at first sight incompatible with the original assumptions. A clear example of this is given by the Carter's equation (Eq. 3.6) which was developed based on the assumption that the fluid flows in a rectangular slit of constant height and width as well as constant flow rate. This assumption is contrary to the different assumed geometries in each model. However, in the absence of other relations and by the fact that it has been giving satisfactory results, it is still in use even with more complicated models such as the 3-D ones.

All the different equations that we have shown so far provide estimates for the geometry of the fracture (length, width or radius). But even if a given geometry is the main goal in hydraulic fracturing, they are useless in monitoring the process because

there is no cost effective way to monitor them on the fly at the current state of the technology.

The main variable that is used in the field to monitor the process as well as to detect screenout is the Bottom Hole Pressure. This variable, measured continuously during the whole process, can provide feedback in monitoring indirectly the development of the fracture geometry. However, none of the equations developed in the previous models showed a direct relation to this parameter. This fact brings up the need to obtain a new set of equations that could provide us a direct estimation of the pressure at any instant of time, *i.e.*, a dynamic model.

The following chapter will focus on the development of this "new model" but it shall be based on the same considerations as the ones outlined above. However, additional assumptions shall be made in order to convert the partial differential equations into control-type equations (dynamic models).

CHAPTER 4

SIMPLIFIED DYNAMIC 2-D MODELS

Overview

A dynamic model for the hydraulic process is indispensable to relate the injection rate, time of treatment, fluid coefficients, and rock mechanics parameters with the Bottom Hole Pressure (BHP). Together, they can provide information about the development of the fracture as well as helping to control the process via analysis of the pressure.

In order to get sufficient and reliable information from these new models, physically based equations should be studied, and as such, the classical 2-D models were chosen to provide those fundamental relations.

As we have seen in the previous chapter, the classical 2-D models provide three different approaches for the same process. Taking this fact into account, we will develop a different dynamic model corresponding to each one of them.

The aim of this chapter shall be to transform the partial differential equations that combine the solid/fluid mechanics relations into ordinary dynamic differential equations, having the pressure as their output. Additional assumptions shall be made in order to do these transformations. We shall show these assumptions throughout this chapter.

The Dynamic PKN Model

The same assumptions outlined in the previous chapter shall be considered in order to develop this dynamic model. However, additional considerations are made in order to gain some generality such as taking into account:

- A variable input flow rate into the fracture, and
- The use of a non-Newtonian fracturing fluid.

The equations that shall be considered are the fracture mechanics equation for the maximum width of the fracture, the local-continuity equation, the cross-sectional area equation of the fracture, and the Carter's equation as they follow

$$w(x,t)\big|_{y=0} = \frac{(1-\upsilon)\Delta p(x,t)}{G} h \tag{3.3}$$

$$\frac{\partial q(x,t)}{\partial x} + q_l(x,t) + \frac{\partial A(x,t)}{\partial t} = 0 \tag{3.4}$$

$$A(x,t) = \frac{\pi h}{4} w(x,t) \tag{3.5}$$

$$q_l(x,t) = \frac{2hK_l}{\sqrt{t-\tau(x)}} \tag{3.6}$$

where $\Delta p(x,t) = p(x,t) - \sigma_H$ is the net pressure acting on the fracture. For the sake of simplicity we have not taken into account the spurt loss volume in the local-continuity equation. On the other hand, we shall approximate $\tau(x)$ by

$$\tau(x) = \frac{t}{L(t)} x \tag{4.1}$$

The fluid pressure gradient inside the fracture will be now calculated for a laminar flow of a power-law fluid between parallel plates according to [12]

$$\frac{\partial \Delta p(x,t)}{\partial x} = -\frac{2K'}{h^n}\left(\frac{4n+2}{n}\right)^n \frac{q(x,t)^n}{w(x,t)^{2n+1}}. \tag{4.2}$$

where K' is the power-law consistency index, and n is the power-law behavior index for a non-Newtonian fluid.

Combining the above equations into the local-continuity equation (Eq. 3.4) we get

$$\frac{\partial q(x,t)}{\partial x} = -\frac{2hK_l}{\sqrt{t-\frac{t}{L}x}} - \left[\frac{\pi h^2(1-\upsilon)}{4G}\right]\frac{\partial \Delta p(x,t)}{\partial t} \tag{4.3}$$

with the boundary conditions

$$q(0,t) = q_i(t)$$

$$q(x,t) = 0, \quad x \geq L(t)$$

where $q_i(t)$ is the variable input flow rate, and

$$\Delta p(x,t) = 0, \quad x \geq L(t)$$

In order to solve Eq. 4.3, we shall assume a linear, time-variant pressure distribution along the fracture. In addition to that, we shall consider that the rate of change of the net pressure, with respect to time, is the same at any point x along the fracture. The following two equations summarize these assumptions:

$$\frac{\partial \Delta p(x,t)}{\partial x} = -\frac{\Delta p(0,t)}{L(t)} = -\frac{\Delta p(t)}{L(t)} \tag{4.4}$$

$$\frac{\partial}{\partial x}\left[\frac{\partial \Delta p(x,t)}{\partial t}\right] = 0 \tag{4.5}$$

Now integrating Eq. 4.3 from $x = 0$ to $x = L(t)$, and taking into account the boundary conditions for $q(x,t)$, and Eq. 4.5, we get

$$q_i(t) = \frac{4hK_I}{\sqrt{t}} L(t) + \frac{\pi h^2 (1-\nu)}{4G} L(t) \frac{\partial \Delta p(x,t)}{\partial t} \tag{4.6}$$

In Eq. 4.6, two terms are still unknown. The first one is the length, $L(t)$, of the fracture, and the second one is the rate of change of the pressure with respect to time at any point x along the fracture. Now we shall proceed to obtain the corresponding expressions for both of them.

First of all, in order to obtain the length of the fracture, $L(t)$, we shall substitute Eqs. 3.3 and 3.4 into Eq. 4.2. Then, we shall evaluate the remaining expression at x=0, and from that, the fracture length can be expressed in terms of the input flow rate, the net BHP and the remaining known parameters as follows

$$L(t) = \left[\frac{n}{4n+2}\right]^n \frac{(1-\upsilon)^{2n+1}}{G^{2n+1}} \frac{h^{3n+1}}{2K'} \frac{\Delta p^{2(n+1)}}{q_i(t)^n} \tag{4.7}$$

Now, regarding the rate of change of the net pressure, with respect to time, along the fracture, we have to take into account Eq. 4.5 that implies that this rate is independent of the fracture position. Therefore we can assume that it changes in the same fashion as the change in time of the net BHP, $\Delta p(0,t)$, according to

$$\frac{\partial \Delta p(x,t)}{\partial t} = \frac{\partial \Delta p(0,t)}{\partial t} = \dot{\Delta p} \tag{4.8}$$

Finally, substituting Eqs. 4.7 and 4.8 into Eq. 4.6, we are able to solve for the net BHP as follows

$$\dot{\Delta p} = \alpha \frac{q_i(t)^{n+1}}{\Delta p^{2(n+1)}} - \beta \frac{1}{\sqrt{t}} \tag{4.9}$$

with the lumped parameters α and β as follow

$$\alpha = \frac{16K'}{\pi}\left[\frac{4n+2}{n}\right]^{n}\left[\frac{G^2}{h^3(1-\upsilon)^2}\right]^{n+1} \tag{4.10}$$

$$\beta = \frac{8GK_l}{\pi h(1-\upsilon)} \tag{4.11}$$

The resulting Eq. 4.9 is a nonlinear, time-variant, ordinary differential equation for the net BHP, Δp and it is linear in its parameters α and β. This equation represents a simplified model of the PKN process, and by no means pretends to provide more accurate results than the original model equation. However it shall facilitate the analysis of the process from the fault detection point of view as we shall see later.

The Dynamic GdK Model

The development of this dynamic model shall be based on the same premises as the ones outlined in Chapter 3. As it was the was for the dynamic PKN model, the following are the additional considerations for this case:

- A variable input flow rate into the fracture, and
- A non-Newtonian fracturing fluid is considered.

In order to develop this dynamic model a different approach will be used with respect to the one outlined in Chapter 3. We shall use the local-continuity equation instead of the mass balance equation so as to solve simultaneously the solid/fluid mechanics equations.

Now, if we express the Eq. 4.2 in terms of the partial fracture length, $f_L = x/L$, we obtain

$$\frac{\partial \Delta p(f_L,t)}{\partial f_L} = -\frac{2K'}{h^n}\left[\frac{4n+2}{n}\right]^n L(t)\frac{q(f_L,t)^n}{w(f_L,t)^{2n+1}} \tag{4.12}$$

Integrating Eq. 4.12 from f_L= 0 to f_L we have

$$\Delta p_w(t) - \Delta p(f_L,t) = \frac{2K' L(t)}{h^n}\left[\frac{4n+2}{n}\right]^n \frac{q(0,t)^n}{w(0,t)^{2n+1}} \int_0^{f_L} \frac{Q(u,t)^n}{W(u,t)^{2n+1}} du \tag{4.13}$$

where $0 \le f_L \le f_{L0}$, and f_{L0} representing the fraction of the wetted fracture length, with f_{L0} close to unity, and

$$Q(u,t) = \frac{q(u,t)}{q(0,t)}$$

$$W(u,t) = \frac{w(u,t)}{w(0,t)}$$

In Eq. 4.13, if we let $f_L = f_{L0}$, we get $\Delta p(f_{L0},t)=0$, and obtain an expression for the net Bottom Hole Pressure

$$\Delta p_w(t) = \frac{2K' L(t)}{h^n}\left[\frac{4n+2}{n}\right]^n \frac{q(0,t)^n}{w(0,t)^{2n+1}} \int_0^{f_{L0}} \frac{Q(u,t)^n}{W(u,t)^{2n+1}} du \tag{4.14}$$

Dividing Eq. 4.13 by Eq. 4.14, taking the derivative with respect to f_L, and evaluating the resulting equation at f_L=0, we get

$$\frac{\partial \Delta p(f_L,t)}{\partial f_L} = \frac{\partial p(f_L,t)}{\partial f_L} = -\frac{\Delta p_w(t)}{I(f_{L0})} \tag{4.15}$$

where

$$I(f_{L0}) = \int_0^{f_{L0}} \frac{Q(u,t)^n}{W(u,t)^{2n+1}} du$$

represents a constant expression given the value of f_{L0}. Therefore the gradient of the pressure along the fracture follows a linear distribution that depends only in the net BHP. Now substituting Eq. 4.15 into Eq. 4.12, and evaluating the resulting expression at $f_L = 0$

$$\frac{\Delta p_w(t)}{I(f_{L0})} = -\frac{2K'}{h^n}\left[\frac{4n+2}{n}\right]^n L(t)\frac{q(0,t)^n}{w(0,t)^{2n+1}} \tag{4.16}$$

In Eq. 4.16, recall that $q(0,t)=q_i(t)$, and that $w(0,t)$ is given by Eq. 3.14. Therefore, substituting these relations into the above equation, we get an estimation for the fracture length as follows

$$L(t) = \left[\frac{I(f_{L0})K'}{2^{2n}h^n}\left[\frac{4n+2}{n}\right]^n\left(\frac{G}{1-\upsilon}\right)^{2n+1}\frac{q_i(t)^n}{\Delta p_w(t)(\overline{p(t)}-\sigma_H)^{2n+1}}\right]^{\frac{1}{2n}} \tag{4.17}$$

Eq. 4.17 provides the length of the fracture in terms of the process parameters, the input flow rate, the net BHP as well as the assumed, statistically equivalent, constant pressure in the fracture. The problem here is that we have two pressures that we have to deal with and, in the field, we only measure one so we shall make use of the approximation proposed by Geertsma [6] that assumes that

$$\Delta p_w(t) = \overline{p(t)} - \sigma_H$$

simplifying the final expression for the fracture length as follows

$$L(t) = C_1\frac{\sqrt{q_i(t)}}{(\overline{p(t)}-\sigma_H)^{\frac{n+1}{n}}} \tag{4.18}$$

with

$$C_1 = \left[\frac{I(f_{L0})K'}{2^{2n}h^n}\left(\frac{4n+2}{n}\right)^n\left(\frac{G}{1-\upsilon}\right)^{2n+1}\right]^{\frac{1}{n}}$$

Now, by substituting Eq. 4.18 into Eq. 3.14, we get an equation for the width of the fracture in terms of variable the input flow rate

$$w(x,t) = \frac{2C_1(1-\upsilon)}{G} \frac{\sqrt{q_i(t)}}{(\overline{p(t)} - \sigma_H)^{\frac{1}{n}}} \sqrt{1-(\frac{x}{L(t)^2})} \tag{4.19}$$

The Eqs. 4.18 and 4.19 provide expressions to evaluate the length, and the width of the fracture if the pressure is known (the input flow rate is considered a known parameter). A dynamic equation of this pressure shall be found by combining these equations with the ones provided by the fluid mechanics. Recall that the local-continuity equation is given as follows

$$\frac{\partial q(x,t)}{\partial x} + q_i(x,t) + \frac{\partial A(x,t)}{\partial t} = 0 \tag{3.4}$$

In order to transform the local-continuity equation into an ordinary differential equation for the pressure, we shall integrate it along the fracture length. But, before doing that, we shall find an equivalent expression for the rate of change of the crossectional area $A(x,t)$ that is now given by

$$A(x,t) = hw(x,t) \tag{4.20}$$

Now, by substituting Eq. 4.19 into Eq. 4.20, we can express the third term of the local-continuity equation as

$$\frac{\partial A(t)}{\partial t} = F(x) + G(x) + H(x) \tag{4.21}$$

where

$$F(x) = -\frac{2hC_1(1-\upsilon)\sqrt{q_i(t)}}{nG} \frac{\dot{\bar{p}}}{(\bar{p} - \sigma_H)^{\frac{n+1}{n}}} \sqrt{1-(\frac{x}{L(t)})^2}$$

$$G(x) = \frac{2hC_1(1-\upsilon)\sqrt{q_i(t)}}{GL(t)^3(\bar{p}-\sigma_H)^{\frac{1}{n}}} \frac{\dot{L}(t)x^2}{\sqrt{1-(\frac{x}{L(t)})^2}}$$

$$H(x) = \frac{2hC_1(1-\upsilon)}{G} \frac{\dot{q_i}(t)}{2\sqrt{q_i(t)}} \frac{1}{(\bar{p}-\sigma_H)^{\frac{1}{n}}} \sqrt{1-(\frac{x}{L(t)})^2}$$

On the other hand, recall that Carter's equation is expressed as

$$q_i(x,t) = \frac{2hK_l}{\sqrt{t-\tau(x)}} \tag{3.6}$$

with

$$q(0,t) = q_i(t)$$

$$q(x,t) = 0, \quad x \geq L(t)$$

where $q_i(t)$ is the variable input flow rate. Now substituting Eqs. 4.21, and 3.6 into the local-continuity equation (Eq. 3.4), and then integrating the resulting equation from x=0 to x=$L(t)$, we get

$$-q_i + \frac{4hK_lL(t)}{\sqrt{t}} - \frac{\pi hC_1(1-\upsilon)\sqrt{q_i(t)}L(t)\dot{\bar{p}}}{2nG(\bar{p}-\sigma_H)^{\frac{n+1}{n}}} + \frac{\pi hC_1(1-\upsilon)\sqrt{q_i}\dot{L}(t)}{2G(\bar{p}-\sigma_H)^{\frac{1}{n}}} + \frac{\pi hC_1(1-\upsilon)\dot{q_i}L(t)}{4G(\bar{p}-\sigma_H)^{\frac{1}{n}}\sqrt{q_i}} = 0 \tag{4.22}$$

an expression that is independent of x.

We now need to replace $L(t)$ and its derivative in Eq. 4.22 in order to have an ordinary differential equation for the pressure. Therefore, substituting Eq. 4.18, and its derivative, into Eq. 4.22, and solving for the pressure, we get

$$\dot{\bar{p}} = -\alpha(\bar{p}-\sigma_H)^{\frac{2(n+1)}{n}} + \beta\frac{(\bar{p}-\sigma_H)^{\frac{n+1}{n}}}{\sqrt{q_i(t)t}} + \gamma\frac{\dot{q_i}}{q_i}(\bar{p}-\sigma_H) \tag{4.23}$$

where

$$\alpha = \frac{8n^2(1-\upsilon)^{\frac{n+1}{n}}}{\pi(n+2)(4n+2)K'I(f_{L0})^{\frac{1}{n}}G^{\frac{n+1}{n}}}$$

$$\beta = \frac{16nK_l}{\pi(n+2)}\left(\frac{hn}{4n+2}\right)^{\frac{1}{2}}\left(\frac{1-\upsilon}{K'I(f_{L0})G}\right)^{\frac{1}{2n}}$$

$$\gamma = \frac{3n}{2(n+2)}$$

The above resulting Eq. 4.23 is again a nonlinear, time-variant, ordinary differential equation for the estimated pressure. Notice that it is also linear in its parameters α, β and γ. The predominant term in this equation is the one corresponding to α, and it is negative so we should expect that the response of the pressure with respect to time should show a negative slope when the pressure reaches high values.

The Dynamic Radial Model

This model is based on the same premises as the ones outlined for the previous model. Therefore a similar approach shall be taken in this case. The local-continuity equation, provided by the fluid dynamics, will be used in conjunction with the fracture mechanics fundamental relations. However, these relations shall be also modified as we did for the GdK dynamic model.

Now, for a radial flow, the pressure gradient of the flow of a power-law fluid between two parallel plates is given by [12]

$$\frac{\partial \Delta p(r,t)}{\partial r} = -\frac{2K'}{\pi^n}\left[\frac{4n+2}{n}\right]^n \frac{q(r,t)^n}{r^n w(r,t)^{2n+1}} \qquad (4.24)$$

Following the same procedure as the one shown for the GdK model, we obtain an expression for the radius of the fracture, $R(t)$, as follows

$$R(t) = \left[\frac{1}{2K'I(f_0)}\left(\frac{\pi n}{4n+2}\right)\frac{w(f_w,t)^{2n+1}\Delta p(t)}{q_i(t)^n}\right]^{\frac{1}{1-n}} \tag{4.25}$$

with

$$I(f_0) = \int_{f_w}^{f_0}\frac{1}{f_r^n}\frac{Q(f_r,t)^n}{W(f_r,t)^{2n+1}}df_r$$

$$Q(f_r,t) = \frac{q(f_r,t)}{q(f_w,t)}$$

$$W(f_r,t) = \frac{w(f_r,t)}{w(f_w,t)}$$

$$\Delta p(t) = p_w(t) - \sigma_H$$

Recall that $I(f_0)$ represents a constant expression as it was the case for the GdK model.

The Eq. 4.25 relates geometry, $R(t)$ and $w(f_w,t)$, with the fracturing process parameters, $\Delta p(t)$ and q_i, from the fluids dynamics perspective. Now, we need to relate this equation to the ones provided by the fracture mechanics. In order to do that, we shall use the following expression for the maximum width of the fracture [12]

$$w(f_w,t) = \frac{4(1-\upsilon)}{\pi G}R(t)\Delta p(t) \tag{4.26}$$

Combining Eqs, 4.25 and 4.26 we get more convenient expressions for $R(t)$, and $w(f_w,t)$ as follows

$$R(t) = C_1 \frac{\sqrt[3]{q_i(t)}}{\Delta p(t)^{\frac{2(n+1)}{3n}}} \tag{4.27}$$

$$w(f_w,t) = C_2 \frac{\sqrt[3]{q_i(t)}}{\Delta p^{\frac{2-n}{3n}}} \tag{4.28}$$

with

$$C_1 = \sqrt[3n]{2K' I(f_0)\left[\frac{\pi G}{4(1-\upsilon)}\right]^{2n+1}\left[\frac{4n+2}{\pi n}\right]^n}$$

$$C_2 = \frac{4(1-\upsilon)}{\pi G} C_1$$

We can now extend Eq. 4.28 into a more general form taking into account that the radial fracture can be taken as an ellipsoid of revolution [13]

$$w(r,t) = w(f_w,t)\sqrt{1-(\frac{r}{R(t)})^2} \tag{4.29}$$

We shall now substitute Eq. 4.29 into the local-continuity equation for a radial fracture. The local continuity equation can be expressed in this case as follows

$$\frac{\partial q(r,t)}{\partial r} + q_l(r,t) + \frac{\partial A(r,t)}{\partial t} = 0 \tag{4.30}$$

This equation can be now rewritten as

$$\frac{\partial q(r,t)}{\partial r} + \frac{2\pi r K_l}{\sqrt{t-\frac{t}{R(t)}r}} + 2\pi r \frac{\partial w(r,t)}{\partial t} = 0 \tag{4.31}$$

In the same way as we did for the dynamic GdK model, we shall integrate Eq. 4.31 along the radius of the fracture. But, before doing that, we shall find the partial derivative of the width of the fracture with respect to time. By doing that, we get

$$\frac{\partial w(r,t)}{\partial t} = E(r) + F(r) + G(r) + H(r) \tag{4.32}$$

with

$$E(r) = -\frac{8(n+1)(1-\upsilon)}{3\pi n G C_1} \frac{\Delta p^{\frac{2(n+1)}{3n}}}{\sqrt[3]{q_i}} \frac{\dot{\Delta p} r^2}{\sqrt{1-(\frac{r}{R(t)})^2}}$$

$$F(r) = \frac{C_1 C_2}{3R^3} \frac{\dot{q}_i}{\sqrt[3]{q_i}} \frac{1}{\Delta p^{\frac{n+4}{3n}}} \frac{r^2}{\sqrt{1-(\frac{r}{R(t)})^2}}$$

$$G(r) = -\frac{(2-n)C_2}{3n} \frac{\sqrt[3]{q_i}\,\dot{\Delta p}}{\Delta p^{\frac{2n+2}{3n}}} \sqrt{1-(\frac{r}{R(t)})^2}$$

$$H(r) = \frac{C_2}{3} \frac{\dot{q}_i}{\sqrt[3]{q_i^2}\,\Delta p^{\frac{2-n}{3n}}} \sqrt{1-(\frac{r}{R(t)})^2}$$

Now substituting Eq. 4.32 into Eq. 4.31, and integrating from $r = 0$ to $r = R$, and recalling that

$$q(0,t) = q_i$$

$$q(R,t) = 0$$

we get a first order differential equation for the net BHP as follows

$$\dot{\Delta p} = -\alpha\ \Delta p^{\frac{2(n+1)}{n}} + \beta\ \frac{\Delta p^{\frac{2(n+1)}{3n}}}{\sqrt[3]{q_i}\sqrt{t}} + \gamma\ \frac{\dot{q}_i}{q_i}\Delta p \tag{4.33}$$

with

$$\alpha = \frac{3n^2}{(n+2)(4n+2)[K' I(f_0)]^{\frac{1}{n}}} \left[\frac{2(1-\upsilon)}{\pi G}\right]^{\frac{n+1}{n}}$$

$$\beta = \frac{nK_l}{n+2}\left[\frac{2^{4n+1}}{K' I(f_0)}\left(\frac{\pi G}{1-\upsilon}\right)^{n-1}\left(\frac{\pi n}{4n+2}\right)^{n}\right]^{\frac{1}{3n}}$$

$$\gamma = \frac{n}{n+2}$$

The Eq. 4.33 is a nonlinear, time-variant, first order differential equation for the net BHP. As in the previous models, it is linear in its parameters α, β, and γ. Notice again that the predominant term is the one corresponding to α which shall produce negative slopes which is the main characteristic of the radial model.

Summary

In this chapter we have developed control-type equations for the 2-D models, and some assumptions were made in order to solve the partial differential equations. Basically we assumed a certain pressure distribution along the fracture because it is still uncertain how the fracture actually develops, and, at our best, we can only guess. Other considerations were put aside as was the case of the spurt loss volume or the building of the filtercake on the walls of the fracture because the main goal of this work was to keep the models as simple as possible but giving them some physically based characteristics.

Even though all the dynamic models are nonlinear and time-variant, they are indeed linear in their parameters. This characteristic makes them suitable for system identification purposes.

Regarding the lumped parameters α, β, and γ, we must notice that they contain important information about the process such as the fluid's parameters, n and K', the in-situ parameters, G and υ, the height of the fracture, h, and the fluid loss coefficient, K_l.

For this reason, we could expect that, by running an appropriate identification algorithm, it will be able to show the signatures of the fracturing process provided that the proposed models adequately represent it.

The following is a brief summary of the hypothesis and results for each one of these models:

The Dynamic PKN Model. The assumptions for this model are:

- The fracture has a constant height, h, independent of fracture length.
- The fracturing fluid pressure, p, is constant in vertical cross sections perpendicular to the direction of the propagation, and it equals the rock stress perpendicular to the fracture plane, σ_H, at the tip of the fracture.
- Each vertical cross section deforms individually and is not affected by its neighbors.
- The injection rate into the fracture, q_i, is variable in time.
- The fracturing fluid is non-Newtonian (power-law fluid).

The equation that calculates the pressure is:

$$\dot{\Delta p} = \alpha \frac{q_i(t)^{n+1}}{\Delta p^{2(n+1)}} - \beta \frac{1}{\sqrt{t}}$$

with

$$\alpha = \frac{16K'}{\pi}\left[\frac{4n+2}{n}\right]^n\left[\frac{G^2}{h^3(1-\upsilon)^2}\right]^{n+1}$$

$$\beta = \frac{8GK_l}{\pi h(1-\upsilon)}$$

The fracture length and width are calculated by

$$L(t) = \left[\frac{n}{4n+2}\right]^{n} \frac{(1-\upsilon)^{2n+1}}{G^{2n+1}} \frac{h^{3n+1}}{2K'} \frac{\Delta p^{2(n+1)}}{q_i(t)^n}$$

$$w(0,t)| = \frac{(1-\upsilon)h}{G} \Delta p$$

The Dynamic GdK model. The assumptions for this model are:

- The height of the fracture, h, is fixed.
- The width of the fracture, $w(x,t)$, is constant in the vertical direction.
- The injection rate into the fracture, q_i, is variable in time.
- The fracturing fluid is non-Newtonian (power-law fluid).

The equation that calculates the pressure is:

$$\dot{\bar{p}} = -\alpha\,(\bar{p}-\sigma_H)^{\frac{2(n+1)}{n}} + \beta \frac{(\bar{p}-\sigma_H)^{\frac{n+1}{n}}}{\sqrt{q_i(t)t}} + \gamma \frac{\dot{q}_i}{q_i}(\bar{p}-\sigma_H)$$

with

$$\alpha = \frac{8n^2(1-\upsilon)^{\frac{n+1}{n}}}{\pi(n+2)(4n+2)K'I(f_{L0})^{\frac{1}{n}}G^{\frac{n+1}{n}}}$$

$$\beta = \frac{16nK_l}{\pi(n+2)}\left(\frac{hn}{4n+2}\right)^{\frac{1}{2}}\left(\frac{1-\upsilon}{K'I(f_{L0})G}\right)^{\frac{1}{2n}}$$

$$\gamma = \frac{3n}{2(n+2)}$$

The fracture length and width are calculated by

$$L(t) = \left[\frac{I(f_{L0})K'}{2^{2n}h^n} \left(\frac{4n+2}{n}\right)^n \left(\frac{G}{1-\upsilon}\right)^{2n+1} \right]^{\frac{1}{n}} \frac{\sqrt{q_i(t)}}{(\overline{p(t)} - \sigma_H)^{\frac{n+1}{n}}}$$

$$w(x,t) = \frac{2C_1(1-\upsilon)}{G} \frac{\sqrt{q_i(t)}}{(\overline{p(t)} - \sigma_H)^{\frac{1}{n}}} \sqrt{1 - \left(\frac{x}{L(t)^2}\right)}$$

The Dynamic Radial Model. The assumptions for this model are:

- The height of the fracture, h, is fixed.
- The width of the fracture, $w(x,t)$, is constant in the vertical direction.
- The injection rate into the fracture, q_i, is variable in time.
- The fracturing fluid is non-Newtonian (power-law fluid).

The equation that calculates the pressure is:

$$\dot{\Delta p} = -\alpha \ \Delta p^{\frac{2(n+1)}{n}} + \beta \ \frac{\Delta p^{\frac{2(n+1)}{3n}}}{\sqrt[3]{q_i}\sqrt{t}} + \gamma \ \frac{\dot{q}_i}{q_i} \Delta p$$

with

$$\alpha = \frac{3n^2}{(n+2)(4n+2)[K' I(f_0)]^{\frac{1}{n}}} \left[\frac{2(1-\upsilon)}{\pi G}\right]^{\frac{n+1}{n}}$$

$$\beta = \frac{nK_l}{n+2} \left[\frac{2^{4n+1}}{K' I(f_0)} \left(\frac{\pi G}{1-\upsilon}\right)^{n-1} \left(\frac{\pi n}{4n+2}\right)^n \right]^{\frac{1}{3n}}$$

$$\gamma = \frac{n}{n+2}$$

The radius and the maximum width of the fracture are calculated by

$$R(t) = \sqrt[3n]{2K^{'} I(f_0)\left[\frac{\pi G}{4(1-\upsilon)}\right]^{2n+1}\left[\frac{4n+2}{\pi n}\right]^{n}} \frac{\sqrt[3]{q_i(t)}}{\Delta p(t)^{\frac{2(n+1)}{3n}}}$$

$$w(f_w,t) = \frac{4(1-\upsilon)}{\pi G} \sqrt[3n]{2K^{'} I(f_0)\left[\frac{\pi G}{4(1-\upsilon)}\right]^{2n+1}\left[\frac{4n+2}{\pi n}\right]^{n}} \frac{\sqrt[3]{q_i(t)}}{\Delta p^{\frac{2-n}{3n}}}$$

CHAPTER 5

STUDIES ON FAULT DETECTION

Overview

In this chapter, we shall apply some system identification techniques to the developed PKN-type dynamic model. We shall concentrate our analysis in this model because we have the chance to apply the outcomes of this research to a real data profile. As we shall see later in this chapter, the data that we have available corresponds to a PKN-type data profile.

Throughout most of this chapter, we will develop estimation algorithms, both off-line and on-line, for the dynamic PKN model. In an effort to validate these estimation algorithms, we shall generate our own PKN-type profile and use it as a test case. This pressure profile shall be generated by using real values for the fracturing process related parameters. These parameters, in turn, shall generate fixed values for the lumped parameters, α and β, as indicated in the Eqs. 4.10 and 4.11, that we will try to recover by using linear system identification techniques in a reverse process.

After developing this estimation algorithm, we shall adequately manipulate its parameters in order to get a clear signature of the screenout fault.

Generated PKN-Type Pressure Profile

In order to run our simulations for system identification purposes, we need to generate our own data with well-known parameters. This model shall serve as a test case in order to validate our results so that we can later apply them to the field data.

As it has been mentioned, we decided to generate our data by using the dynamic PKN differential equation (Eq. 4.9). In addition to that, we shall add a screen-out type behavior at the end of that profile. The main idea is just to generate a different profile with respect to the one provided by Eq. 4.9.

The following are the assumed values for the corresponding parameters of Eq. 4.9. Most of these values have been taken from the well's profile provided by Halliburton Services (see Appendix B) while others have been taken from the literature.

$K_l = 0.00046 \text{ m}/\sqrt{\text{min}}$
$G = 1.45e6 \text{ psi}$
$\upsilon = 0.2$
$n = 0.715$
$K' = 0.00056/60'' \text{ psi.min}^n$
$h = 39 \text{ m}$

For this set of parameters, the corresponding values for α and β are (see Eqs. 4.10 and 4.11)

$$\alpha = 1.449 \times 10^{10} \ \frac{\text{psi}^{2n+3}\text{min}^n}{\text{m}^{3(n+1)}}$$

$$\beta = 54.44 \ \frac{\text{psi}}{\sqrt{\text{min}}}$$

In order to generate and plot the PKN-type pressure profile, a Matlab algorithm (PK.M) was written. This algorithm is included in Appendix A. The following is the resulting plot of this generated pressure profile.

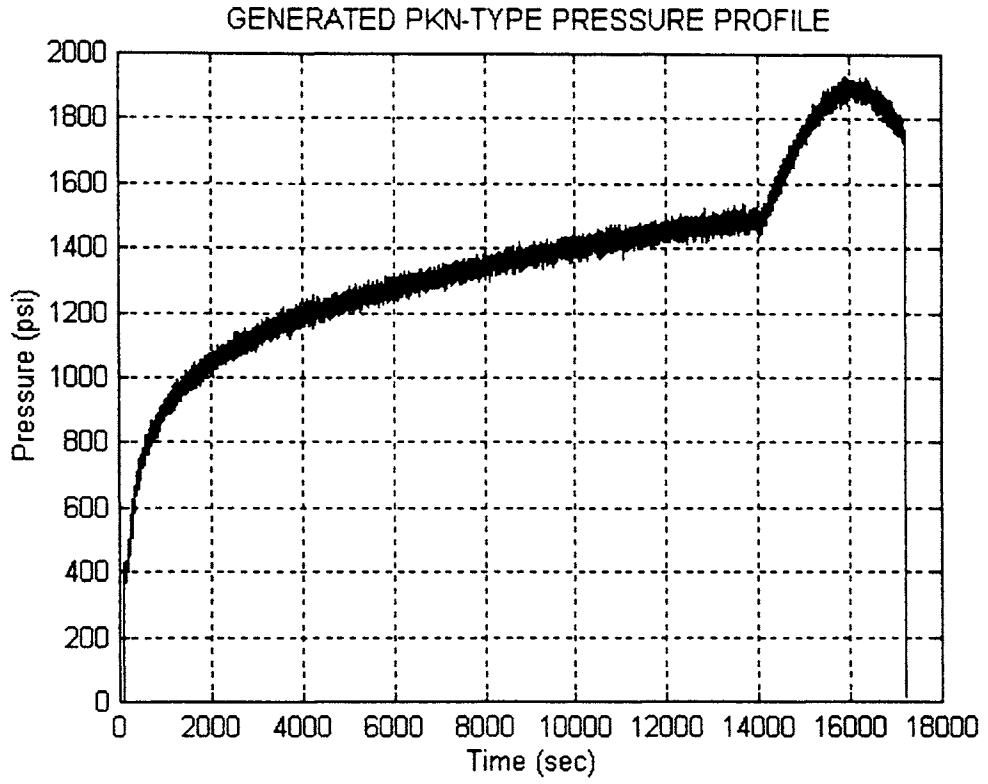

Fig. 5.1 Generated pressure profile

As we can see from Fig. 5.1, the first part of this plot represents a PKN-type pressure profile; while, the second part, a screen-out type behavior. The orders of magnitude of the pressure, and time values agree with the ones observed in the field. In addition to that, in order to simulate some perturbations in the process (such as noise in the measurements), random noise was added on top of the generated profile but not exceeding 3% of the maximum generated pressure. Another important profile that we

shall use for our simulations will be the one corresponding the input slurry rate to the fracture (see Appendix B), and that is shown in Fig. 5.2.

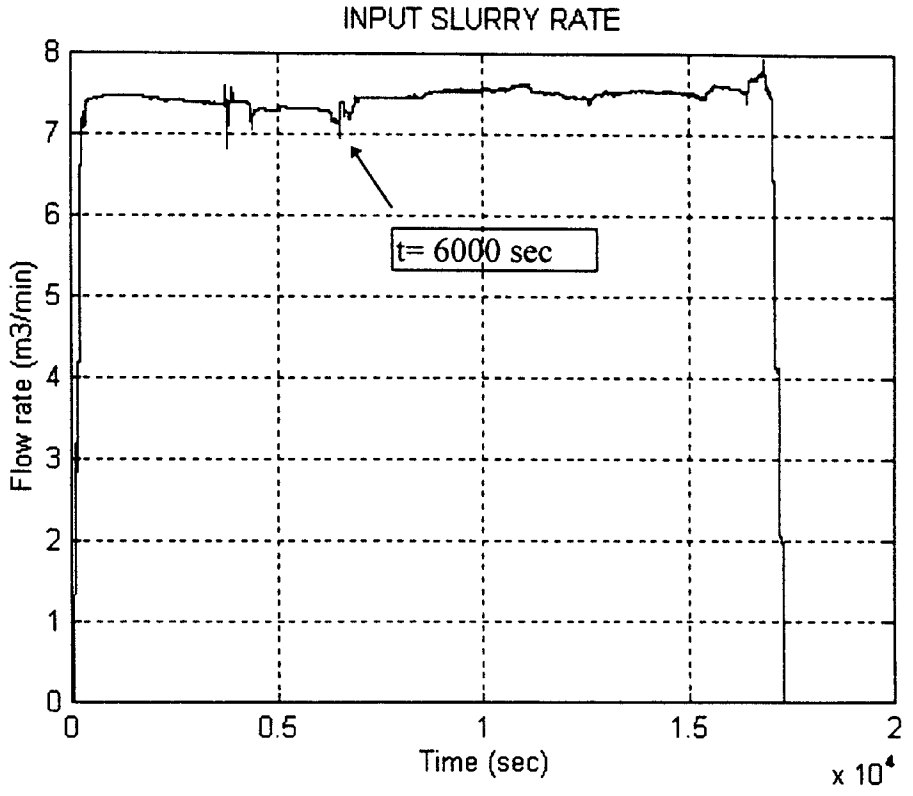

Fig. 5.2 Input Slurry rate to the fracture

In Fig. 5.2 we can see that the input slurry rate is kept approximately constant around 7.5 m^3/min. However, we should notice that there has been a change in the job schedule at approximately t=6000 sec. At this time in the process, the proppant concentration is increased, and it causes some perturbations as well as a slight increase in the input Slurry rate. It is very important to point out that the effect of the proppant concentration has not been modeled in the dynamic PKN model, and as such we expect that the model should be able to show this change in the behavior in some fashion. A profile of the proppant concentration can be seen in Appendix B.

Off-line Parameter Estimation

As a first step, in order to develop an on-line estimation algorithm, we shall first develop an off-line estimation algorithm that will be later made recursive for fault identification purposes.

First of all, we shall analyze the sensitivity of the model with respect to its related parameters, α and β. Recall that the dynamic PKN model is expressed as

$$\dot{\Delta p} = \alpha \frac{q_i(t)^{n+1}}{\Delta p^{2(n+1)}} - \beta \frac{1}{\sqrt{t}} \tag{4.9}$$

In order to speed up the simulation time, avoiding to solve directly the continuous time differential equation, we shall now discretize Eq. 4.9 by replacing the derivative term with a backward difference. By doing so, we get

$$\hat{P}(k) = \alpha \frac{q_i(k-1)^{n+1}}{P(k-1)^{2(n+1)}} \Delta t_k - \beta \frac{\Delta t_k}{\sqrt{t_{k-1}}} + P(k-1) \tag{5.1}$$

where $\hat{P}(k)$ represents the predicted value for the net Bottom Hole Pressure (BHP) for the step k, $P(k\text{-}1)$, the last measured value at the step k-1, and Δt_k the sampling rate. In addition to that, we should take into account that in a hydraulic process, the pressure, $P(k)$, and the time, t_k, exhibit a large range of variation. Therefore, we need to normalize this equation in order to make it more suitable to such large variations. The Eq. 5.2 shows this new normalized equation

$$\hat{P}_N(k) = \alpha_N \frac{q_N(k-1)^{n+1}}{P_N(k-1)^{2(n+1)}} - \beta_N \frac{1}{\sqrt{t_N(k-1)}} + P_N(k-1) \tag{5.2}$$

with

$$\hat{P}_N(k) = \frac{\hat{P}(k)}{P_{\max}}, \quad q_N(k) = \frac{q(k-1)}{q_{\max}}, \quad t_N(k) = \frac{t_k}{t_{\max}},$$

$$\alpha_N = \frac{\alpha\, q_{\max}^{n+1}}{P_{\max}^{2n+3}} \Delta t_k$$

$$\beta_N = \frac{\beta}{P_{\max}\sqrt{t_{\max}}} \Delta t_k$$

P_{max}, and t_{max} have been taken from the generated PKN-type pressure profile, and q_{max} from the provided field data. The corresponding values for them are

$$P_{\max} = 1541 \text{ psi}$$
$$q_{\max} = 7.944 \text{ m}^3 / \text{min}$$
$$t_{\max} = 233 \text{ min}$$
$$\Delta t_k = 1 \text{ sec}$$

For this set of values, the normalized exact parameters α_N and β_N are:

$$\alpha_N = 5.0375e-5$$
$$\beta_N = 3.8545e-5$$

Before we proceed to estimate these parameters in an off-line fashion, we shall analyze the sensitivity of Eq. 5.2 to find out how sensitive that equation is with respect to its normalized parameters.

The Sensitivity of the Dynamic PKN Model

Recall that the sensitivity, S, of any function F with respect to its parameter x is expressed as

$$S_x^F = \frac{dF}{dx}\frac{x}{F} \tag{5.3}$$

By applying Eq. 5.3 to the normalized Eq. 5.2, we get the sensitivity of the normalized output pressure with respect to α_N

$$S_{\alpha_N}^{\hat{P}_N}(k) = \frac{1}{1-\frac{\beta_N}{\alpha_N}\left[\frac{P_N(k-1)^{2(n+1)}}{q_N(k-1)^{n+1}\sqrt{t_N(k-1)}}\right]+\frac{1}{\alpha_N}\left[\frac{P_N(k-1)^{2n+3}}{q_N(k-1)^{n+1}}\right]} \tag{5.4}$$

Now, with respect to β_N

$$S_{\beta_N}^{\hat{P}_N}(k) = \frac{1}{1-\frac{\alpha_N}{\beta_N}\left[\frac{q_N(k-1)^{n+1}\sqrt{t_N(k-1)}}{P_N(k-1)^{2(n+1)}}\right]-\frac{1}{\beta_N}\left[P_N(k-1)\sqrt{t_N(k-1)}\right]} \tag{5.5}$$

The above Eqs. 5.4 and 5.5 evaluate the sensitivity of the function at each time step *k*. Figures 5.2 and 5.3 show the corresponding sensitivity values for α_N and β_N. The algorithm (SENS.M) that was used to calculate these sensitivities is shown in Appendix A. We have computed the sensitivity values up to *k*=14000 because that is the range in which the PKN dynamic model was used to generate that data.

We can see, from Figs. 5.3 and 5.4, that the sensitivity of Eq. 5.2 with respect to its parameters α_N and β_N is very poor after *t*=2000 sec. Moreover the sensitivity of this equation, before this time, is not the kind we would like to have as they are indicating very low values. This leads us to the conclusion that we must get an estimation of the parameters at the beginning of the simulation otherwise no major contribution to the estimation will be made after that.

The Weighted Least Square Estimator

Now we shall proceed to generate the off-line estimator algorithm. Taking into account the results given by the sensitivity analysis, we shall use a WLSE such it weighs

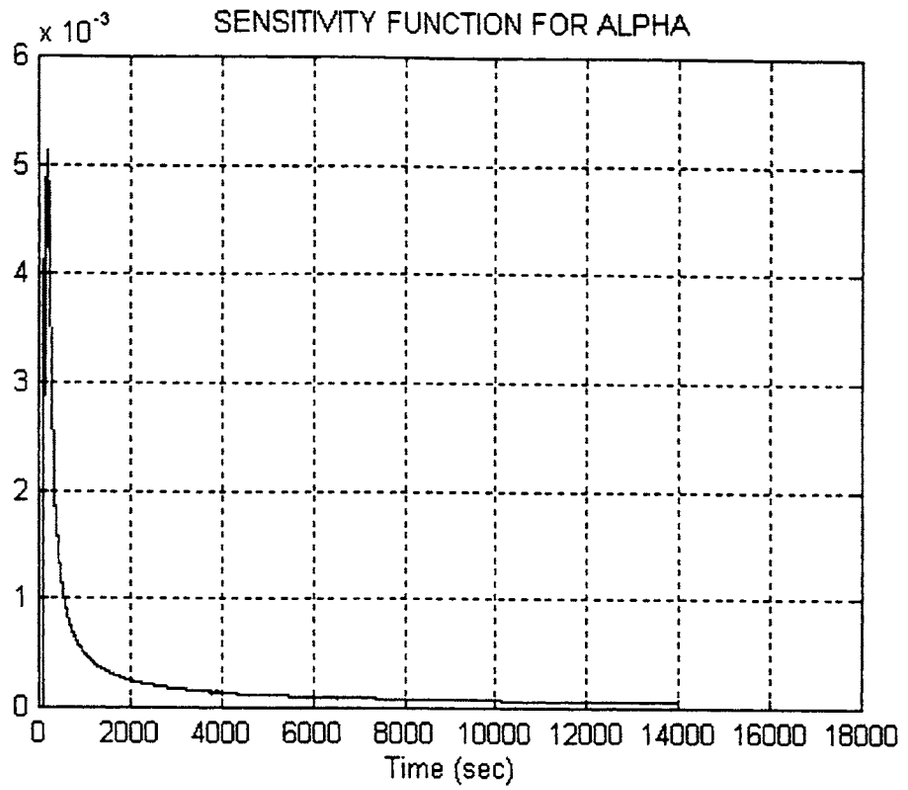

Fig. 5.3 Sensitivity of the output pressure with respect to α_N

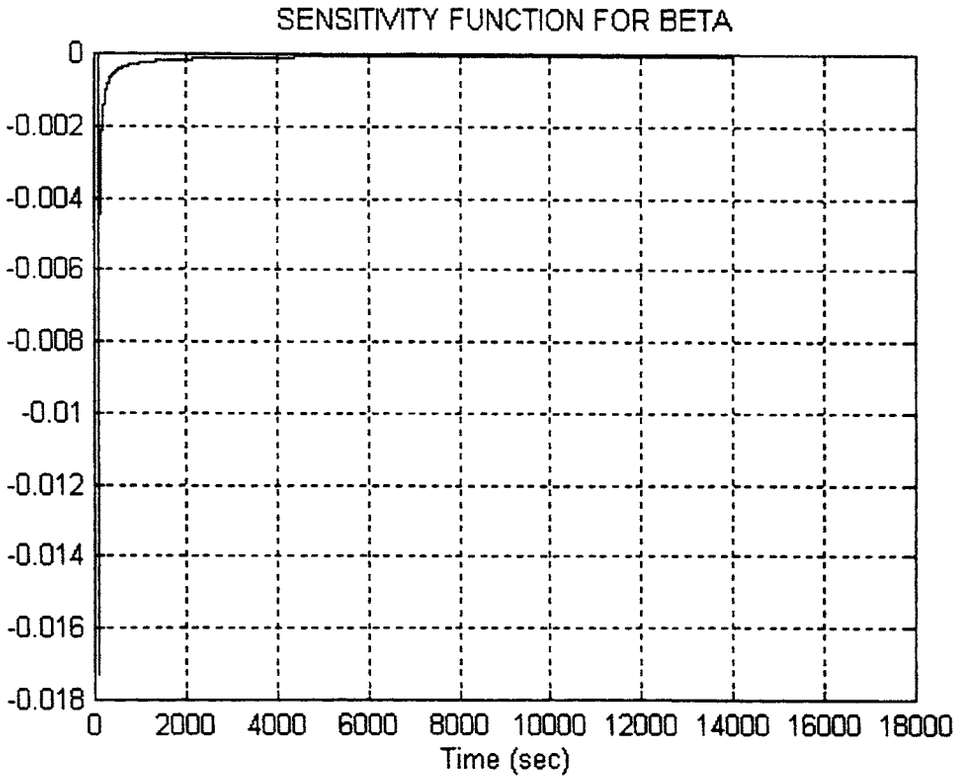

Fig. 5.4 Sensitivity of the output pressure with respect to β_N

more the data at the beginning of the simulation. Thus, we shall start defining our cost index function as

$$J = \frac{1}{2}\sum_{k=1}^{n} w(k)e(k)^2 \tag{5.6}$$

where $w(k)$ is the corresponding weight at the time k, and

$$e(k) = P_N(k) - \hat{P}_N(k) \tag{5.7}$$

represents the error in the estimation in which $P_N(k)$ represents the normalized measured value, and $\hat{P}_N(k)$ represents the predicted value. Now, substituting Eq. 5.2 and Eq. 5.7 into Eq. 5.6, and taking the gradient of the cost function J, we have

$$\nabla J = \left[-\sum_{k=1}^{n} w(k)e(k)\frac{q_N(k-1)^{n+1}}{P_N(k-1)^{2(n+1)}} \qquad \sum w(k)e(k)\frac{1}{\sqrt{t_N(k-1)}} \right] \tag{5.8}$$

Now, by equating both elements of the row vector to zero, in order to minimize the cost function, we get a set of two linear equations for α_N and β_N. The first equation is

$$a\,\alpha_N + b\,\beta_N = c \tag{5.9}$$

with

$$a = \sum_{k=1}^{n} w(k)\left[\frac{q_N(k-1)}{P_N(k-1)^2}\right]^{2(n+1)}$$

$$b = -\sum_{k=1}^{n} \frac{w(k)q_N(k-1)^{n+1}}{P_N(k-1)^{2(n+1)}\sqrt{t_N(k-1)}}$$

$$c = \sum_{k=1}^{n} \frac{w(k)q_N(k-1)^{n+1}}{P_N(k-1)^{2(n+1)}}\left[P_N(k) - P_N(k-1)\right.$$

and the second equation is

$$d\,\alpha_N + e\,\beta_N = f \tag{5.10}$$

with

$$d = \sum_{k=1}^{n} \frac{w(k) q_N (k-1)^{n+1}}{\sqrt{t_N (k-1) P_N (k-1)^{2(n+1)}}}$$

$$e = -\sum_{k=1}^{n} \frac{w(k)}{t_N (k-1)}$$

$$f = \sum_{k=1}^{n} \frac{w(k)}{\sqrt{t_N (k-1)}} \left[P_N (k) - P_N (k-1) \right]$$

We shall solve this set of equations by using both a flat weighting factor, $w(k)$=1, and a triangular weighting factor. The triangular weighting factor shall show values between zero and one, and the early data in the simulation will be more heavily weighted. Fig. 5.5 shows the distribution of this weighting factor.

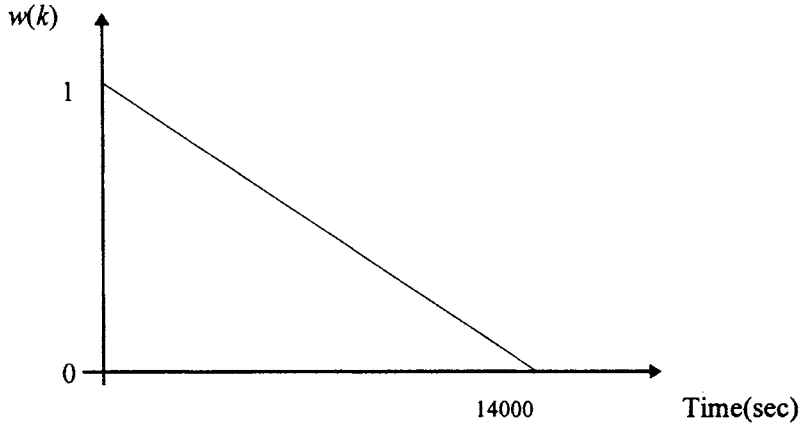

Fig. 5.5 Weighting factor $w(k)$

In order to solve the off-line equations, an algorithm was created in Matlab (OFFLINE.M). It solves simultaneously Eq. 5.9 and 5.10, and it runs a batch of N samples. Different results were obtained for this case: ones with and without weighting

factor, and others for batches of 1000 and 14000 samples respectively. Tables 5.1 and 5.2 show the results obtained for the normalized values, α_N and β_N, in all those cases.

Time (sec)	α_N (5.0375e-5)	β_N (3.8545e-5)
1000	2.1637e-5	6.6538e-6
14000	2.1726e-5	6.799e-6

Table I. Estimation of the generated parameters without weighting factor.

Time (sec)	α_N	β_N
1000	2.1634e-5	6.7023e-6
14000	2.1686e-5	6.4663e-6

Table II. Estimation of the generated parameters for a triangular weighting factor.

As we can see from both tables, there is no significant difference when estimating these parameters by running either a batch of 1000 or 14000 samples nor by applying a weighting factor. Therefore, in order to show how well these parameters match the exact values for α_N and β_N, we shall plot the estimated pressure profile for the parameters α_N and β_N corresponding to the first row of Table 5.1. In all the other three cases, we get very similar plots. This estimated pressure profile as well as the generated one are shown in Fig. 5.6 (the estimated pressure profile has been only calculated until t= 14000 sec), and we can see that they are reasonably close.

With these results, we conclude the off-line estimation. We can see from Tables 5.1 and 5.2 that we have obtained only approximate results of the exact parameters. The results provided by the sensitivity analysis had already indicated that it would be very difficult to improve our estimators even if we let the simulation run a longer time unless we obtained a good estimation of the parameters at the beginning of the simulation. The use of the weighting factor did not improve our results either.

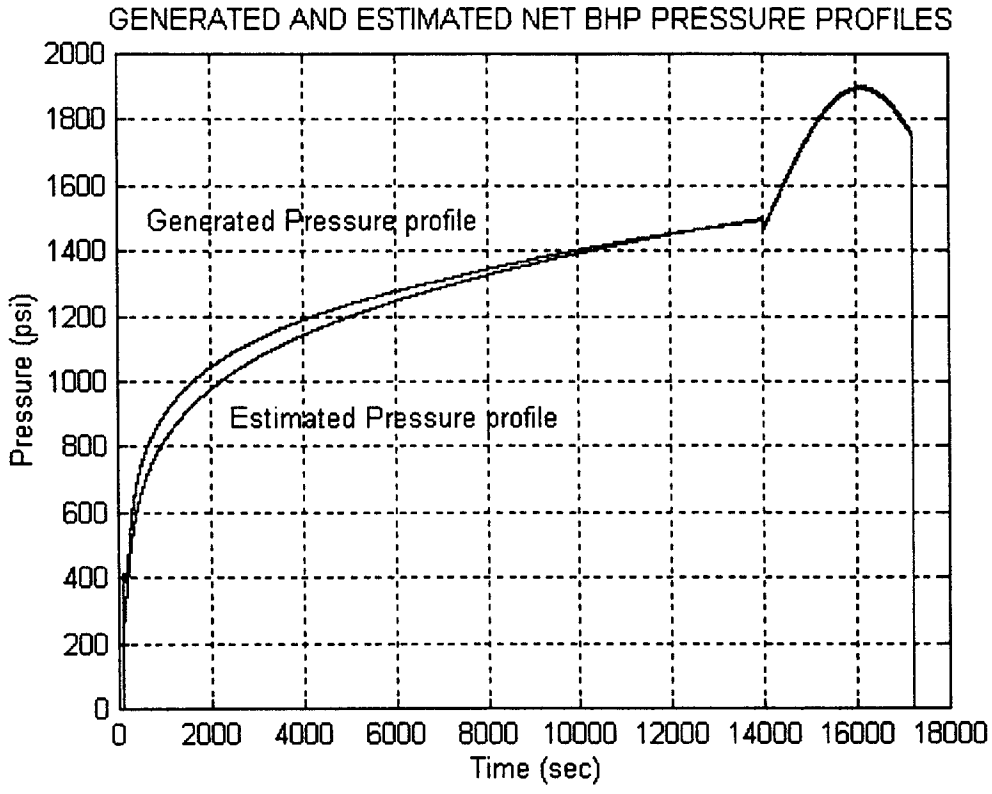

Fig. 5.6 PKN-type generated pressure profile and the estimated one for α_N =2.1637e-5 and β_N=6.6538e-6

We believe that these results can be considered reasonably adequate, given the characteristics of the dynamic equation, and as such we shall now analyze, in the next section, whether or not we can obtain approximately the same accuracy by making this off-line estimation algorithm recursive.

On-line Parameter Estimation

As a first step, in order to proceed with the on-line estimation, we shall write the Eq. 5.2 in a form that is familiar for system identification purposes

$$\hat{P}_N(k) = \varphi^T(k)\,\theta(k) + P_N(k-1) \tag{5.11}$$

with

$$\varphi(k) = \left[\left(\frac{q_N(k-1)}{P_N(k-1)^2}\right)^{n+1} \quad -\frac{1}{\sqrt{t_N(k-1)}}\right]^T \tag{5.12}$$

$$\theta(k) = \left[\alpha_N(k) \quad \beta_N(k)\right]^T \tag{5.13}$$

If we now compute the estimate that minimizes the cost index function

$$J = \sum_{k=1}^{n} w(k)[P_N(k) - (\varphi^T(k)\theta(k) - P_N(k-1))]^2 \tag{5.14}$$

where the weighting sequence has the following property, also known as the *forgetting factor*,

$$\begin{aligned} &w(t,k) = \lambda\, w(t-1,k), \qquad 1 \le k \le t-1 \\ &w(t,t) = 1 \end{aligned} \tag{5.17}$$

we can compute the recursive algorithm version of this estimator by just following the same procedures suggested by Ljung [14]. After dealing with the algebra, we get the recursive algorithm to estimate the new vector parameter $\hat{\theta}(k)$ as follows

$$L(k) = \frac{R(k-1)\varphi(k)}{\lambda + \varphi^T(k)R(k-1)\varphi(k)} \tag{5.16}$$

$$\hat{\theta}(k) = \hat{\theta}(k-1) + L(k)\left[P_N(k) - P_N(k-1) - \varphi^T(k)\hat{\theta}(k-1)\right] \tag{5.17}$$

$$R(k) = \frac{1}{\lambda}\left[R(k-1) - \frac{R(k-1)\varphi(k)\varphi^T(k)R(k-1)}{\lambda + \varphi^T(k)R(k-1)\varphi(k)} \right] \tag{5.18}$$

With the above equations, we are now able to compute the estimation of the parameter vector $\theta(k)$ in an on-line fashion. However, we shall still provide adequate initial values for both $R(0)$ and $\hat{\theta}(0)$. We shall do so by following the recommendations of Ljung [14] that computes these initial values by running a small batch of data according to

$$R(0) = \left[\sum_{k=1}^{k_0} w(k_0, k)\varphi(k)\varphi^T(k) \right]^{-1} \tag{5.19}$$

$$\hat{\theta}(0) = R(0)\sum_{k=1}^{k_0} w(k_0, k)\varphi(k)[P_N(k) - P_N(k-1)] \tag{5.20}$$

We are now ready to proceed with the on-line estimation. An algorithm was developed in Matlab (ONLINE.M) that evaluates Eqs. 5.16, 5.17 and 5.18, and also computes a set of initial values, according to Eqs. 5.19 and 5.20, for a batch of 10 points, and, from there on, estimates the parameter vector $\hat{\theta}(k)$ on-the-fly from t=111 sec up to t=14000 sec. We have chosen to run the simulation until t= 14000 sec because the PKN pressure profile was generated for that range.

The corresponding estimated values for α_N and β_N, when using a forgetting factor equal to 1, and other using 0.9993, have been plotted in Figs. 5.7 and 5.8. The reason why such a particular value of forgetting factor was used shall be explained below.

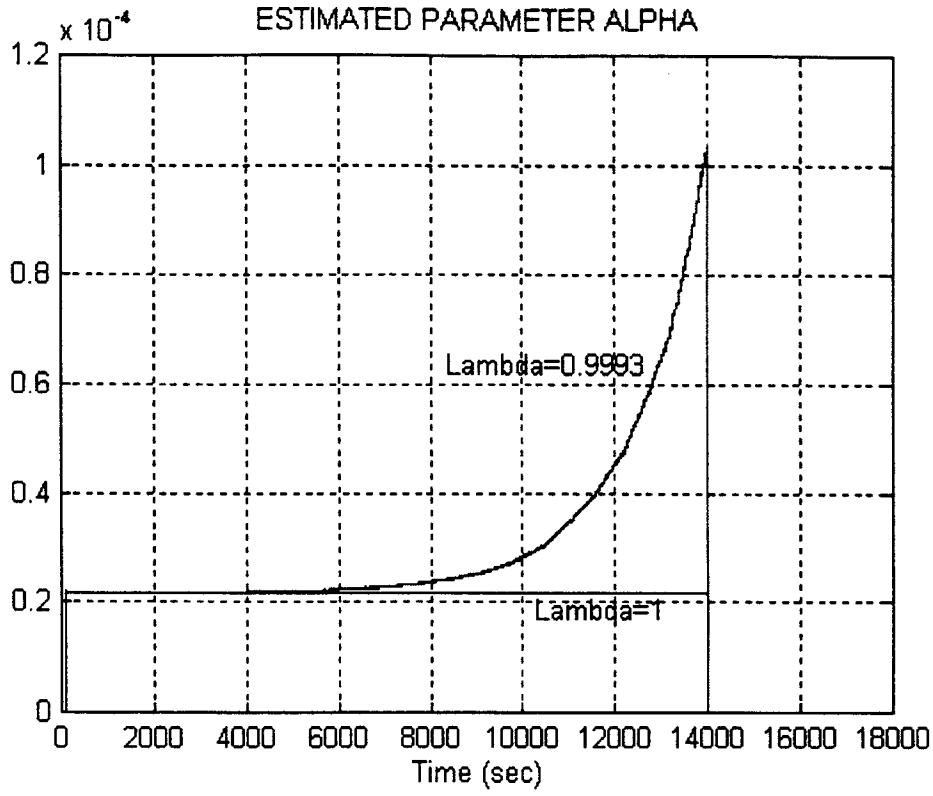

Fig. 5.7 Estimated parameter α_N for λ=1 and λ=0.9993

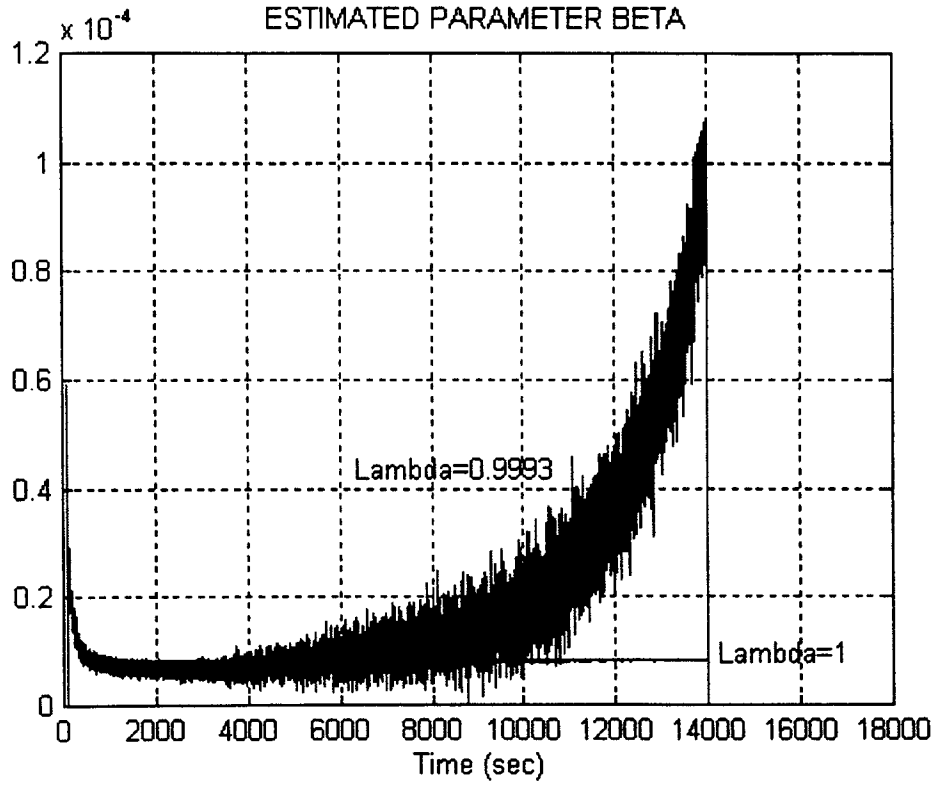

Fig. 5.8 Estimated parameter β_N for λ=1 and λ=0.9993

We can see from Figs. 5.7 and 5.8 that the estimation of the parameters diverge when using a forgetting factor less than one, and this tendency is even worse when using values lower than the one shown. However, when using no forgetting factor, these parameters converge to a definite set of values ($\hat{\alpha}_N = 2.2e-5, \hat{\beta}_N = 8e-6$) that are close to the exact values (α_N=5.0375e-5, β_N=3.8545e-5) but still showing an offset.

In the above results, we have to take into account that we have added a random perturbation on top of the generated PKN-type pressure profile. This effect is more noticeable in the case of the parameter β_N. The presence of this unmodeled disturbance, in Eq. 5.2, makes the estimation of the generated parameters diverge when using a forgetting factor less than one. This was also clear when adding less random disturbances on top of the PKN-type generated profile. Disturbances as low as 0.5% of the maximum pressure were also tested, and gave similar results.

Now we would like to see how well this on-line algorithm performs if we take the disturbance out of the PKN-type pressure profile. For this case, Figs. 5.9 and 5.10 show the estimated values of α_N and β_N, again, for two different values of the forgetting factor. In these cases, we have an excellent convergence in the parameters when using a forgetting factor equal to 0.96. Both parameters, α_N and β_N, converge relatively fast to their exact values with the above forgetting factor. Values bigger than 0.96 produce slow convergence, and values lower than that do not improve very much the rate of convergence.

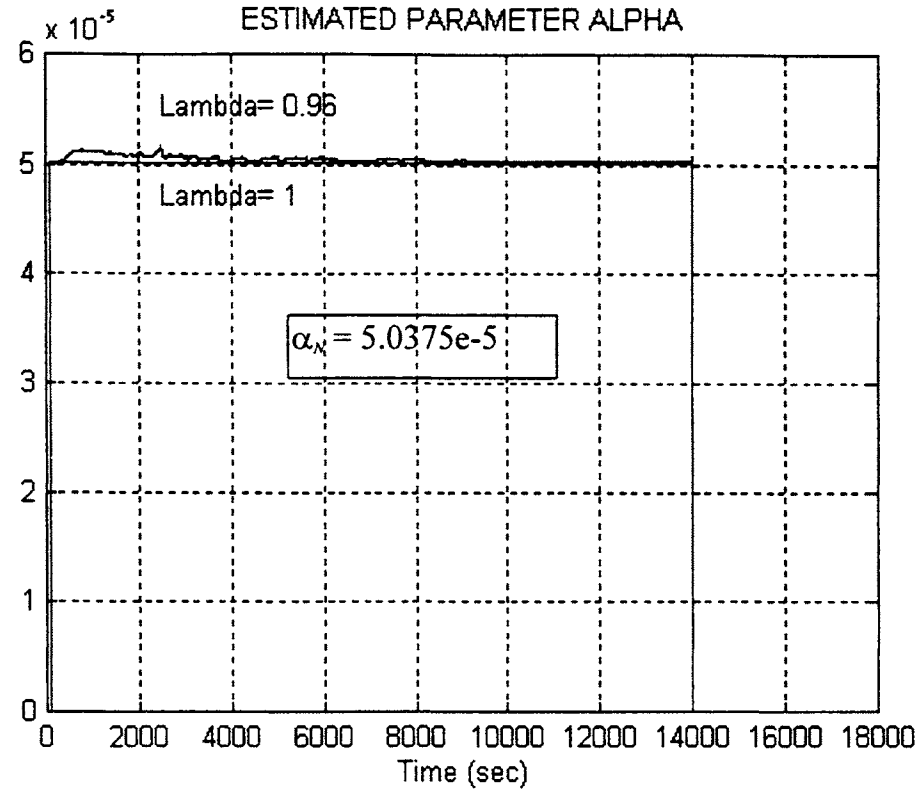

Fig. 5.9 Estimated parameter α_N for λ=1 and λ=0.96 (without noise)

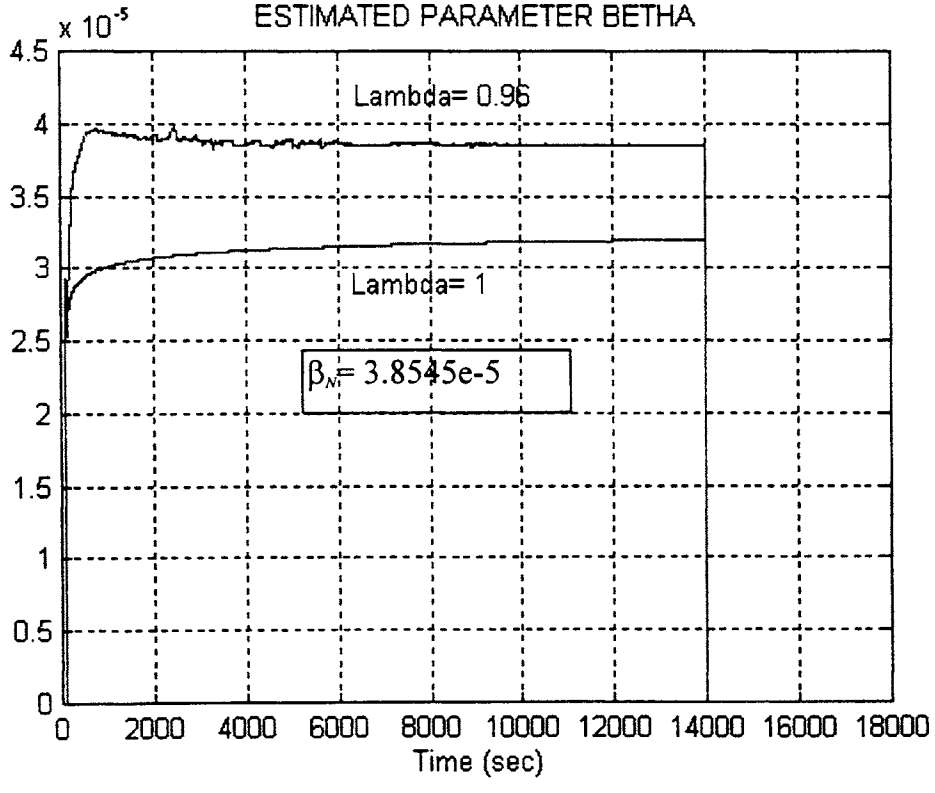

Fig. 5.10 Estimated parameter β_N for λ=1 and λ=0.96 (without noise)

Also, when using a forgetting factor equal to one, the performance was better than the ones obtained when noise was added on top of the generated pressure profile, indicating that the estimation algorithm performs relatively well in the absence of unmodeled errors. These results lead us to conclude that the estimation algorithm is not very reliable in the presence of unmodeled errors. For this reason, we shall continue the analysis of this dynamic model by eliminating these random disturbances from our generated pressure profiles from here on.

We shall now modify the generated pressure profile such that we will have two different sets of parameters for α_N and β_N. In this way, we shall be able to see whether or not the algorithm is capable of estimating a sudden change in these parameters while the process is running as well as to show the new signatures of the parameters. The new pressure profile for this case is shown in Fig. 5.11, and it has been developed by using Eq. 5.1 for two different values for n and K' (all the other related parameters remain the same). The algorithm (PK1.M) to generate this profile is shown in Appendix A. The following are the sets of values for this new generated pressure profile

$K_{I1} = 0.00046 \text{ m} / \sqrt{\text{min}}$
$G_1 = 1.45e6 \text{ psi}$
$\upsilon_1 = 0.2$
$n_1 = 0.715$
$K_1' = 0.00056 / 60^n \text{ psi.min}^n$
$h_1 = 39 \text{ m}$

$K_{I2} = 0.00046 \text{ m} / \sqrt{\text{min}}$
$G_2 = 1.45e6 \text{ psi}$
$\upsilon_2 = 0.2$
$n_2 = 0.41$
$K_2' = 0.0375 / 60^n \text{ psi.min}^n$
$h_2 = 39 \text{ m}$

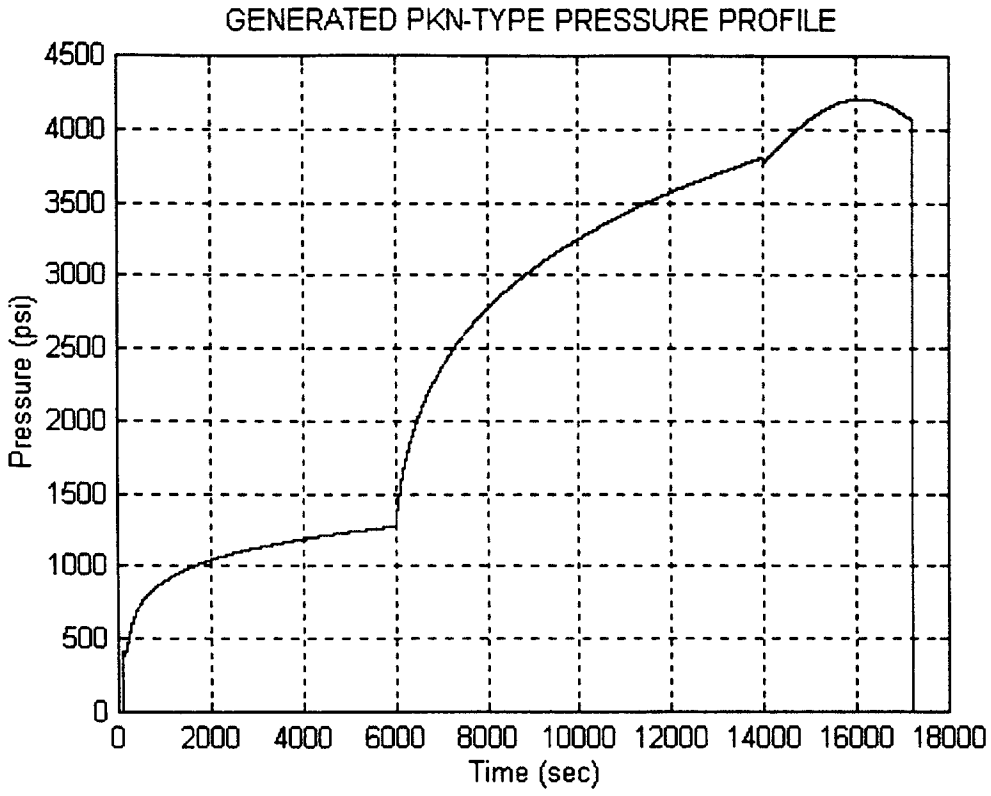

Fig. 5.11 Generated pressure profile for two different sets of parameters

The new set of normalized parameters for this profile are

$$\alpha'_{N1} = 5.8882e-7 \qquad \alpha'_{N2} = 3.208e-5$$
$$\beta'_{N1} = 1.2813e-5 \qquad \beta'_{N2} = 1.2813e-5$$

for

$$P_{\max} = 4207\ psi$$
$$q_{\max} = 7.9440\ m^3 / \min$$
$$t_{\max} = 283\ \min$$

Now we shall plot the results obtained by running the estimator algorithm for a forgetting factor equal to 0.96 because that was the one that gave the best results in our previous analysis when we used a single set of parameters. Figs. 5.12 and 5.13 show these results for the first 14000 sec.

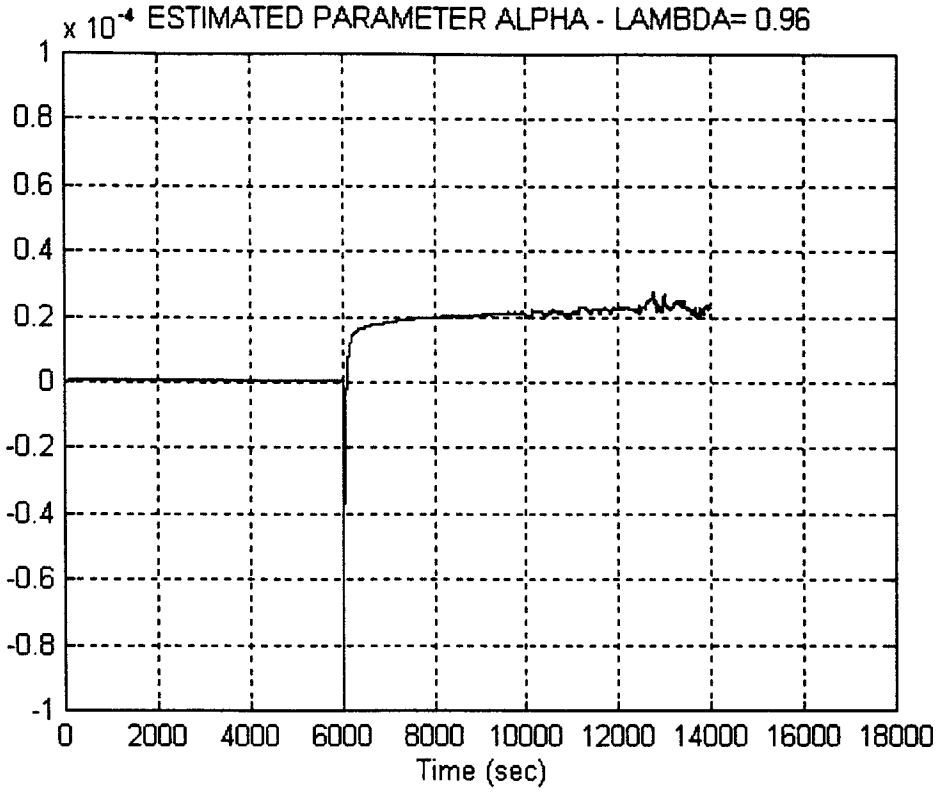

Fig. 5.12 Estimated parameter α_N for λ=0.96 for two different sets of parameters

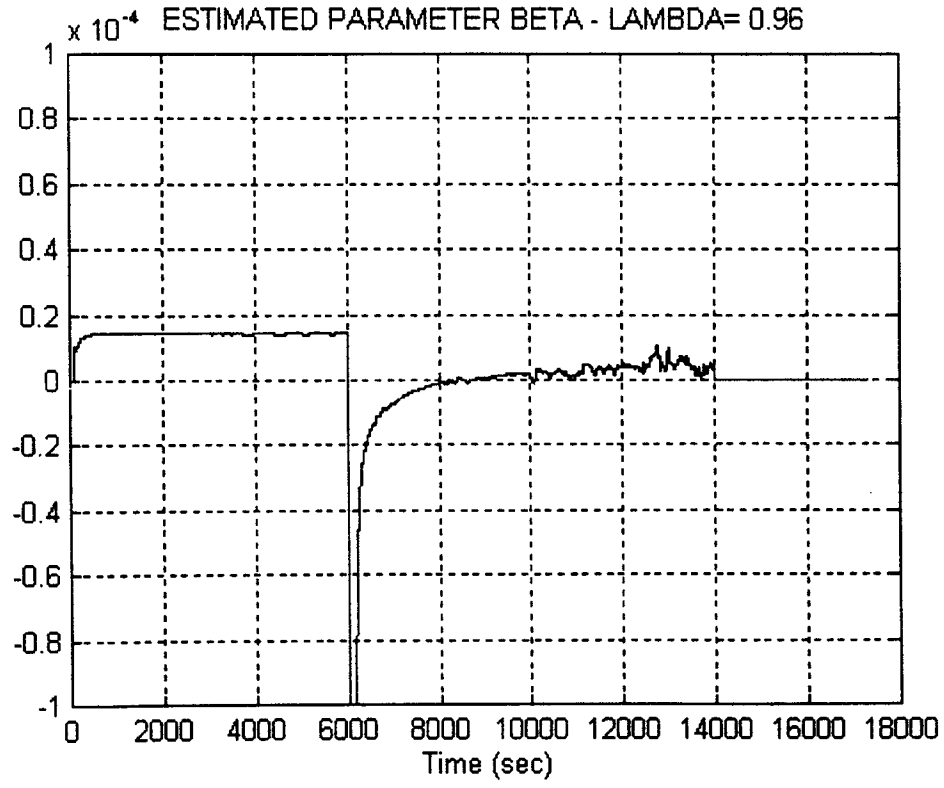

Fig. 5.13 Estimated parameter β_N for λ=0.96 for two different sets of parameters

It is not difficult to understand that the accuracy in the estimation of the first set of parameters (α_{N1}, β_{N1}) must be the same as it was for the single case. The fact that we are using a new set of normalizing values does not affect the convergence in the first case. Regarding the second set of parameters, we can see that they converge approximately to $\hat{\alpha}_N = 2.2e-5$, and $\hat{\beta}_N = 5e-6$. Even though we have not obtained the same accuracy for this case, we can see a tendency in the algorithm to converge to the exact parameters ($\alpha'_{N2} = 3.21e-5$, $\beta'_{N2} = 1.28e-5$) even when the sensitivity of the equation is very low at this point in the process.

Figs. 5.14 and 5.15 show the estimation of the parameters throughout the whole pressure profile. In any of these plots, we can see that the algorithm is able to detect a sudden change in the parameters by showing a peak of relatively large magnitude with respect to the order of magnitude of the parameters. These peaks are located at t=6000 and t= 14000 seconds respectively. This kind of pattern is very important in Fault Detection Diagnosis, and that is something that we expect to find when applying this algorithm to the field data.

In the next section, we will precisely apply this on-line estimation algorithm to the field data, and see whether or not it is able to show the signatures of a screenout fault.

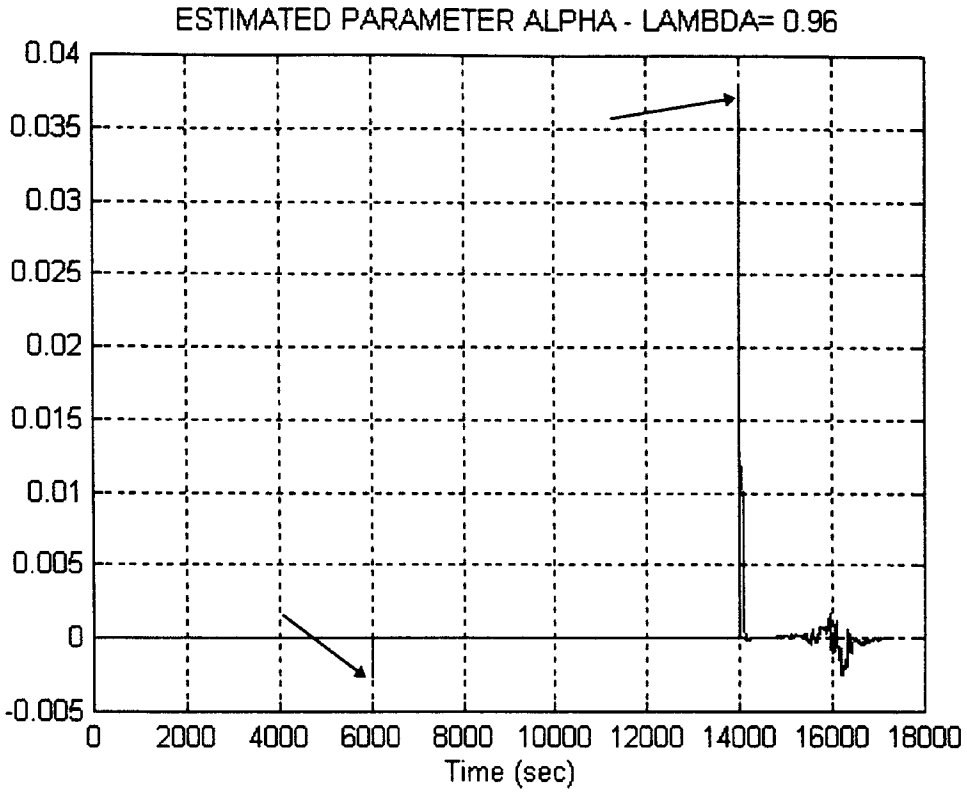

Fig. 5.14 Estimated parameter α_N for λ=0.96 for two different sets of parameters

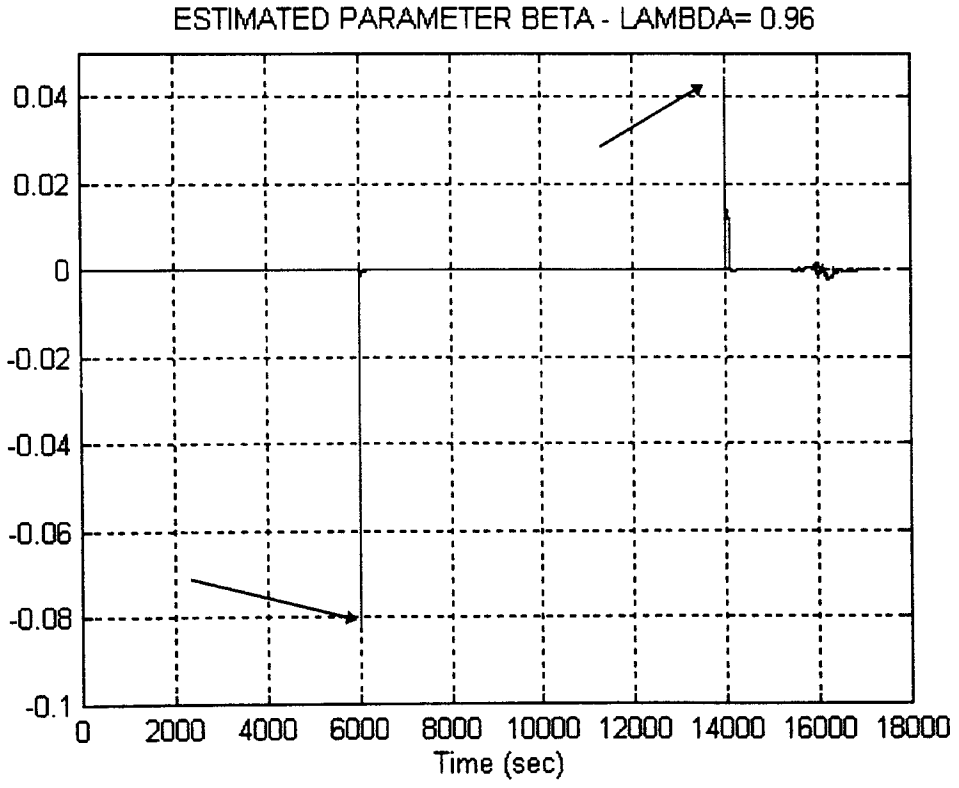

Fig. 5.15 Estimated parameter β_N for λ=0.96 for two different sets of parameters

Screenout Detection

In order to detect screenout in a real BHP profile, we shall use the same algorithm developed in the previous Section. The only modification will be the input pressure. In the previous section, we used the generated pressure profile as the input pressure for this algorithm. In this case, we shall use the field data profile that is shown in Fig. 5.16.

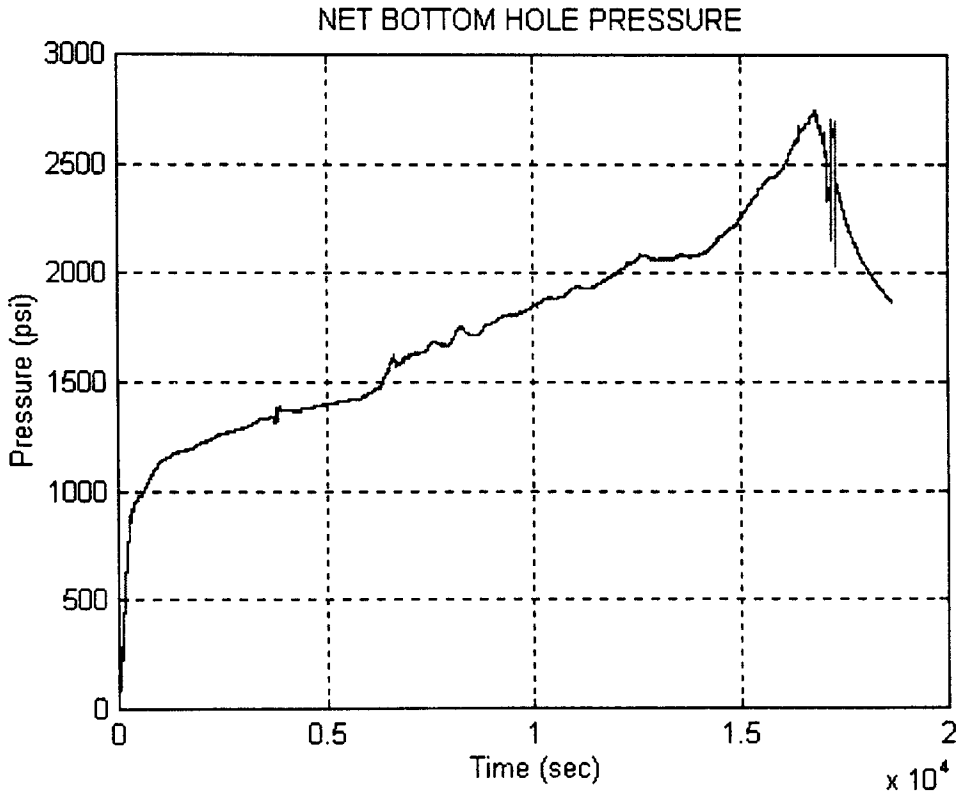

Fig. 5.16 Net Bottom Hole Pressure measured in the field

The above net Bottom Hole Pressure profile has been measured during the hydraulic fracturing of a well at approximately 9500 ft. This pressure profile shows a PKN-type behavior [15]. It also shows the so called screenout starting at approximately t= 14000 sec. At this time, the pressure started to increase, and the operators needed to shut down the process so as to avoid loosing the well. This shutdown is shown at

approximately t=16000 when the pressure starts to decrease very quickly. After this shut down, a clean up of the well was needed in order to save the process.

We are here interested in detecting sudden variations in the parameters when screenout occurs. If the proposed dynamic PKN model represents adequately the hydraulic fracturing process, the on-line estimator algorithm should be able to show these variations as this phenomenon has not been modeled in the dynamic equation. Success in detecting variations in these parameters will be very helpful for fault diagnosis purposes because the detection of this malfunctioning in the process could now be automated. Nowadays, only experienced field operators can diagnose screenout on-the-fly.

We applied the estimator algorithm (ONLINE.M) to the field data for a forgetting factor equal to 0.96 because that was the maximum value that produced a good match of the net BHP profile. Bigger values of the forgetting factor produce bigger BHP residuals. The simulation was run with the following normalizing values

$$P_{\max} = 2743 \text{ psi}$$
$$q_{\max} = 7.944 \text{ m}^3 / \text{min}$$
$$t_{\max} = 283 \text{ min}$$

Fig. 5.17 shows the estimated pressure profile, and Fig. 5.18 shows the BHP residual that is the result of subtracting the estimated BHP pressure from the net Bottom Hole Pressure profile. As we can see from both figures, we obtained a very good match of the BHP with a very low pressure residual. However, these residual does not provide conclusive information about the screen-out that starts at t=14000 sec.

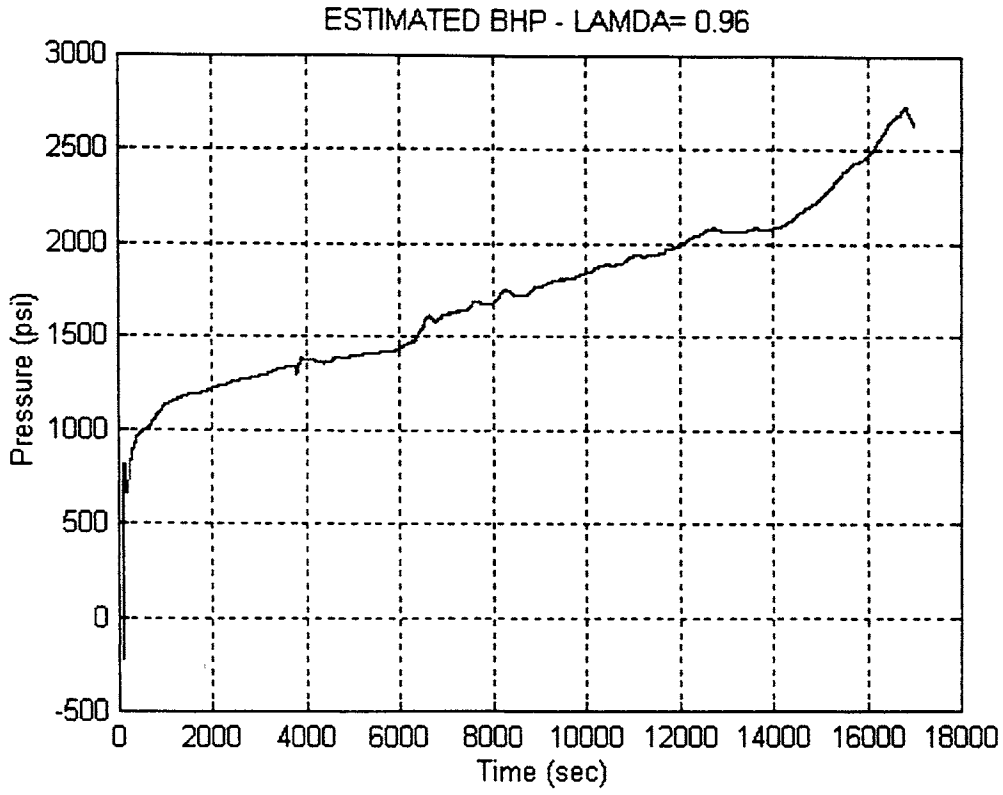

Fig. 5.17 Estimated net Bottom Hole Pressure for $\lambda = 0.96$

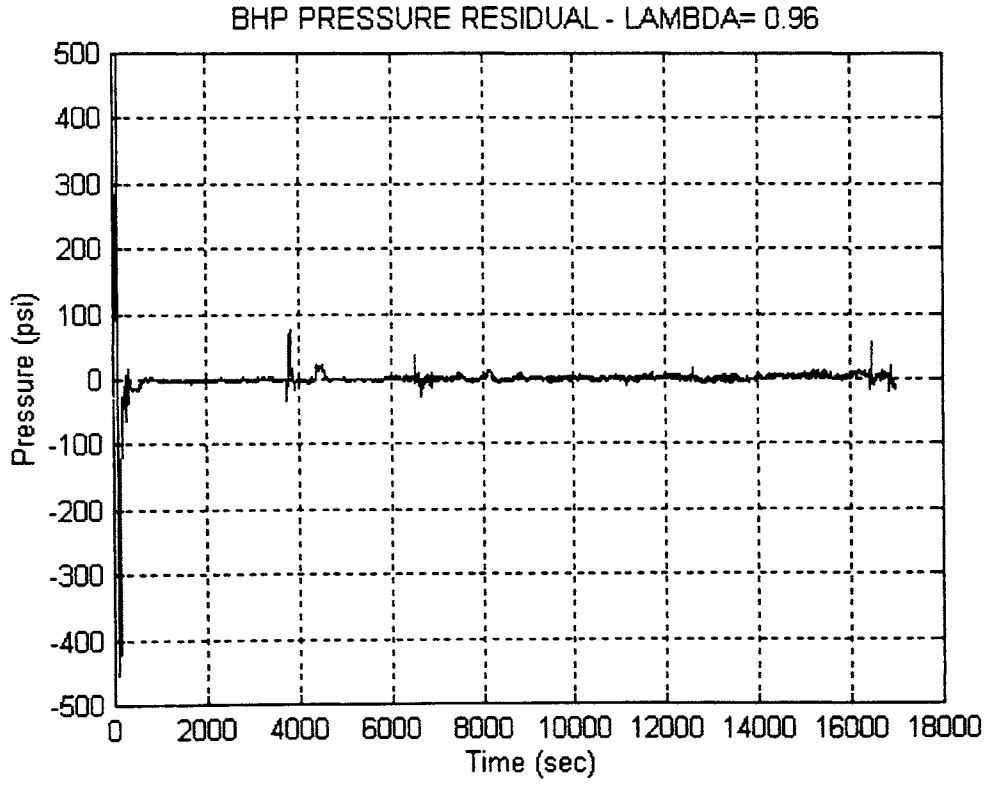

Fig. 5.18 Net Bottom Hole Pressure residual for $\lambda = 0.96$

Regarding the parameters' profiles (Figs. 5.19 and 5.20), we can also verify that no conclusive information can be obtained in this case either. The plots show a big change in their pattern at approximately t=3800 sec but it is due to a small perturbation in the measurement of the pressure profile. Nothing is shown at t=6000 sec when the proppant concentration is increased. Also, when screenout occurs at t=14000 sec, the estimator algorithm is not able to show this change in the process. Notice that some negative values are returned for both parameters, but this is not that important because we are here interested in detecting sudden variations in the parameters rather than the type of values themselves.

As we can see from both plots, the parameters show a high rate of variation. This may possibly indicate that the measurements are strongly affected by noise or that the forgetting factor should be made closer to one in order to reduce the sensitivity due to small perturbations. For these reasons, we shall filter out the measured pressure profile, and try different values of the forgetting factor.

In order to filter the BHP profile we will use a first order filter. The criterion to select such a filter shall be that it will eliminate most of the unwanted noise without either distorting the pressure profile or introducing unmodeled errors into the system. This filter will have the following Laplace transfer function

$$\frac{FP(s)}{P(s)} = \frac{a}{s+b} \tag{5.21}$$

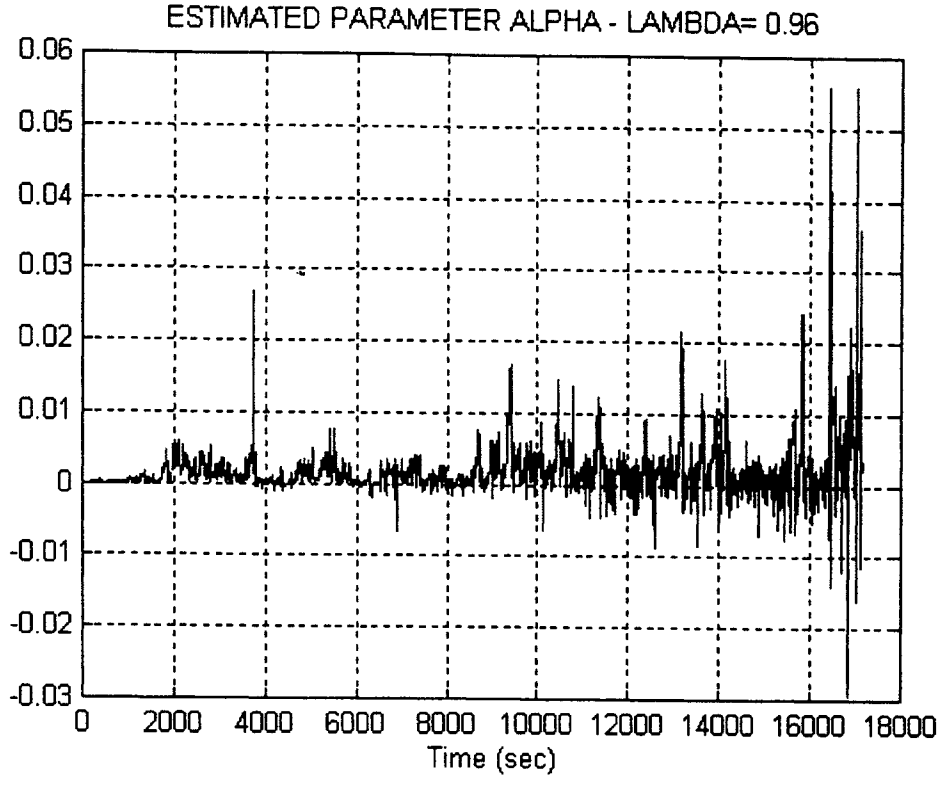

Fig. 5.19 Parameter α_N for λ=0.96 for the net BHP

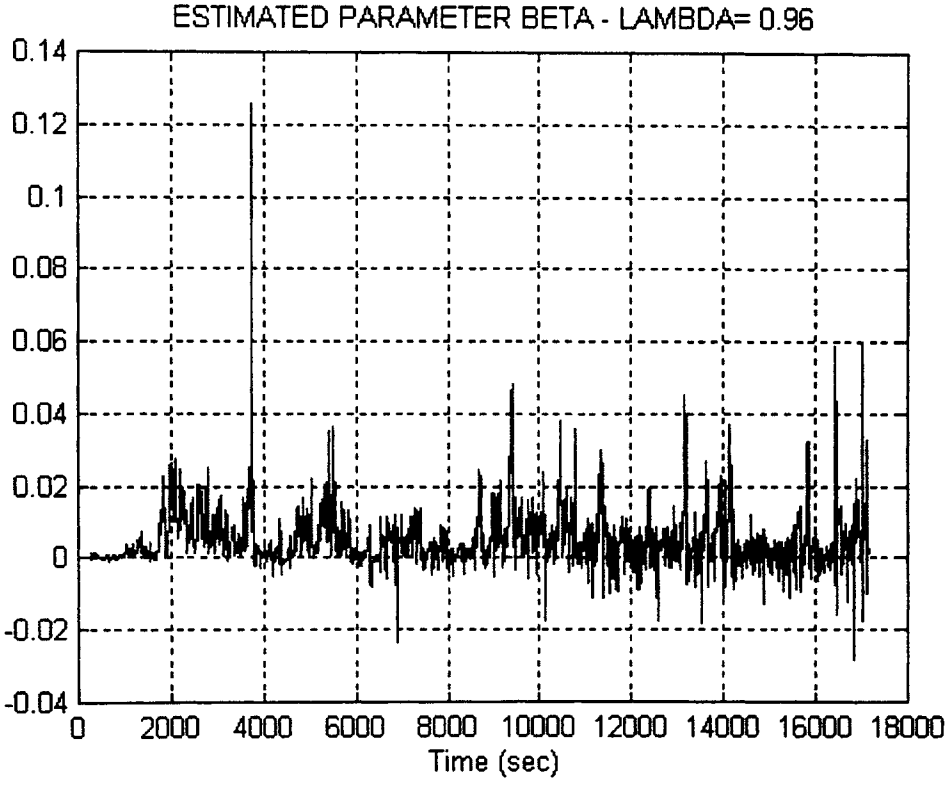

Fig. 5.20 Parameter β_N for λ=0.96 for the net BHP

In order to keep a DC gain equal to one, we shall make a equal to b. After a series of tests, the best pair of values found were a=b=0.1. Figs. 5.21 to 5.24 show the results obtained for this set of values and for different values of the forgetting factor.

Fig. 5.21 shows the parameter α_N for six different values of the forgetting factor. This plot shows that values of λ close to one do not provide much information about the change in the proppant schedule nor the screen-out phenomenon. However, a value of λ equal to 0.9990 shows a clear variation of α_N at t=6000 sec and t=14000 sec respectively. We observe the same pattern in Fig. 5.22 regarding the parameter β_N. These sudden changes in the behavior of these parameters could be used to activate some alarms to indicate a change in the process.

However, we must still be able to distinguish between a desirable change, such as the change in the proppant concentration, and an undesirable one such as the unwanted screenout phenomenon. None of these parameters, in the way they are presented, will be useful for this purpose so, in order to be able to distinguish among these different events, we also estimated the pressure profiles obtained for the corresponding parameters α_N and β_N. shown in Figs. 5.20 and 5.21. These results are plot in Figs. 5.23 and 5.24.

Fig. 5.23 shows the estimated BHP profile corresponding to the above tested values of the forgetting factor. In this case we can see that a value of λ equal to 0.9995 provides the best pressure residual (Fig. 5.24) without affecting the detection of screenout. In this case we can better distinguish the changes at t =6000 sec and at t = 14000 sec respectively.

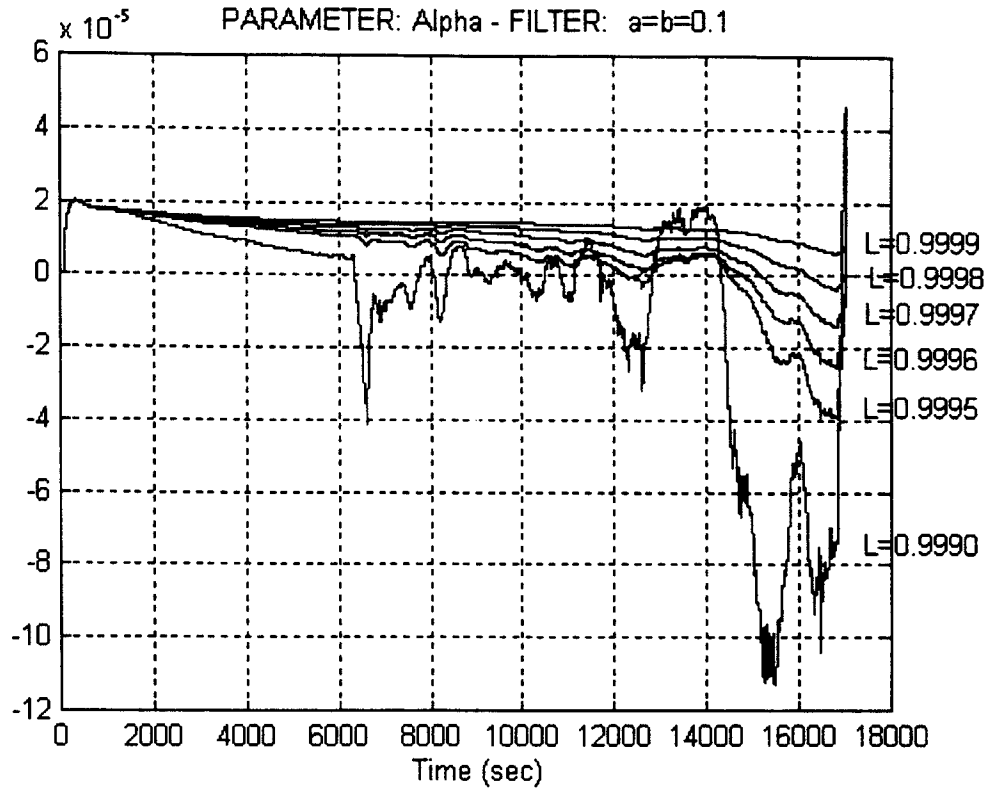

Fig. 5.21 Parameter α_N for various forgetting factors

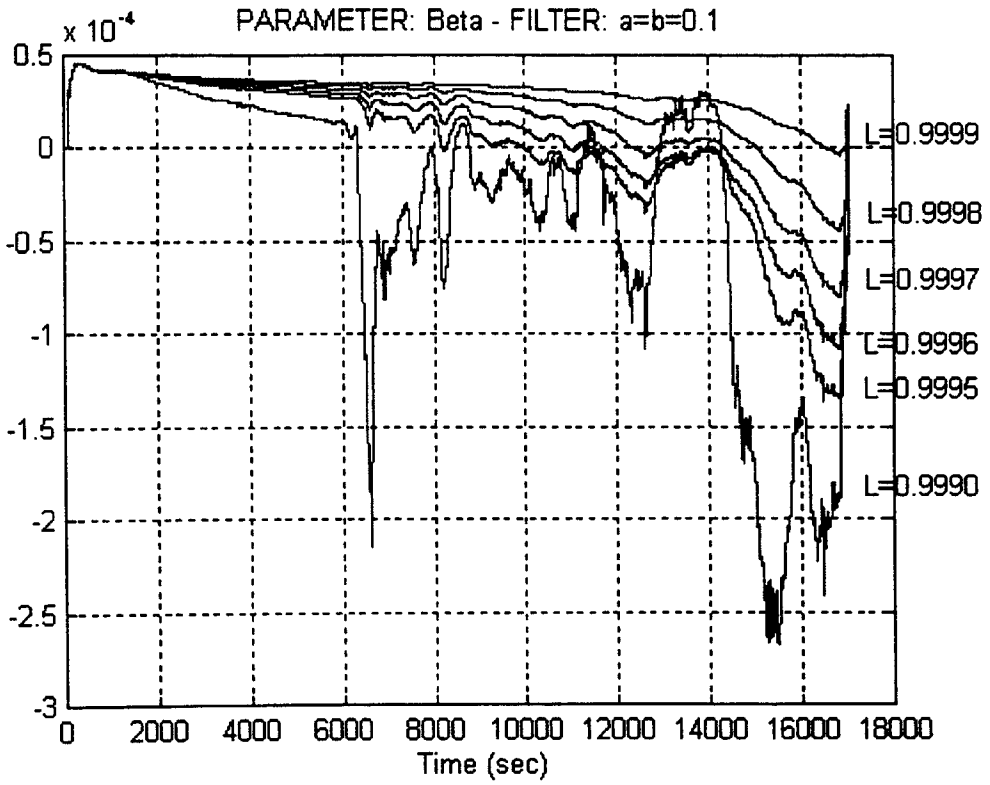

Fig. 5.22 Parameter β_N for various forgetting factors

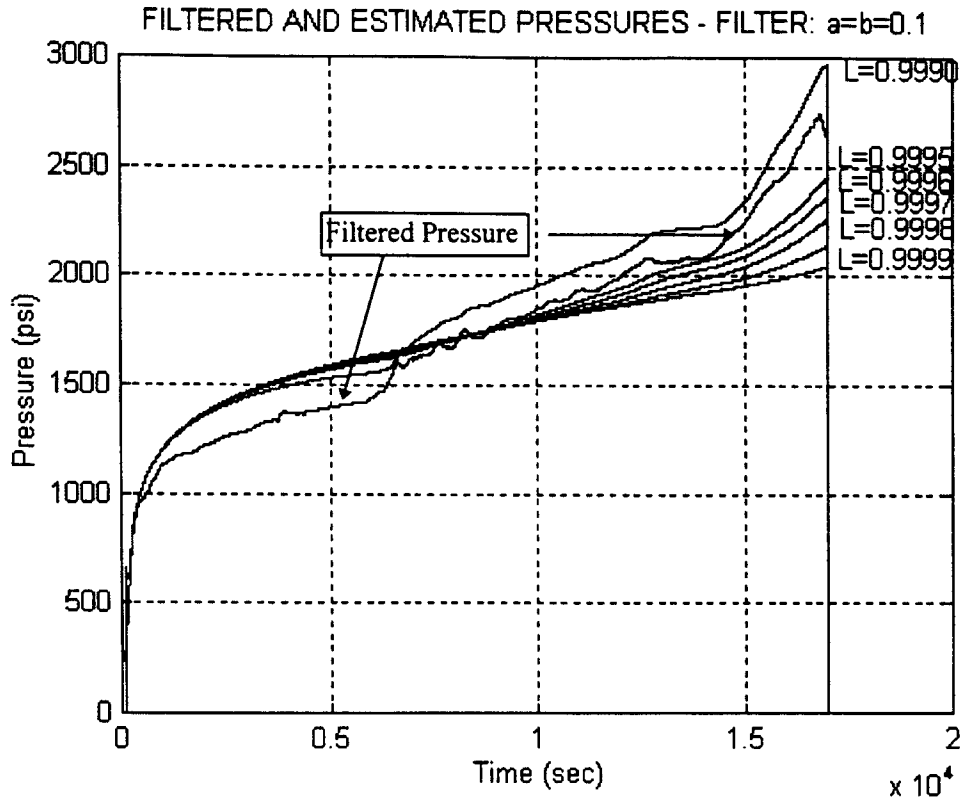

Fig. 5.23 Filtered and estimated Pressure residuals for different λ's

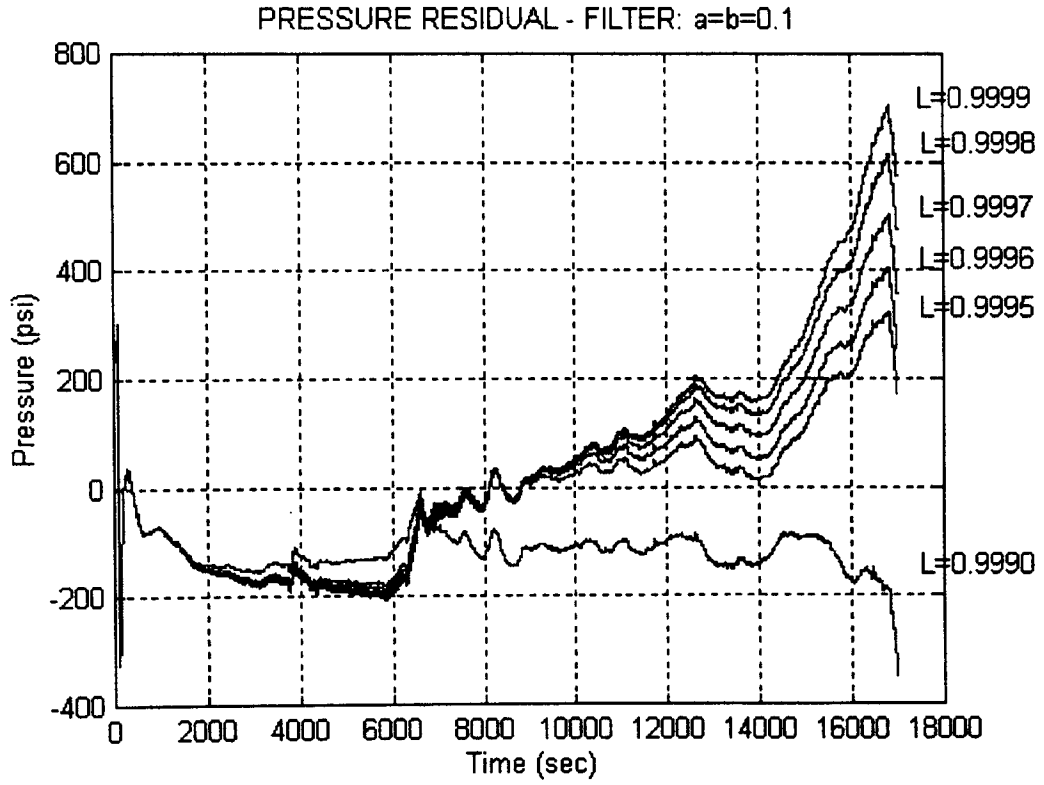

Fig. 5.24 Pressure residuals for different λ's

In order to get clearer indications of the different situations that we are handling in this case, we shall combine the above plots together, and see whether or not they show some relationship with each other when the change in proppant concentration and screenout occur. Figs. 5.25 and 5.26 depict this situation for a forgetting factor equal to 0.9990 which was the value that provided the best results in this case. Similar results for other values of the forgetting factor are shown in Appendix C.

Fig. 5.25 shows the plot of α_N vs. β_N, indicating the instant of time when the change of proppant concentration and screenout occur. We can see from this plot a strong correlation between both parameters. This correlation varies slightly when the change of proppant concentration (t = 6000 sec) and screenout (t = 14000 sec) occur. However they are not showing distinctive changes that could help to characterize them.

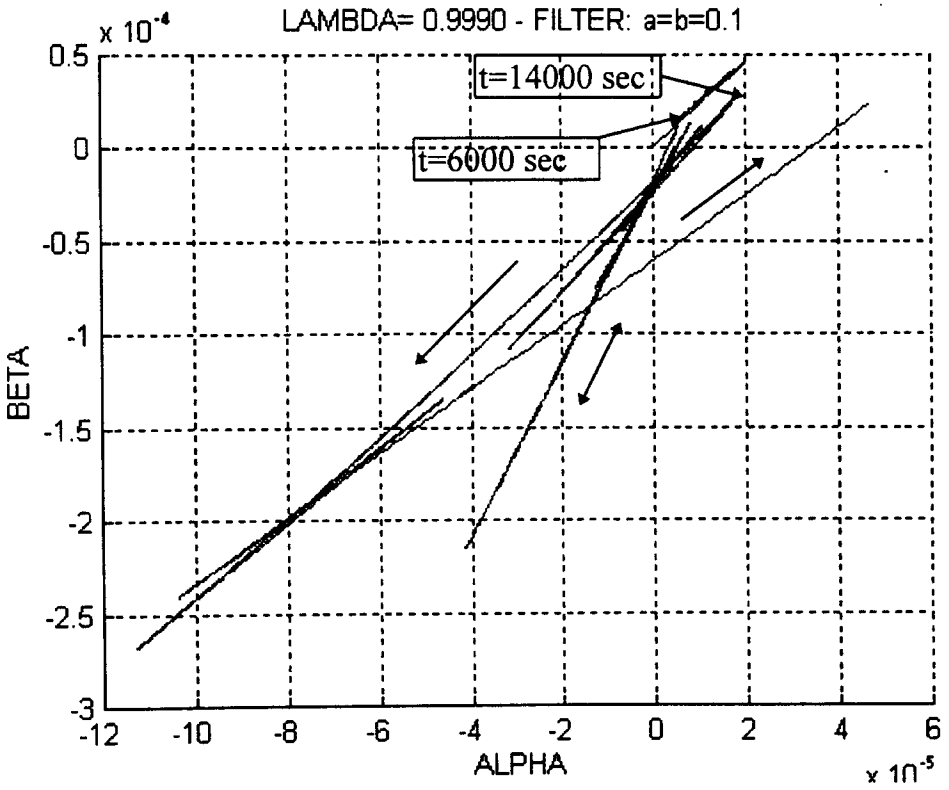

Fig. 5.25 α_N versus β_N for λ=0.9990

Fig. 5.26 shows the plot of α_N vs. the Pressure Residual. As it was the case for the previous figure, we can see here distinctive peaks starting at t = 6000 sec and t = 14000 indicating a change in the process. We see that the change in the vector α_N-Pressure Residual is bigger than any other in this plot. This peak could be used to activate an alarm warning the operators about a possible screenout. However we can not neglect the other peak occurring at t = 6000 sec that may also activate the same alarm.

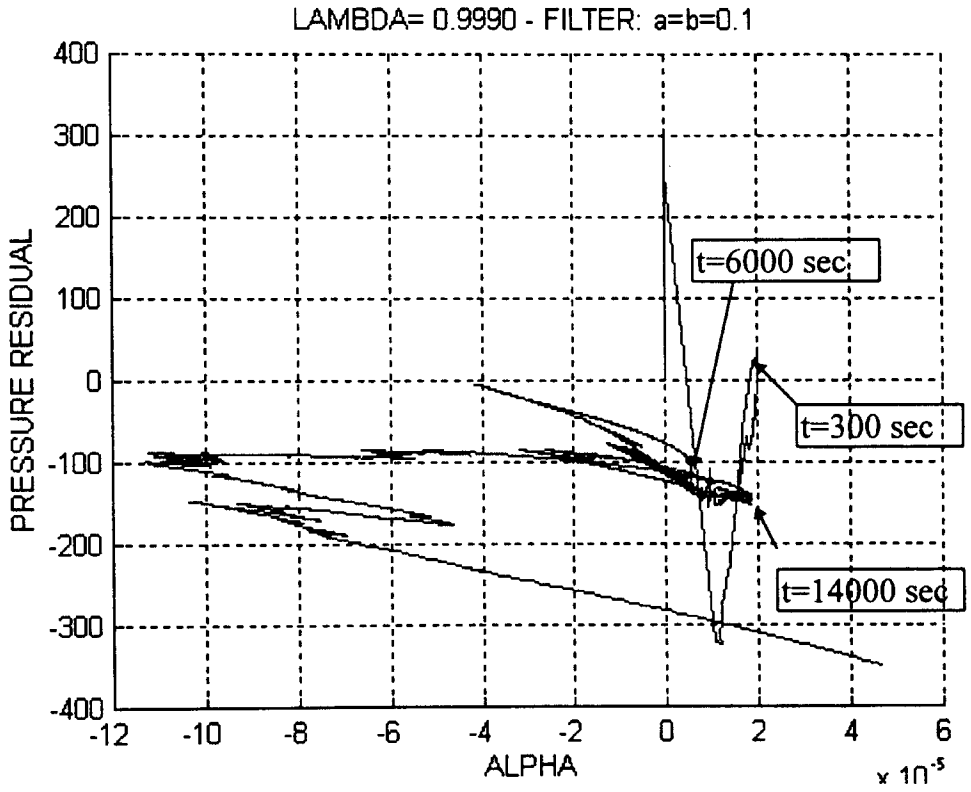

Fig. 5.26 α_N versus Pressure residual for λ=0.9990

Taking into account the above reasons, we see the need to rely on additional information to help distinguishing between these two events. Recall that the change occurring at t= 6000 sec is related to change in proppant concentration, and as such it modifies the density of the fracturing fluid. The measurement of the fracturing fluid's

density is also available in the output data. From Appendix B, we can notice a change in density from stage 5 to stage 6. This fact could be of relevant importance because we could correlate the event occurring at t=6000 sec with the change in density, and, in this way, be able to identify this event.

CHAPTER 6

RESULTS AND ANALYSIS

Throughout this work, we focused our attention on developing dynamic models, and an estimation algorithm that could help us to detect the so-called screenout phenomenon.

By working under the same premises proposed by the classical 2-D models, we developed their equivalent dynamic models. These models calculated the resulting pressure of the process having as their main input the input Slurry Rate pumped into the formation. Other involved parameters such as the fracturing fluid's viscosity parameters, the fluid loss coefficient, the in-situ stress, and the shear rate have also been added into these models. All of them were lumped into unique parameters, α and β.

We also developed both off-line and on-line estimation algorithms for the generated PKN-type pressure profile that served as a test case to improve our estimation algorithms. These algorithms showed a reasonable convergence to the exact generated parameters when the models did not take into account unmodeled errors. But they did not prove to be very reliable in the presence of unmodeled errors. We observed this divergence when we tried to estimate the generated PKN-type pressure profile's parameters by applying the on-line estimation algorithm. It was clear here that the proposed algorithm could not perform very well in the presence of unmodeled errors. However, this algorithm proved to provide convergent parameters when no random disturbances were added on top of the generated profile.

Finally, we applied the resulting estimation algorithm to a real case expecting to detect some distinctive patterns in the behavior of the equation's parameters when changes in the process occurred. In this case the model showed significant changes in the behavior of the parameters (α_N, and β_N) and the pressure residual when the proppant concentration and screenout occurred. However, we were not able to distinguish very clearly between the events happening in both cases. These results proved the necessity to rely on additional information in order to correlate these changes with the variation of other fracture related parameters as maybe the case of the fracturing fluid's density.

Despite of the lack of conclusive results, we believe that this model still provided some valuable information about particular events occurred in this process such as screenout. As it was the main concern of this research, we were satisfied with the results obtained in this work up to this point. Further research should take into account some of the limitations of this work.

One of the limitations of this model was the assumption that we had a fixed height. We assumed this condition as a first step towards developing a dynamic model but nothing in the provided field data indicated so.

Another factor that must be also taken into account is that we applied linear estimation techniques to a model that presented unmodeled errors. We did so because there is almost no research in system identification techniques regarding unmodeled errors nor nonlinear systems, and this work was aware of these limitations from the beginning of this research.

Finally recall that we have not modeled other variables that may affect the hydraulic process. These omissions certainly introduced unmodeled errors that affected the accuracy in the estimation, and made the screenout detection more difficult.

CHAPTER 7

CONCLUSIONS

The models developed in Chapter 4 are physically based models that, given a definite set of commonly used parameters, as the ones used in the field, calculate pressures and geometry in the same order of magnitude as the ones measured in real life. This fact indicates that these dynamic models still modelate the hydraulic process to some extent.

For the reasons explained above, we can verify that the additional assumptions, such as the assumption of the pressure distribution along the fracture, did not undermine significantly the solution of these dynamic models.

The results obtained in this work indicate that the proposed dynamic model is able to detect some changes in the behavior of the net BHP

The results also indicated that the availability of the fracturing fluid's density profile might be very helpful in identifying the change in the proppant concentration during the process. In this way, the isolation and detection of the screenout fault would be better accomplished.

CHAPTER 8

FUTURE RESEARCH

As suggested research about this work, I can recommend the following:

1. Apply a nonlinear estimation technique to overcome the problems presented for the unmodeled errors.
2. Incorporate additional considerations into the model such as to allow the models to grow in the vertical direction.
3. Correlate the fracturing fluid's density with the obtained parameters in order to identify one of the causes of the sudden changes in the behavior of the net BHP.

REFERENCES

1. Veatch Jr., R.W. et al., An Overview of Hydraulic Fracturing, Monograph Series, SPE, V.12, pp.1-38, 1989.

2. Daneshy, A., Proppant Transport, Monograph Series, Monograph Series, SPE, V.12, pp 210-22, 1989.

3. Geertsma, J., Two-Dimensional Fracture-Propagation Models, Monograph Series, SPE, V.12, pp.81-94, 1989.

4. Daneshy, A. A., On the Design of Vertical Hydraulic Fractures, JPT, pp.83-93, Jan 1973; Trans, AIME, 255

5. Perkins, T.K. and Kern, L.R., Widths of Hydraulic Fractures, JPT, pp.937-949, September 1961; Trans, AIME, 222.

6. Geertsma, J and de Klerk, F.A., A Rapid Method of Predicting Width and Extent of Hydraulically Induced Fractures, JPT, pp.1571-1581, Dec 1969; Trans, AIME, 246.

7. Nordgren, R.P., Propagation of a Vertical Hydraulic Fracture, Society of Petroleum Engineers Journal, pp.306-314, Aug 1972; Trans, AIME, 253.

8. Sneddon, I.N. and Elliot, H.A., The Opening of a Griffith Crack Under Internal Pressure, Quarterly of Applied Mathematics, V.4, pp.262, 1946.

9. Khristianovic, S.A. and Zheltov, Y.P., Formation of Vertical Fractures by Means of Highly Viscous Fluid, Proc., Fourth World Pet. Cong., V.II, pp.579, 1955.

10. Barenblatt, G.I., Mathematical Theory of Equilibrium Cracks, Advances in Applied Mechanics, V.7, pp.55, 1962.

11. Cameron, J.R., and Prud'homme, R.K., Fracturing-Fluid Flow Behavior, Monograph Series, SPE, V.12, pp.177-209, 1989.

12. Paulsen, D.K., Fracturing Net Pressure Analysis for Variable-Rate Injection, paper SPE 23434, SPE Eastern Regional Meeting, Lexington, KY, pp.49-64, Oct1991.

13. Paulsen, D.K., Net Pressure Fracture Design, paper CIM/SPE 90-42, International Technical Meeting, Calgary, pp. 1-21, June 1990.

14. Ljung, L, System Identification, Prentice Hall, Inc., pp.305-07, 1987.

15. Nolte, K.G. and Smith, M.B., Interpretation of Fracturing Processes, JPT, pp.1767-75, Sept. 1981

16. Warpinsky, N.R. et al., Comparison Study of Hydraulic Fracturing Models - Test Case: GRI Staged Field Experiment No. 3, SPE, pp.7-16, Feb. 1994.

17. Clifton, R.J., Three-Dimensional Fracture-Propagation Models, Monograph Series, SPE, V.12, pp.95-108, 1989.

APPENDIXES

APPENDIX A

MATLAB M-FILES

```
% PK.M
% This program generates a PK pressure profile using the
% PK difference equation for a given set of parameters
% indicated in this file:
%
%                P = PK(SLR)
%
% where P is the generated pressure (psi); and SLR is the
% input Slurry Rate (bpm).

function P = pk(SLR)

SLR= SLR(1:18700,1);

% Process parameters
Kl= 0.00046;          % Over all fluid-loss coefficient [m/min^.5]
G= 1.45e6;            % shear rate [psi]
v= 0.20;              % Poisson's ratio
n= 0.715;             % Power-law flow behavior index
K= 0.00056/60^n;      % Power-law consistency index [psi*min^n]
h= 39;                % height of the fracture [m]

% Calculate the lumped parameters alpha and beta
a= 16*K/pi*( (4*n+2)/n )^n* (G^2/h^3/(1-v)^2)^(n+1)
b= 8*G*Kl/pi/h/(1-v)

P= zeros(17200,1);

% Sampling period
deltam= 1/60;         % [min]
DELTA=1;

% Initializing sampling time
tk= 0;

% Initial guess for the pressure
P(100)= 85;
t1=clock;
for i=101:17199

        % Get the Slurry Rate
        q = SLR(i-1)*0.16;
        tk= tk + DELTA;
        if i < = 14000
        P(i)= [a b] * [q^(n+1)/P(i-1)^(2*n+2) -1/sqrt(tk/60)]'*deltam+ P(i-1);

% Generate a sine plot
        else
                P(i)= 400 *sin(2*pi/8000*(tk-14000)) + P(14000);
        end
end
etime(clock,t1)
figure(3)
plot(P),grid
```

```
% FILE: OFFLINE.M
% This file computes the ordinary difference equation's parameters in
% an off-line fashion.  It uses a triangular weighting factor.  The syntaxis is:
%
%                [A,B]= offline(PK,SLR,N)
%
% where A and B represent the returned parameters alpha, and beta;
% PK is the input pressure profile (psi), SLR is the input Slurry Rate (bpm),
% and N is the number of samples (sec).


function [A,B]=offline(PK,SLR,N)

T= triang(28000);
w=T(14001:28000);

% Power-law flow behavior index
n= 0.715;

% Sampling period
delta= 1/60;              % [min]

% Normalizing values
pmax= 1541;               % [psi]
qmax= 49.65*0.16;         % [m^3/min]
tmax= 14000/60;           % [min]

a=0;
b=0;
c=0;
d=0;
e=0;
f=0;

% Get the initial values for the input flow rate and pressure
q_1=SLR(100)*0.16/qmax;                 % [m^3/min]
p_1=PK(100)/pmax;                       % [psi]

t1=clock;
for i=101:N                             % i represents [sec]
                                        % It must be transformed to [min]
        p=PK(i)/pmax;
        q=SLR(i)*0.16/qmax;
        tk_1= (i-100)/60/tmax;

        a= a + w(i)*(q_1/p_1^2)^((n+1)*2);
        b= b + w(i)*(q_1/p_1^2)^(n+1)/sqrt(tk_1);
        c= c + w(i)*(q_1/p_1^2)^(n+1)*(p - p_1);

        d= d + w(i)*(q_1/p_1^2)^(n+1)/sqrt(tk_1);
        e= e + w(i)* 1/tk_1;
        f= f + w(i)*(p - p_1)/sqrt(tk_1);

        p_1=p;
```

```
        q_1=q;
end
t=etime(clock,t1)

b=-b;
e=-e;

% Solution of the linear equations
dt=det([a b;d e]);
A=det([c b;f e])/dt;
B=det([a c;d f])/dt;
```

```
% PK1.M
% This program generates a PK pressure profile using the
% PK difference equation for a set of vector parameters
% A and B.
%
%                P = PK1(SLR,A,B)
%
% where P is the generated pressure (psi), and SLR is the
% input Slurry Rate (bpm).  The parameters A and B are normalized.

function P = pk1(A,B)

SLR= SLR(1:18700,1);

% Power-law flow behavior index
n= 0.715;

% Normalizing values
delta= 1/60;                    % Sampling period [min]
pmax= 2743                      % [psi], BHP
qmax= 49.65*0.16;               % [m^3/min]
tmax= 17000/60;                         % [min]

% Denormalizing parameters A and B
A= A*pmax^(2*n+3)/qmax^(n+1)/delta;
B= B*pmax*sqrt(tmax)/delta;

P= zeros(17200,1);

% Initializing sampling time
tk= 0;

% Initial guess for the pressure
P(100)= 85;

t1=clock;
for i=101:17000

        % Get the Slurry Rate
        q = SLR(i-1)*0.16;
        p=P(i-1);

        tk= tk + DELTA;

P(i)= [A(i) B(i)] * [(q/p^2)^(n+1) -1/sqrt(tk/60)]'*delta + P(i-1);

end
etime(clock,t1)

figure(3)
plot(P),grid
```

```
% FILE: SENS.M
% This file computes the sensitivity values for ALPHA and BETA for
% the PK type dynamic model.
%
%                [SA,SB]= SENS(PK, SLR,A,B)
%
% where SA, and SB return the sensitivity vectors for ALPHA and
% BETA; PK and SLR are the pressure (psi) and input flow rate process (bpm)
% vector profiles, and A, and B are the correspondent scalar values
% for the parameters ALPHA, and BETA.

function [SA,SB]= sens(PK, SLR,a,b)

SA= zeros(17200,1);
SB= zeros(17200,1);

% Power-law flow behavior index
n= 0.715;

% Normalizing parameters
delta= 1/60;                    % [min]
pmax= 1541;                     % [psi]
qmax= 49.65*0.16;               % [m^3/min]
tmax= 14000/60;                 % [min]

% Normalization of the parameters ALPHA and BETA.
A= a*qmax^(n+1)/pmax^(2*n+3)*delta;
B= b/pmax/sqrt(tmax)*delta;

t1=clock;
for i=101:14000                 % i represents [sec]
                                        % It must be transformed to [min]

        p= PK(i)/pmax;          % [psi]
        q= SLR(i)*0.16/qmax;    % [m^3/min]
        tk_1= (i-100)/60/tmax;  % [min]

        sa= 1-B/A*(p^2/q)^(n+1)/sqrt(tk_1)+1/A*(p^2/q)^(n+1)*p;
        sb= 1-A/B*(q/p^2)^(n+1)*sqrt(tk_1)-1/B*sqrt(tk_1)*p;
        SA(i)= 1/sa;
        SB(i)= 1/sb;
end
t=etime(clock,t1)

plot(SA),grid,
pause
plot(SB),grid
```

```
% FILE: ONLINE.M
% This file calculates the parameters of the PK-type
% model in an on-line fashion.
%
%       [A,B]= online(PK, SLR,LAMBDA,N)
%
% where A, and B return the vector process parameters
% alpha, and beta; PK and SLR are the pressure (psi) and
% input flow rate (bpm) profiles of the process, LAMBDA
% is the forgetting factor, and N is the number of samples (sec).

function [A,B]=online(PK, SLR,LAMBDA,N)

% Process parameters
n= 0.715;                       % Power-law flow behavior index
Kl= 0.00046;                    % Overall fluid loss coefficient [m/min^.5]
G= 1.45e6;                      % Shear rate [psi]
v= 0.20;                        % Poisson's ratio
K= 0.00056/60^n;                % Power-law consistency index [psi*min^n]
h= 39;                          % heigth of the fracture [m]
delta= 1/60;                    % Sampling period [min]

pmax= 2743;                     % [psi], BHP
qmax= 49.65*0.16;               % [m^3/min]
tmax= 17000/60;                 % [min]

theta= zeros(2,17200);
R= zeros(2,2);
F= zeros(2,1);

% Get the initial values for the input flow rate and pressure

q_1=SLR(100)*0.16/qmax;         % [m^3/min]
p_1=PK(100)/pmax;               % [psi]

% Compute the initial estimates for P and theta
for i=101:110

        q= SLR(i)*0.16/qmax ;   % [m^3/min]
        p= PK(i)/pmax;          % [psi]

        phi1= (q_1/p_1^2)^(n+1);
        phi2= -1/sqrt((i-100)/60/tmax);
        phi = [phi1 phi2]';
        R= R + phi*phi';
        F= F + phi*(p - p_1);

        p_1= p;
        q_1= q;
end

P=inv(R);
th= P * F;
```

```
% Running the recursive algorithm now

t1=clock;
for i=111:N                          % i represents [sec]
                                     % It must be transformed to [min]
        p=PK(i)/pmax;
        q=SLR(i)*0.16/qmax;
        tk_1= (i-110)/60/tmax;

        phi1= (q_1/p_1^2)^(n+1);
        phi2= -1/sqrt(tk_1);
        phi=[phi1 phi2]';

        L= P*phi/(LAMBDA + phi'*P*phi);
        th= th + L*(p - p_1 - phi'*th);
        P= (P - (P*phi*phi'*P)/(LAMBDA + phi'*P*phi))/LAMBDA;

        theta(:,i)=th;

        p_1=p;
        q_1=q;

end
t=etime(clock,t1)

A= theta(1,:);
B= theta(2,:);

figure(1)
plot(A),grid
figure(2)
plot(B),grid
```

APPENDIX B

JOB SCHEDULE

Customer:
Well Desc: 3-3
Formation: COTTON VALLEY LIME

Date: MARCH 16, 1993
Ticket #: 30108700
Job Type: VERSAGEL HT FRAC

JOB SCHEDULE

STAGE INFORMATION

	1	2	3	4	5	6	7
Fluid Type	Gel (Lord)	Gel (Lord)	Gel (Lord)	Gel (Lord)	Gel (Lord)	Gel (Lord)	Gel (Lord)
Planned Clean Volume (gal)	2000	6000	15000	210000	175000	80000	58000
Planned Slurry Volume (gal)	2000	6000	15000	210000	199505	95005	70230
Actual Slurry Volume (gal)	1257	5701	12339	209884	198520	94436	52705
Base Fluid Density (lb/gal)	15.00	15.00	15.00	9.00	8.28	8.31	8.34
n'	0.7150	0.7150	0.7150	0.4100	0.4100	0.4100	0.4100
K' (#s**n/ft2)	0.000560	0.000560	0.000560	0.037500	0.037500	0.037500	0.037500
Proppant Size					20/40	20/40	20/40
Proppant Type					Resin-coat	Resin-coat	Resin-coat
Abs. Proppant Volume (gal/lb)	0.04530	0.04530	0.04530	0.00000	0.04689	0.04689	0.04689
Planned Fluid Rate (bpm)	6.00	6.00	20.00	45.00	45.70	47.00	47.00
Starting Prop Conc (lb/gal)	0.00	0.00	0.00	0.00	2.00	4.00	4.00
Ending Prop Conc (lb/gal)	0.00	0.00	0.00	0.00	4.00	4.00	5.00

	8	9
Fluid Type	Gel (Lord)	Gel (Lord)
Planned Clean Volume (gal)	50000	10926
Planned Slurry Volume (gal)	61723	10926
Actual Slurry Volume (gal)	34	10888
Base Fluid Density (lb/gal)	8.34	9.50
n'	0.4100	0.7150
K' (#s**n/ft2)	0.037500	0.000560
Proppant Size	20/40	
Proppant Type	Resin-coat	
Abs. Proppant Volume (gal/lb)	0.04689	0.00000
Planned Fluid Rate (bpm)	47.00	45.00
Starting Prop Conc (lb/gal)	5.00	0.00
Ending Prop Conc (lb/gal)	5.00	0.00

Customer:
Well Desc: 3-3
Formation: COTTON VALLEY LIME

Date: MARCH 16, 1993
Ticket #: 30108700
Job Type: VERSAGEL HT FRAC

WELLBORE CONFIGURATION

Wellbore Segment Number	Actual Length (feet)	TVD (feet)	Casing ID (inch)	Casing OD (inch)	Tubing ID (inch)	Tubing OD (inch)
1	11731	11731	4.778	5.500	0.000	0.000

PERFORATIONS DATA

NO DATA ENTERED FOR THIS REPORT

PERFORATED INTERVALS

FROM (feet)	TO (feet)	SPF
9480	9578	1

Customer:
Well Desc: 3-3
Formation: COTTON VALLEY LIME

Date: MARCH 16, 1993
Ticket #: 30108700
Job Type: VERSAGEL HT FRAC

MISCELLANEOUS JOB PARAMETERS

Well Treated Down		Casing	
Static Column Available		No	
Gel System		VERSAGEL HT	
Delayed Crosslinker Used		Yes	
Surface Earth Temperature		80.0	(deg. F)
Surface Slurry Temperature		60.0	(deg. F)
Bottom Hole Treating Temp		120.0	(deg. F)
Initial Bottom Hole Pressure		5500	(psi)
Wellbore Fluid Density		8.33	(lb/gal)
Wellbore Fluid n'		1.0000	
Wellbore Fluid K'		0.000018	(#s**n/ft2)
Volume used for Stage Info		Slurry	
Rheology Unit Fluid Type		Base Gel	
n',K' for Friction		Book Values	
RS232 Input Type		Generic	
RS232 Setup -	Port	TTA3	
	Baud Rate	1200	
	Parity	N	
	Data Bits	8	
	Stop Bits	1	
Data Signal -	Record Length	49	
	Terminator Char	10	
	Index	15	
	Index	25	

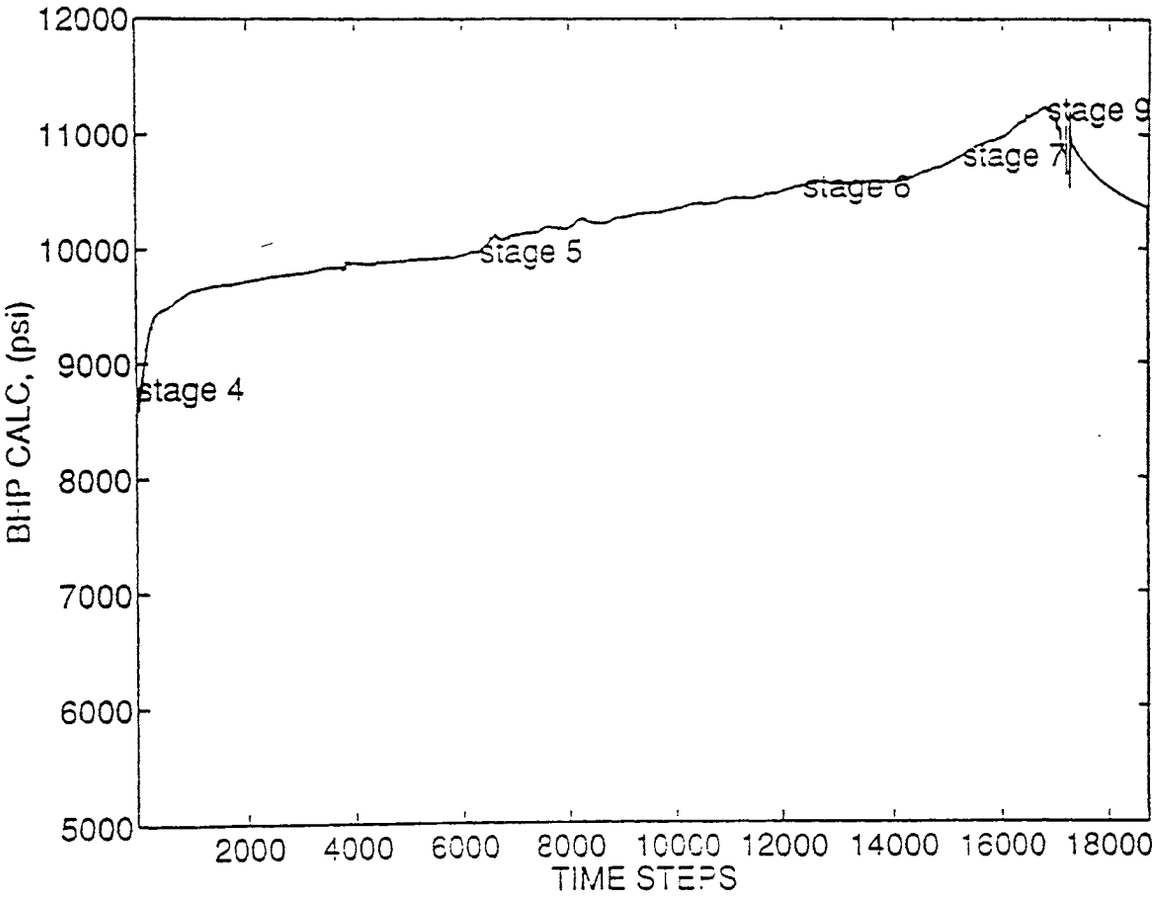

Fig. B-1. Bottom hole pressure profile (psi)

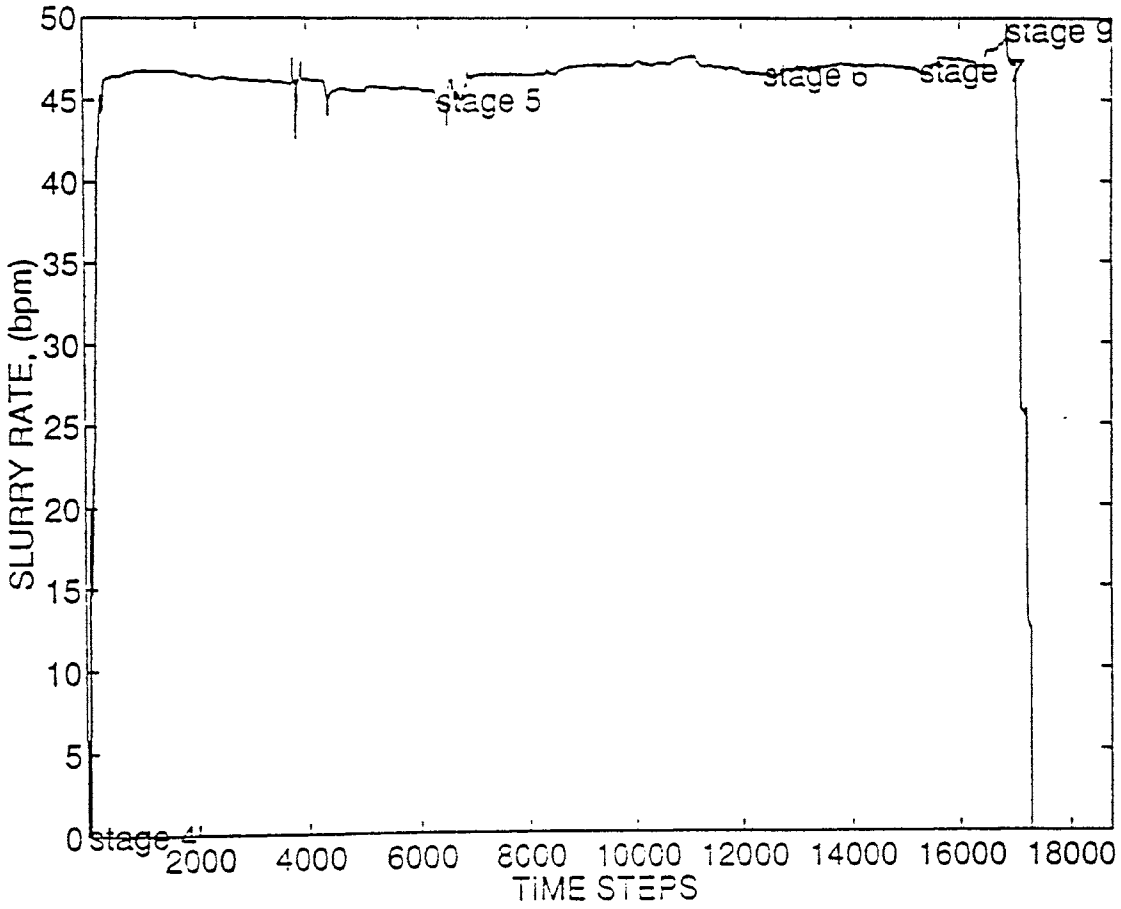

Fig. B-2. Input slurry rate (bpm)

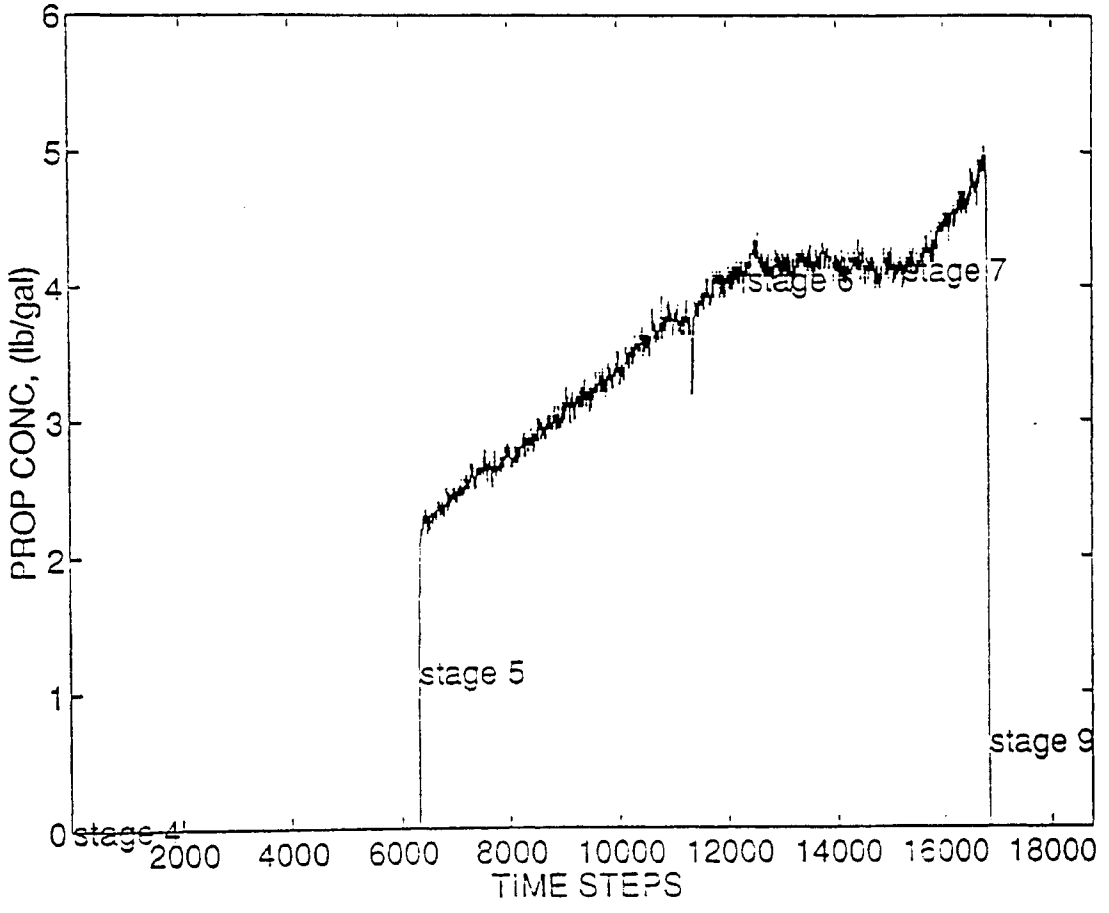

Fig. B-3. Proppant concentration (lb/gal)

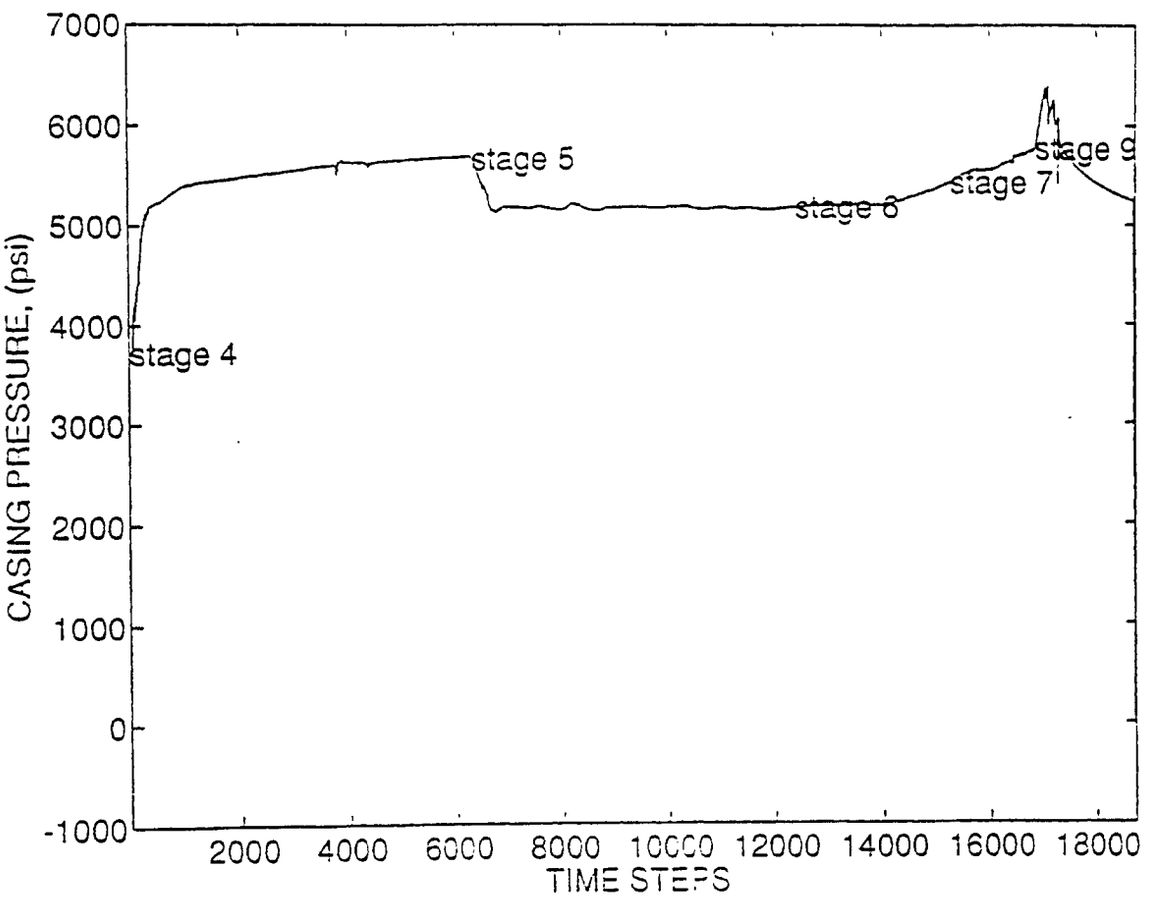

Fig. B-4. Casing pressure (psi)

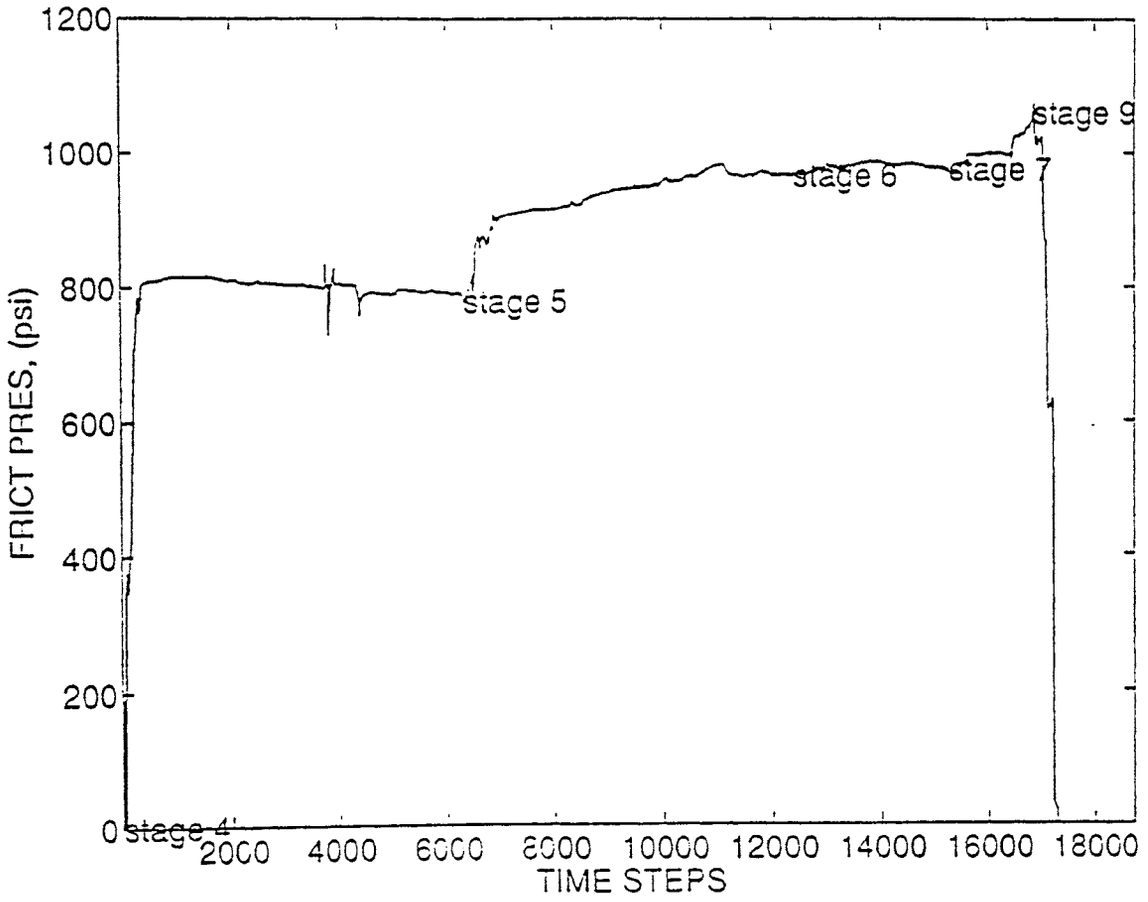

Fig. B-5. Friction pressure (psi)

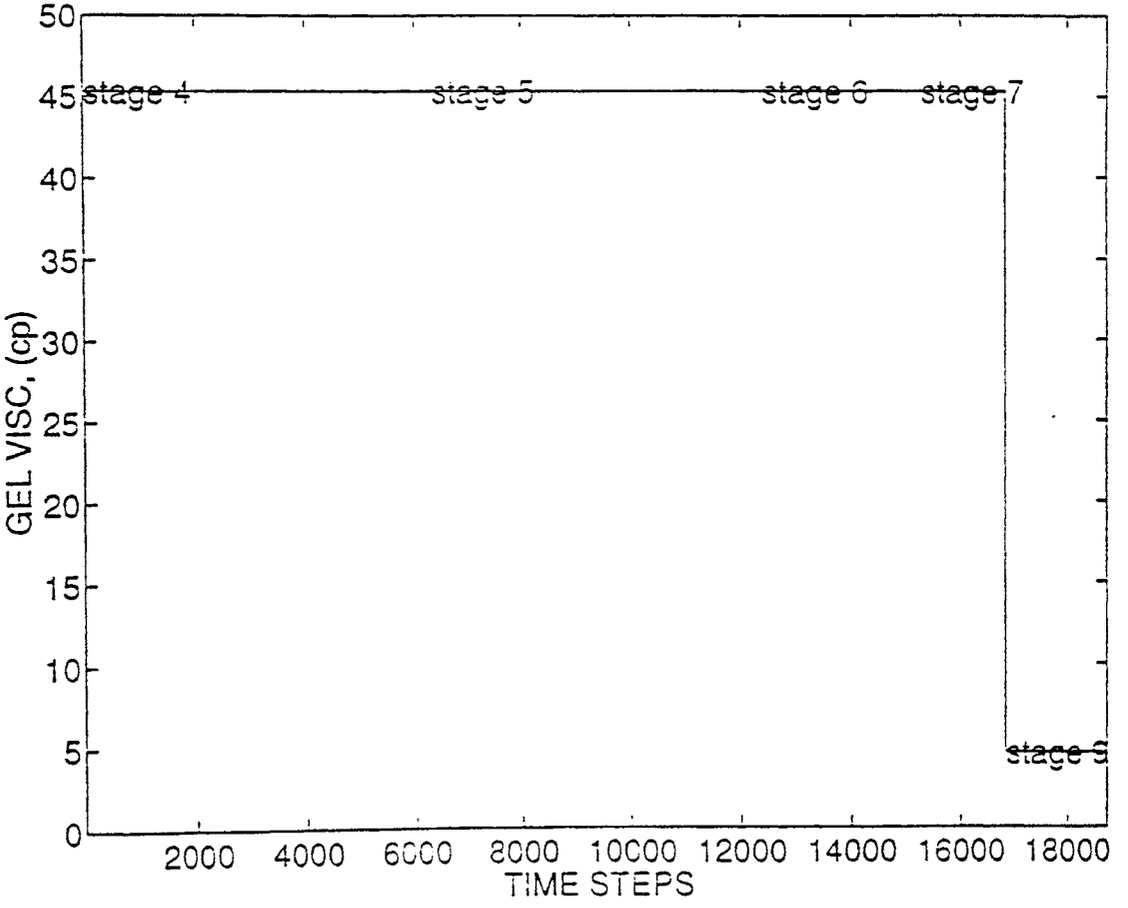

Fig. B-6. Gel viscosity (cp)

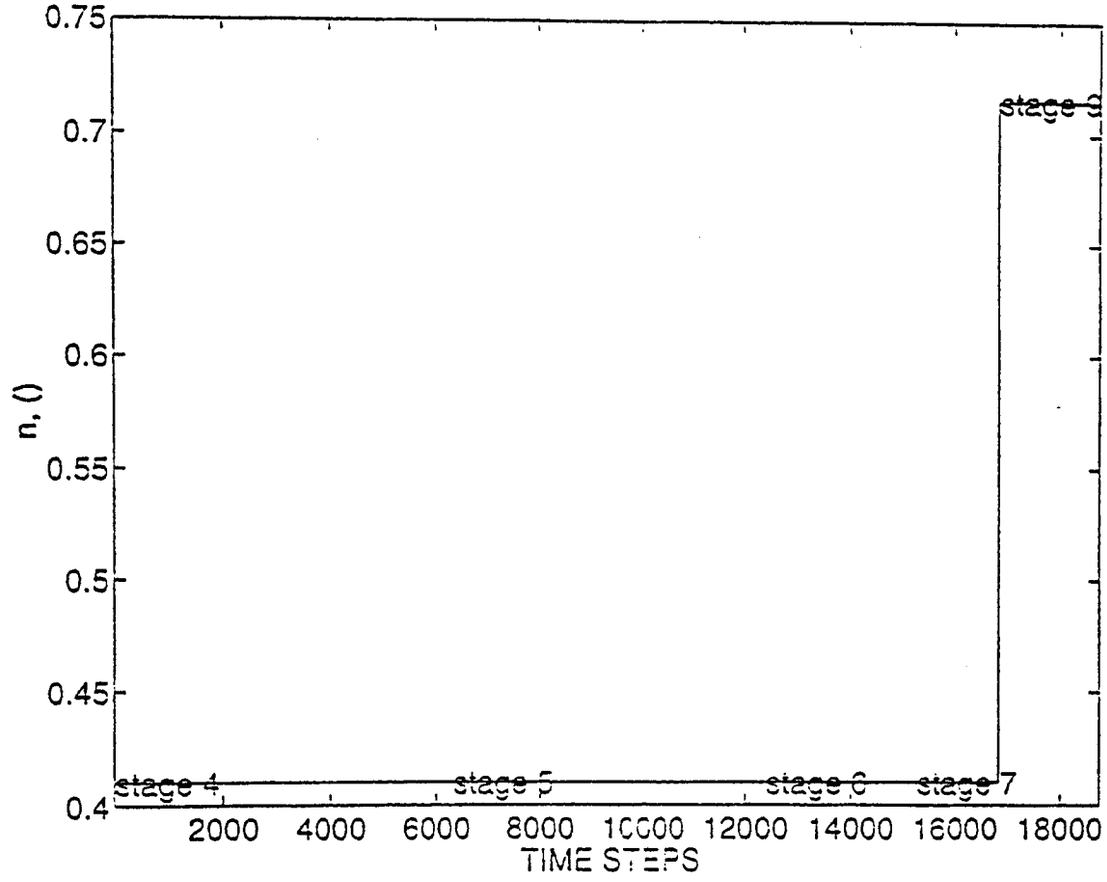

Fig. B-7. Power-law behavior index

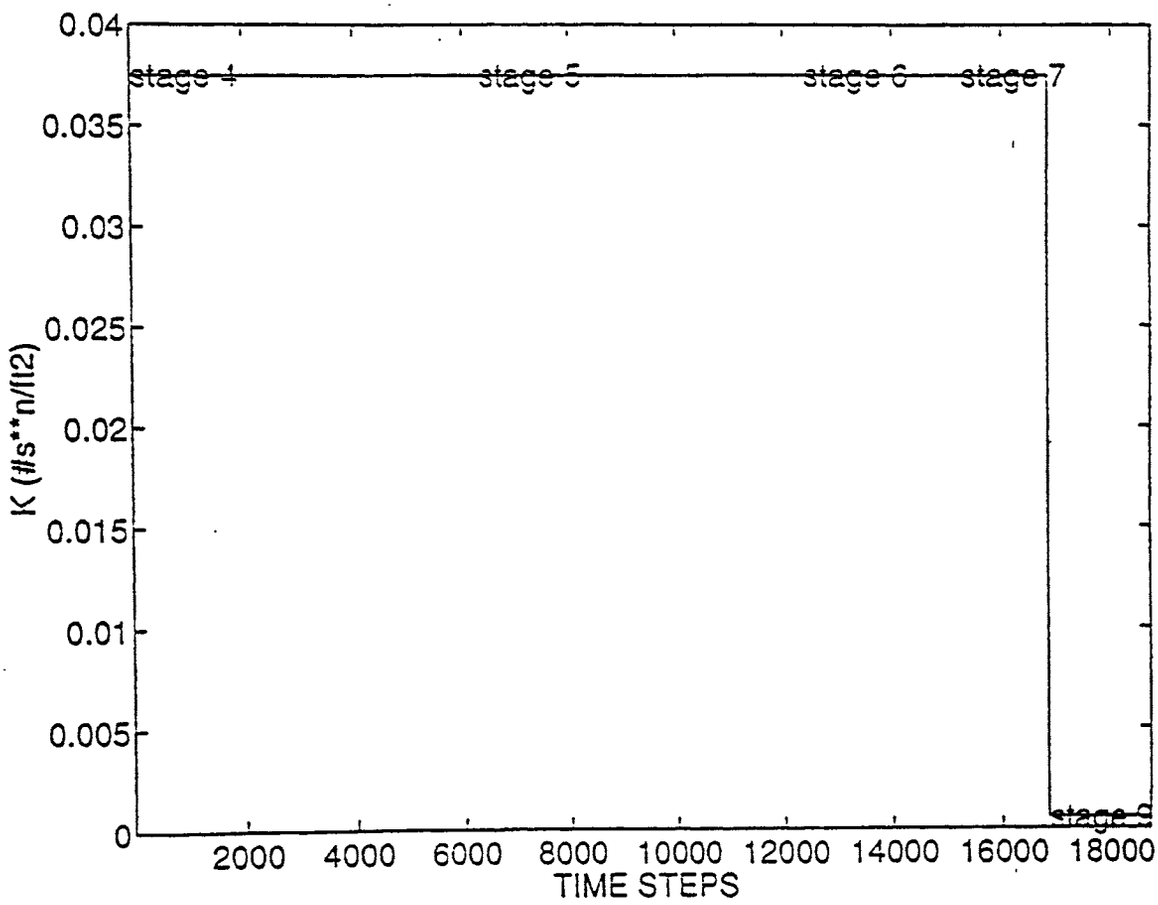

Fig. B-8. Power-law consistency index (lb-sec^n/ft^2)

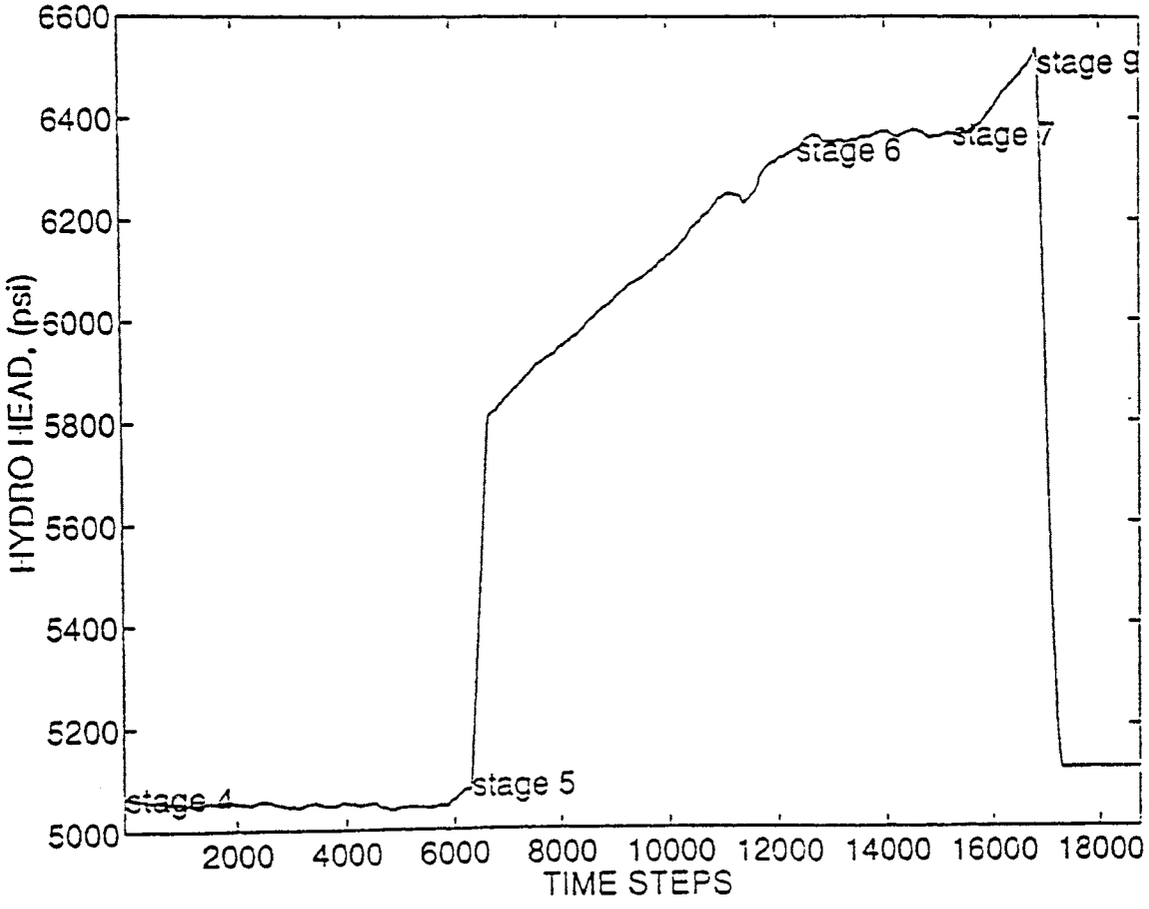

Fig. B-9. Hydro head (psi)

APPENDIX C

ADDITIONAL SIMULATIONS

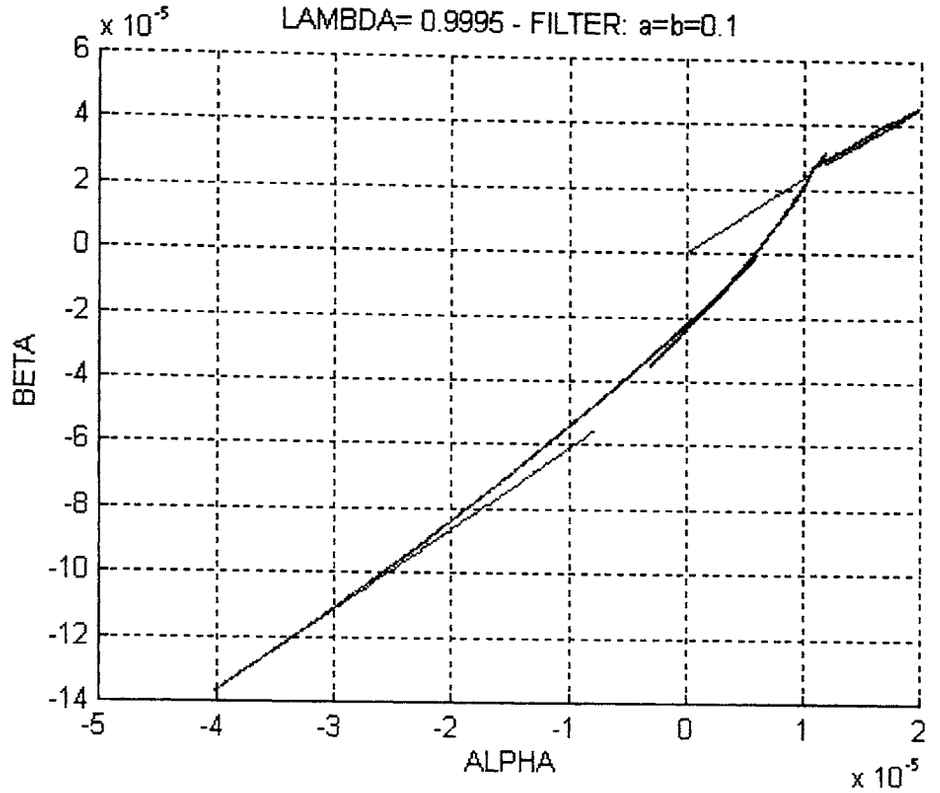

Fig. C-1. Parameters α_N and β_N for $\lambda=0.9995$

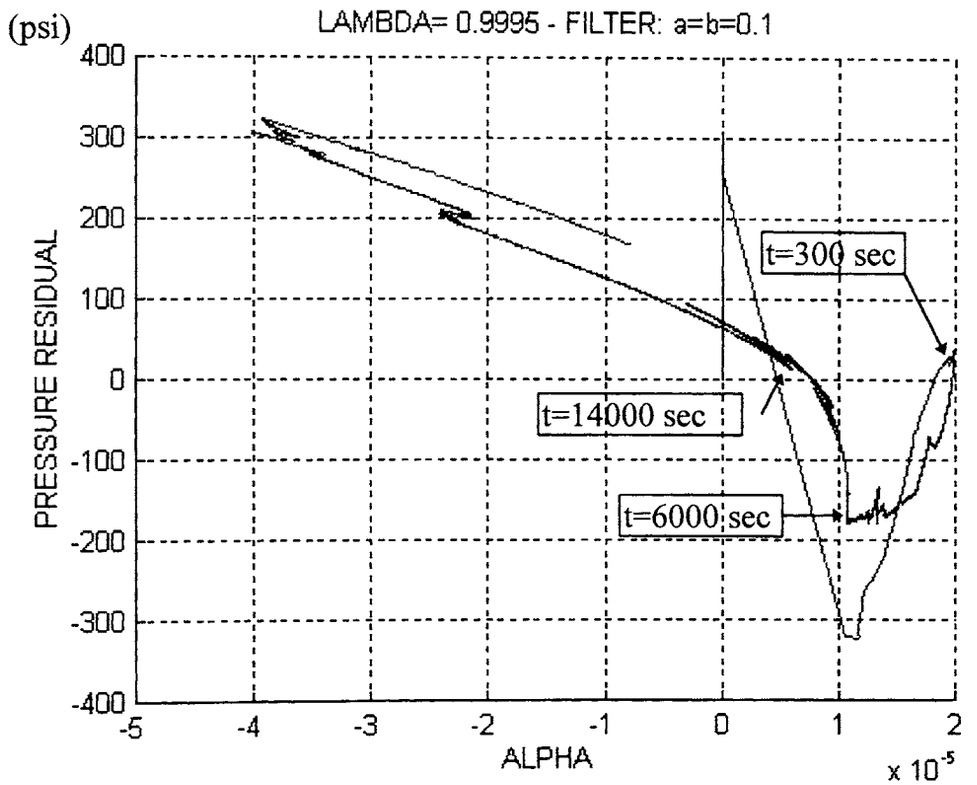

Fig. C-2. Pressure residual versus parameter α_N for $\lambda=0.9995$

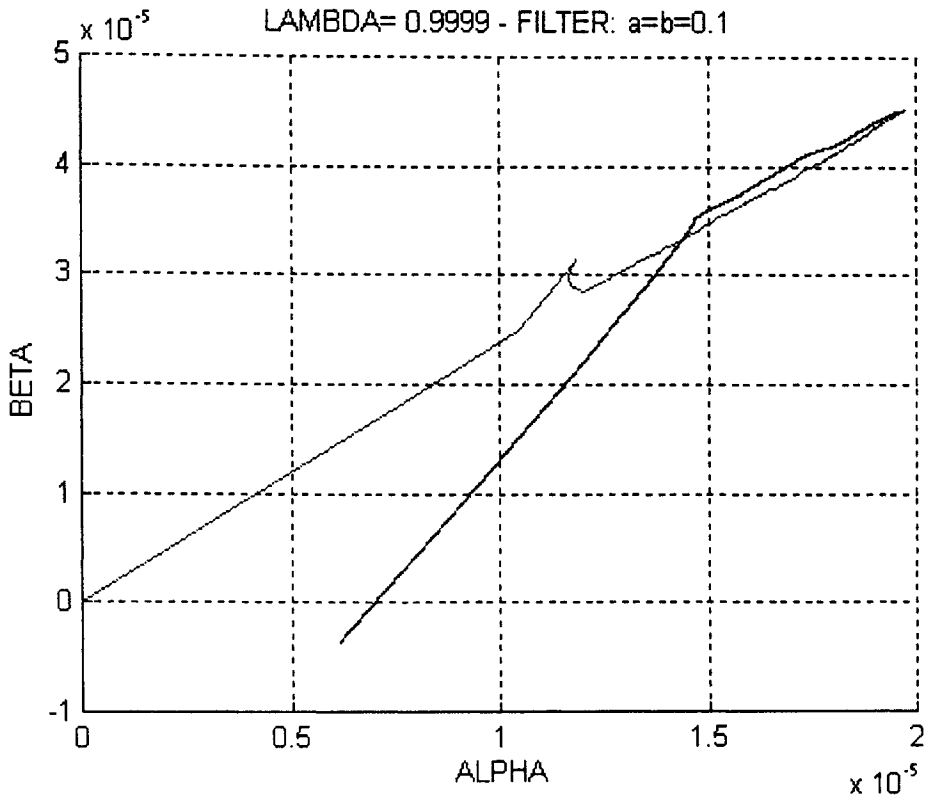

Fig. C-3. Parameters α_N and β_N for $\lambda=0.9999$

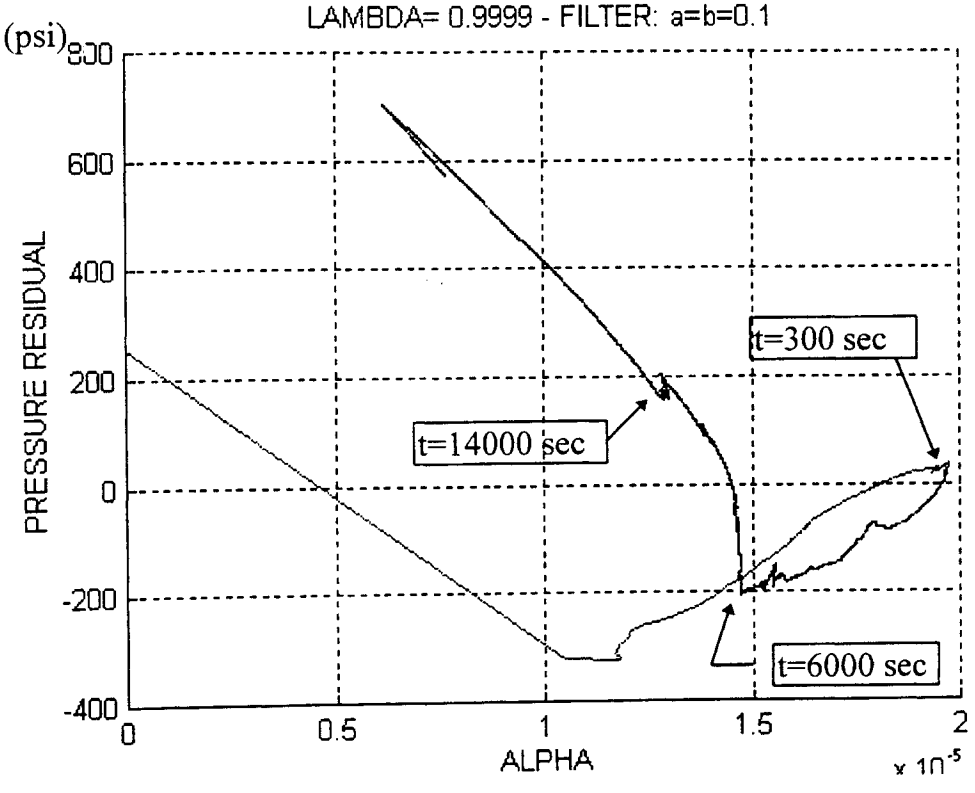

Fig. C-4. Pressure residual versus parameter α_N for $\lambda=0.9999$

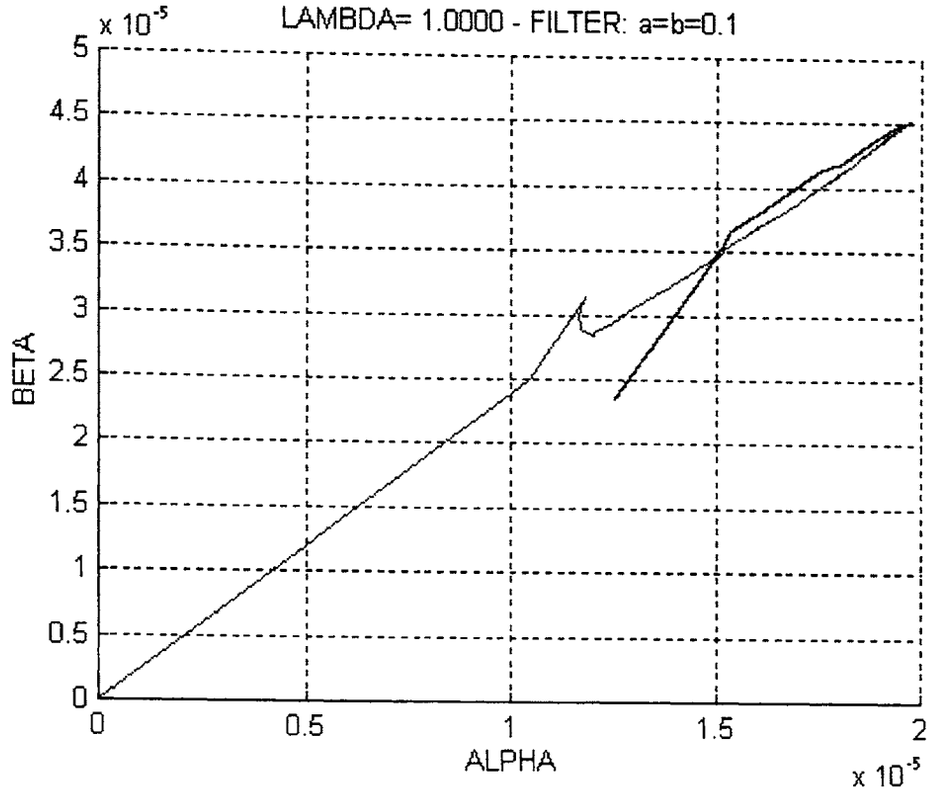

Fig. C-5. Parameters α_N and β_N for $\lambda = 1.0000$

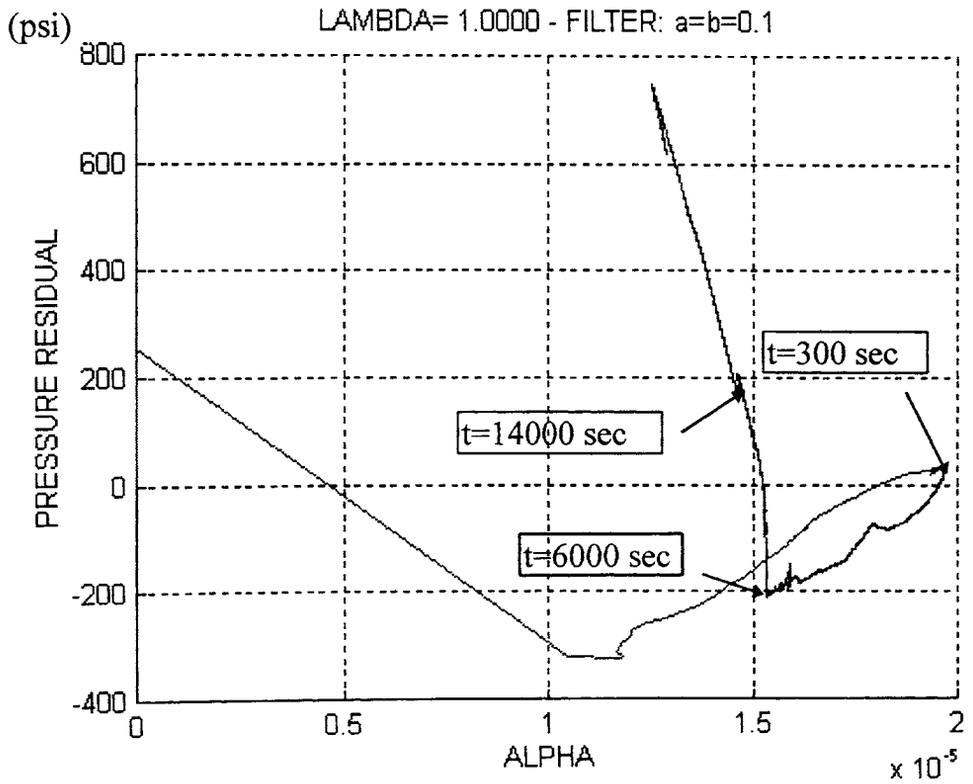

Fig. C-6. Pressure residual versus parameter α_N for $\lambda = 1.0000$

VITA

Jorge Chiriboga

Candidate for the Degree of

Master of Science

Thesis: ON THE MODELING AND SCREENOUT DETECTION BASED ON A SIMPLIFIED MODEL OF HYDRAULIC FRACTURING

Major Field: Mechanical Engineering

Biographical:

Personal Data: Born in Lima, Peru, April 12, 1963, the son of Carlos and Victoria Chiriboga.

Education: Received Bachelor of Science degree in Mechanical Engineering from the Pontificia Universidad Catolica del Peru at Lima, Peru in January 1990; completed requirements for the Master of Science degree at Oklahoma State University in December 1994.

Professional Experience: Graduate Research and Teaching Assistant, Department of Mechanical and Aerospace Engineering, Oklahoma State University, January 1994, to December 1994; Teaching Instructor, Seccion de Electricidad y Electronica, Pontificia Universidad Catolica del Peru, July 1991 to July 1992; Teaching Assistant, Seccion de Electricidad y Electronica, Pontificia Universidad Catolica del Peru, January 1988 to June 1991.

Professional Memberships: American Society of Mechanical Engineers, Society of Hispanic Professional Engineers.